HOKKAIDO UNIVERSITY

Title	Mechanism of redox potential dependent chalcopyrite dissolution in acidic ferric chloride solutions
Author(s)	Nguyen, Thi Phuong Thao
Degree Grantor	北海道大学
Degree Name	博士(工学)
Dissertation Number	甲第14246号
Issue Date	2020-09-25
DOI	https://doi.org/10.14943/doctoral.k14246
Doc URL	https://hdl.handle.net/2115/90546
Type	doctoral thesis
File Information	Nguyen_Thi_Phuong_Thao.pdf

Hokkaido University Collection of Scholarly and Academic Papers : HUSCAP

Doctoral Thesis

Mechanism of redox potential dependent chalcopyrite dissolution in acidic ferric chloride solutions

by

NGUYEN THI PHUONG THAO



Laboratory of Mineral Processing and Resources Recycling

Division of Environmental and Resources Engineering

Graduate School of Engineering

Hokkaido University, Japan

September 2020

Abstract

Chalcopyrite ($CuFeS_2$) is the most abundant mineral in copper ore bodies, accounting for more than 70% of the world copper reserves. However, with increasing the consumption of copper worldwide, high-grade ores are depleting. To guarantee the sustainable supply of copper, nowadays, low-grade ores are explored, mined, and concentrated with high amounts of impurities that are toxic such as arsenic. The concentrate of chalcopyrite together with arsenic as impurities are then processed for copper metal extraction. The conventional method to extract copper from chalcopyrite concentrate is pyro-metallurgy. However, the pyro-metallurgical process is facing the problem of high running cost and environmental issues related to the release of arsenic through stack emission.

Thus, hydrometallurgy is considered as a promising alternative approach to extract copper from low-grade chalcopyrite concentrate, owning to its low cost and safe removal and handling of arsenic that concomitantly dissolved in aqueous solution. Leaching is the first step of hydrometallurgy, where the metal ions are released (leached) into the solution from the solid particles (minerals). The biggest challenge of copper hydrometallurgy is to overcome the extremely slow leaching rate of chalcopyrite. To propose a good method to improve the chalcopyrite leaching rate, it is important to understand the chalcopyrite leaching mechanism. Therefore, this study aims to clarify the mechanism of chalcopyrite leaching in acidic chloride solution through an understanding of redox potential dependence of chalcopyrite leaching and the effect of chloride ions.

Chapter 1 gave the general introduction including overview of the study, statement of the problem, and outline of dissertation.

Chapter 2 gave a literature review on chalcopyrite leaching.

Chapter 3 investigated the effects of temperature and solution composition on the redox potential dependence of chalcopyrite leaching. The leaching experiments were carried out in acidic ferric chloride solutions using a specially designed batch leaching experimental setup that accurately determined and monitored the redox potential changes with time. Assuming that chalcopyrite oxidation with Fe(III) occurred stoichiometrically, the concentration ratio of Fe(III) to Fe(II) and the relationship between leaching rate versus redox potential were then determined from the redox potential data.

A peak behavior was observed in the copper extraction rate versus the redox potential plot. The leaching rate increased with increasing redox potential reaching a (local) maximum (i.e., the peak rate) at a certain redox potential (i.e., the peak redox potential) followed by the

gradual decrease in leaching rate at higher redox potentials.

The effects of temperature and solution composition (Cu(II), Fe(III), and Cl^- concentrations) on the peak rate and peak redox potential were investigated. The results showed that the peak rate increased with increasing temperature, and decreased with increasing HCl and Fe(III) concentrations but was not strongly affected by the concentration of Cu(II). In comparison, the peak redox potential was less dependent on the temperature and the concentrations of HCl and Fe(III). Although Cu(II) concentration was not crucial in the peak rate, it was a major factor affecting the peak redox potential, that is, the peak redox potential increased with increasing the cupric ion concentration. Based on these results, an empirical equation for the relationship between the peak redox potential and Cu(II) concentration was derived.

Chapter 4 investigated the effects of solution composition on the anodic polarization curve of chalcopyrite. Anodic polarization experiments were carried out using a conventional three-electrode system, with chalcopyrite as a working electrode, at 298 K under the nitrogen atmosphere.

The results indicated that in the absence of Cu(II) and/or Fe(II), the current density increased monotonically with increasing applied redox potential. Only in the presence of both Cu(II) and Fe(II) in solution, the peak behavior was observed in anodic polarization curve, which was similar to the peak leaching rate, reported in leaching experiments. At low redox potential region (lower than 0.50 V), the current density in the presence of Cu(II) and Fe(II) was much higher than that in the absence of these ions. This result indicated that the coexistence of Cu(II) and Fe(II) promoted the dissolution of chalcopyrite at low redox potentials.

The effects of chloride ions on the anodic dissolution of chalcopyrite in the presence of both Cu(II) and Fe(II) were investigated. In the solutions containing 0.1 M HCl, 0.05 M Cu(II), 0.05 M Fe(II), and various concentration of NaCl, current density increased with increasing NaCl concentration. It indicated that chloride ions were promoters for the dissolution of chalcopyrite. From the thermodynamic point of view, when both Cu(II) and Fe(II) present in solution, they react to form Cu(I). From the result of Geochemist's Workbench® with MINTEQ database, Cu(I) formed cuprous chloride complexes with chloride ions and thus, became more stable at high chloride concentration. It suggested that Cu(I) might play an important role in the chalcopyrite leaching.

The effects of Cu(I) on the anodic dissolution of chalcopyrite were examined using a solution containing 0.1 M HCl with 0.001 M CuCl. The result showed that Cu(I) promoted the chalcopyrite dissolution rate at low redox potentials and the peak behavior appeared on the anodic polarization curve even with only Cu(I) present in solution. Considering the promotion effect of Cu(I), the

effects of coexistence Cu(II) and Fe(II), as well as chloride ions could be explained as follows. The high leaching rate achieved at low redox potential in the presence of both Cu(II) and Fe(II) was due to the formation of promoter Cu(I). The stability of Cu(I) at high chloride ions concentration resulted in a faster chalcopyrite leaching rate at higher chloride ions concentration.

In Chapter 5, the electrochemical impedance spectroscopy (EIS) was conducted to understand different processes happening at the electrode surface. The measurements were done at varied applied potentials on the chalcopyrite electrode in an electrolyte containing 0.05 M Cu(II) and 0.05 M Fe(II) in 0.1 M HCl at 298 K under the nitrogen atmosphere. The results of EIS measurements were plotted in complex plane plots and fitted using equivalent circuits.

At redox potentials lower than 0.45 V, the impedance data were plotted on a straight line of 45 degrees in the complex plane plots and fitted using an equivalent circuit composed of solution resistant (R_s) and constant phase element (CPE) in series. The results suggested that chalcopyrite dissolution at the low redox potential was controlled by a diffusion process.

At redox potentials higher than 0.45 V, the impedance data were plotted on a compressed semi-circle (at high frequencies) connected with a straight line (at low frequencies). The data were fitted with an equivalent circuit containing a parallel circuit of R and CPE, which corresponds to a product layer formed on the surface of the chalcopyrite electrode. With increasing redox potential, the value of R in the parallel circuit increased, suggesting that the product layer grew on chalcopyrite surface and the layer thickness increased with increasing redox potential. This passivation layer hindered the further dissolution of chalcopyrite, resulted in a slow reaction kinetics and leading to a decrease in current density at high redox potential.

In Chapter 6, based on the experimental results in previous chapters, a reaction model assuming the formation of an intermediate Cu_2S at low redox potentials were proposed for chalcopyrite leaching in acidic chloride solutions. The intermediate Cu_2S is easier to dissolve than chalcopyrite, thus enhanced the copper extraction rate at low redox potentials. The formation reaction of intermediate Cu_2S involved three steps. Firstly, chalcopyrite reacted with H^+ in solution to release Cu(II), Fe(II), and H_2S into the solution. Then Cu(II) and Fe(II) reacted to form Cu(I). Finally, Cu(I) reacted with H_2S to form Cu_2S precipitated on the chalcopyrite surface. The intermediate Cu_2S was oxidatively decomposed to release Cu(II) and form elemental sulfur. Once elemental sulfur was formed, it acted as a passivation layer suppressing further chalcopyrite dissolution. Using the reaction model, the experimental results observed in the previous chapters were discussed.

Chapter 7 gave the summary, implications, and conclusion of the dissertation.

Contents

CHAPTER 1: GENERAL INTRODUCTION 1
1.1 Overview of the study 1
1.2 Statement of problem 2
1.3 Outline of the dissertation 3
1.4 References 4
CHAPTER 2: LITTERATURE REVIEW 6
2.1 Copper extractive metallurgy 6
2.2 Leaching reaction of chalcopyrite 6
2.3 Effect of chloride ions 7
2.3.1 The promotion effect of chloride ions 7
2.3.2 The effect of chloride ions concentration 7
2.3.3 The morphology of elemental sulfur 8
2.3.4 Other candidates for passivation layer 9
2.3.5 The formation of Cu (I) species 10
2.3.6 The role of Cu (I) species 10
2.4 Redox potential dependence for chalcopyrite leaching 11
2.4.1 The role of Fe^{2+} 11
2.4.2 High leaching rate was obtained at low redox potential 12
2.4.3 Controlling leaching at low redox potentials yields high copper recovery 13
2.5 References 13
CHAPTER 3: EFFECTS OF TEMPERATURE AND SOLUTION COMPOSITION ON THE REDOX POTENTIAL DEPENCE OF CHALCOPYRITE DISSOLUTION 18
3.1 Introduction 18
3.2 Materials and methods 19
3.2.1 Materials 19
3.2.2 Methods 20
3.3 Results and discussions 21
3.3.1 An example of the results and calculation method 21
3.3.2 Effects of temperature 24
3.3.3 Effects of HCl concentration 26
3.3.4 Effects of ferric ion concentration 27
3.3.5 Effects of cupric ion concentration 29
3.4 Summary 31
3.5 References 32

CHAPTER 4: EFFECTS OF SOLUTION COMPOSITION ON THE ANODIC DISSOLUTION OF CHALCOPYRITE ELECTRODE 34
4.1 Introduction 34
4.2 Materials and methods 35
4.2.1 Materials 35
4.2.2 Methods 35
4.3 Results and discussions 36
4.3.1 Effects of cupric and ferrous ions on anodic polarization curves for chalcopyrite electrode in acidic chloride solutions 36
4.3.2 Comparison of the anodic polarization curves in sulfate and chloride solutions 38
4.3.3 Effects of chloride ion and proton 39
4.3.4 Effect of cuprous ion concentration 41
4.4 Summary 44
4.5 References 45
CHAPTER 5: ELECTROCHEMICAL IMPEDANCE spectroscopy for CHALCOPYRITE ELECTRODE during anodic dissolution in ACidic Chloride solutions 46
5.1 Introduction 46
5.2 Materials and methods 47
5.2.1 Materials 47
5.2.2 Methods 47
5.3 Results and discussions 48
5.3.1 EIS for chalcopyrite electrode in the absence of both cupric and ferrous ions ... 48
5.3.1.1 EIS data 48
5.3.1.2 Fitting of EIS data 50
5.3.2 EIS for chalcopyrite electrode in the presence of both cupric and ferrous ions .. 54
5.3.2.1 EIS data 54
5.3.2.1.1 EIS data at active region I (E < 0.45 V) 54
5.3.2.1.2 EIS data at transition region II (E = 0.46 V) 56
5.3.2.1.3 EIS data at passive region III (E > 0.46 V) 57
5.3.2.2 Fitting of EIS data 59
5.4 Summary 61
5.5 References 62
CHAPTER 6: MECHANISM OF CHALCOPYRITE LEACHING IN ACIDIC CHLORIDE SOLUTIONS 64
6.1 Introduction 64
6.2 A brief review on the reaction model reported in previous studies 65
6.3 Overview of modified reaction model proposed in this study 66

6.3.1 The 1st stage (formation of intermediate Cu_2S) 66
6.3.2 The 2nd stage (dissolution of intermediate Cu_2S) 67
6.4 Thermodynamic and kinetic aspects of chalcopyrite leaching in acidic chloride solutions and factors affecting the leaching 67
6.4.1 Thermodynamics of intermediate formation 68
6.4.2 Roles and effects of chloride ions 68
6.4.3 Roles and effects of proton 68
6.4.4 Thermodynamics of intermediate oxidation 69
6.4.5 Effect of Cu^{2+} on peak redox potentials 69
6.5 Summary 70
6.6 References 71
CHAPTER 7: GENERAL CONCLUSION 73

LIST OF FIGURES

Fig. 3-1. A schematic diagram of the leaching experimental set up. 21

Fig. 3-2. An example of experimental data and calculated results: A redox potential vs. leaching time, B copper extracted amount vs. leaching time, C copper extraction rate vs. leaching time, and D copper extraction rate vs. redox potential. (Conditions: temperature of 343 K, initial Fe^{3+} concentration of 0.01 kmol m^{-3}, initial Cu^{2+} concentration of 0.01 kmol m^{-3}, solid-to-liquid ratio of 0.3 g $CuFeS_2$/15 ml, and agitation speed of 400 rpm). 23

Fig. 3-3. Effects of temperature on the redox potential dependence of chalcopyrite leaching: A copper extraction rate as function of redox potential, B the peak rate as a function of leaching temperature, and C the peak redox potential as a function of leaching temperature. (Conditions: HCl concentration of 0.1 kmol m^{-3}, initial Fe^{3+} concentration of 0.01 kmol m^{-3}, initial Cu^{2+} concentration of 0.01 kmol m^{-3}, solid-to-liquid ratio of 0.3 g $CuFeS_2$/15 ml, and agitation speed of 400 rpm). 25

Fig. 3-4. Effects of HCl concentration on the redox potential dependence of chalcopyrite leaching: A copper extraction rate as function of redox potential, B the peak rate as functions of HCl concentration, and C the peak redox potential as functions of HCl concentration. (Conditions: temperature of 343 K, initial Fe^{3+} concentration of 0.01 kmol m^{-3}, initial Cu^{2+} concentration of 0.01 kmol m^{-3}, solid-to-liquid ratio of 0.3 g $CuFeS_2$/15 ml, and agitation speed of 400 rpm). 27

Fig. 3-5. Effects of ferric ion concentration on the redox potential dependence of chalcopyrite leaching: **A** copper extraction rate as a function of redox potential, **B** the peak rate as functions of Fe^{3+} concentration, and **C** the peak redox potential as functions of Fe^{3+} concentration. (Conditions: temperature of 343 K, HCl concentration of 0.1 kmol m^{-3}, initial Cu^{2+} concentration of 0.01 kmol m^{-3}, a solid-to-liquid ratio of 0.3g $CuFeS_2$/15 ml, and agitation speed of 400 rpm). 28

Fig. 3-6. Effects of cupric ion concentration on the redox potential dependence of chalcopyrite leaching: **A** copper extraction rate as a function of redox potential, **B** the peak rate as functions of Cu^{2+} concentration, and **C** the peak redox potential as functions of Cu^{2+} concentration. (Conditions: temperature of 343 K, HCl concentration of 0.1 kmol m^{-3}, initial Fe^{3+} concentration of 0.01 kmol m^{-3}, a solid-to-liquid ratio of 0.3 g $CuFeS_2$/15 ml, and agitation speed of 400 rpm). 30

Fig. 3-7. Relationship between total Cu^{2+} concentration and peak redox potential (E_p) (Conditions: temperature of 343K, HCl concentration of 0.1 kmol m^{-3}, initial Fe^{3+} concentration of

0.01 kmol m^{-3}, a solid-to-liquid ratio of 0.3 g $CuFeS_2$/15 ml, and agitation speed of 400 rpm)..... 31
Fig. 4-1. Electrochemical experiment setup..... 36
Fig. 4-2. Effects of cupric and ferrous ions on anodic-polarization curves for the chalcopyrite electrode. (Condition: HCl concentration of 0.1 kmol m^{-3} at 298 K in a nitrogen atmosphere, stirring speed 300 rpm.)..... 38
Fig. 4-3. Anodic polarization curves for chalcopyrite electrode in a chloride solution (condition: 0.1 kmol m^{-3} HCl containing 0.1 kmol m^{-3} $FeCl_2$ and 0.1 kmol m^{-3} $CuCl_2$) and a sulfate solution (condition: 0.1 kmol m^{-3} H_2SO_4 containing 0.1 kmol m^{-3} $FeSO_4$ and 0.1 kmol m^{-3} $CuSO_4$). Black dots: in chloride solution, red dots: in sulfate solution..... 39
Fig. 4-4. Effects of chloride ions concentration on anodic-polarization curves for the chalcopyrite electrode. (Condition: $[Cu^{2+}] = [Fe^{2+}]$ =0.05 kmol m^{-3}, HCl concentration of 0.1 kmol m^{-3} at 298 K in a nitrogen atmosphere, stirring speed 300 rpm.)..... 40
Fig. 4-5. Effects of HCl concentration on anodic polarization curves for the chalcopyrite electrode. (Condition: $[Cu^{2+}] = [Fe^{2+}]$ =0.05 kmol m^{-3}, at 298 K in a nitrogen atmosphere, stirring speed 300 rpm.) 41
Fig. 4-6. The Eh-log aCl^- diagram for the Cu^+/Cu^{2+}-Cl^- - H_2O system..... 42
Fig. 4-7. Effects of cuprous ions on anodic polarization curves for the chalcopyrite electrode. (Condition: HCl concentration of 0.1 kmol m^{-3} at 298 K in a nitrogen atmosphere, stirring speed 300 rpm.)..... 43
Fig. 4-8. A cyclic voltammogram obtained using a platinum electrode in the electrolyte containing 0.1 kmol m^{-3} HCl, 0.05 kmol m^{-3} Cu^{2+} and 0.05 kmol m^{-3} Fe^{2+} at 298 K in a nitrogen atmosphere..... 43
Fig. 5-1. Anodic-polarization curves for the chalcopyrite electrode in the absence of cupric and ferrous ions. (Condition: HCl concentration of 0.1 kmol m^{-3} at 298 K in a nitrogen atmosphere, stirring speed 300 rpm.)..... 48
Fig. 5-2. The Bode plot, magnitude of impedance as a function of frequency (Condition: 140 ml electrolyte containing HCl 0.1 M, at 25 ºC, under N2 atmosphere)..... 50
Fig. 5-3. The Bole plot, phase angle as a function of frequency. (Condition: 140 ml electrolyte containing HCl 0.1 M, at 25 ºC, under N2 atmosphere)..... 50
Fig. 5-4. The complex plane plot (Condition: 140 ml electrolyte containing HCl 0.1 M, at 25 º C under N2 atmosphere)..... 50
Fig. 5-5. Equivalent circuit in the case of without Cu^{2+} and Fe^{2+} in solution..... 51
Fig. 5-6. Fitting result of solution resistance (Condition: 140 ml electrolyte containing HCl 0.1 M,

at 25 °C, under N_2 atmosphere)..... 52
Fig. 5-7. Fitting result of constant phase element, CPE-P (Condition: 140 ml electrolyte containing HCl 0.1 M, at 25 °C, under N2 atmosphere)..... 52
Fig. 5-8. Fitting result of constant phase element, CPE-T (Condition: 140 ml electrolyte containing HCl 0.1 M, at 25 °C, under N2 atmosphere)..... 53
Fig. 5-9. Fitting result of charge transfer resistance, R (Condition: 140 ml electrolyte containing HCl 0.1 M, at 25 °C, under N2 atmosphere)..... 53
Fig. 5-10. Anodic-polarization curves for the chalcopyrite electrode in the presence of 0.05 M cupric and ferrous ions. (Condition: HCl concentration of 0.1 kmol m^{-3} at 298 K in a nitrogen atmosphere, stirring speed 300 rpm.) 54
Fig. 5-11. The complex plane plot at active region I (E < 0.45 V) (Condition: 140 ml electrolyte containing Cu^{2+} 0.05 M Fe^{2+} 0.05 M in HCl 0.1 M, at 25 °C, under N2 atmosphere). 55
Fig. 5-12. The Bode plot, magnitude of impedance as a function of frequency at active region I (E < 0.45 V) (Condition: 140 ml electrolyte containing Cu^{2+} 0.05 M Fe^{2+} 0.05 M in HCl 0.1 M, at 25 °C, under N2 atmosphere). 56
Fig. 5-13. The Bode plot, phase angle as a function of frequency at active region I (E < 0.45 V) (Condition: 140 ml electrolyte containing Cu^{2+} 0.05 M Fe^{2+} 0.05 M in HCl 0.1 M, at 25 ° C, under N2 atmosphere). 56
Fig. 5-14. The complex plane plot at transition region II (E = 0.46 V) (Condition: 140 ml electrolyte containing Cu^{2+} 0.05 M Fe^{2+} 0.05 M in HCl 0.1 M, at 25 °C, under N2 atmosphere)..... 57
Fig. 5-15. The Bode plot, phase angle as a function of frequency at transition region II (E = 0.46 V) (Condition: 140 ml electrolyte containing Cu^{2+} 0.05 M Fe^{2+} 0.05 M in HCl 0.1 M, at 25 ° C, under N2 atmosphere). 57
Fig. 5-16. The complex plane plot at passive region II (E > 0.46 V) (Condition: 140 ml electrolyte containing Cu^{2+} 0.05 M Fe^{2+} 0.05 M in HCl 0.1 M, at 25 °C, under N2 atmosphere). 58
Fig. 5-17. The Bode plot, magnitude of impedance as a function of frequency at passive region II (E > 0.46 V) (Condition: 140 ml electrolyte containing Cu^{2+} 0.05 M Fe^{2+} 0.05 M in HCl 0.1 M, at 25 °C, under N2 atmosphere). 59
Fig. 5-18. The Bode plot, phase angle as a function of frequency at passive region II (E > 0.45 V) (Condition: 140 ml electrolyte containing Cu^{2+} 0.05 M Fe^{2+} 0.05 M in HCl 0.1 M, at 25 °C, under N2 atmosphere)..... 59
Fig. 5-19. Equivalent circuit used for fitting the impedance data at active region I (E =< 0.45 V) 59

Fig. 5-20. Equivalent circuit used for fitting the impedance data at transition region II (E = 0.46 V). 60
Fig. 5-21. Equivalent circuit used for fitting the impedance data at passive region II (E > 0.46 V). 60
Fig. 5-22. Fitting result of constant phase element, CPE-T (Condition: 140 ml electrolyte containing Cu^{2+} 0.05 M Fe^{2+} 0.05 M in HCl 0.1 M, at 25 ^{o}C, under N2 atmosphere). 61
Fig. 5-23. Fitting result of charge transfer resistance, R (Condition: 140 ml electrolyte containing Cu^{2+} 0.05 M Fe^{2+} 0.05 M in HCl 0.1 M, at 25 ^{o}C, under N2 atmosphere)..... 61
Fig. 6-1. Formation of intermediate Cu_2S in the proposed model..... 66
Fig. 6-2. Two-step oxidation of intermediate Cu2S in the proposed model..... 67

CHAPTER 1: GENERAL INTRODUCTION

1.1 Overview of the study

Chalcopyrite ($CuFeS_2$) is the most abundant mineral in copper ore bodies, accounting for more than 70% of the world copper reserves (Muñoz-Ribadeneira and Gomberg, 1971; Mikhlin *et al.*, 2004; Wang, 2005; Aguirre *et al.*, 2016). However, with an increase in the consumption of copper worldwide, high-grade copper ores are exhausting and the exploitation of vast low-grade copper ores has become the norm (Deepak and Das, 1981; Plumb, McSweeney and Franzmann, 2008; Gericke, Govender and Pinches, 2010; A. Baba *et al.*, 2012b; Watling, 2013; Ghosh and Pandey, 2015; Fagan-Endres *et al.*, 2017). To guarantee the sustainable supply of copper, nowadays, low-grade ores are mined and concentrated with high amounts of impurities that are toxic such as arsenic. The concentrate of chalcopyrite together with arsenic as impurities are then processed for copper metal extraction. The conventional method to extract copper from chalcopyrite concentrate is pyro-metallurgy (Yoo *et al.*, 2010; Sohn, 2019b). However, the pyro-metallurgical process is facing the problem of high running cost and environmental issues related to the release of arsenic through stack emission.

Hydrometallurgy is considered as a promising alternative approach to extract copper from low-grade chalcopyrite concentrate, owning to its low cost and safe removal and handling of arsenic that concomitantly dissolved in aqueous solution (Hiroyoshi et al., 1997, Sandstrom et al., 2005). Leaching is the first step of hydrometallurgy, where the metal ions are released (leached) into the solution from the solid particles (minerals). Chalcopyrite is the major copper mineral. Among many lixiviant to leach chalcopyrite, sulfuric acid is most commonly used, owning to its cheap price. However, leaching rate of chalcopyrite in sulfuric acid solutions is extremely slow (Hirato, Majima and Awakura, 1987; Third, Cord-Ruwisch and Watling, 2000; Tshilombo, Petersen and Dixon, 2002; Li *et al.*, 2010), making hydrometallurgical process not commercial applicable.

Many researches have been attempted to find a better leaching lixiviant for chalcopyrite, one of the outstanding candidates is chloride solution. It was widely accepted that leaching rate of chalcopyrite in chloride solutions is higher than that in sulfuric solutions (Dutrizac, 1980). However, the mechanism of chalcopyrite leaching in acidic chloride solutions is still topic of controversial.

It was reported that in both sulfate and chloride solutions, high leaching of chalcopyrite can be achieved at low redox potential. In sulfate system, the redox potential dependence of chalcopyrite leaching has been intensively studied and mechanism is well establish. In chloride system, Yoo et al (2010) reported that increasing chloride ions concentration can broaden the potential range where high chalcopyrite leaching rate takes place. However, this study mostly based on the thermodynamic calculation and many parameters were assumed to be constant. Therefore, more detail study is required.

Furthermore, the roles of chloride ions in the mechanism of chalcopyrite leaching remains unclear. Published data in literature indicated that chloride ions promoted the leaching rate of chalcopyrite. Some authors reported the elemental sulfur formed as a product layer on chalcopyrite surface in the presence of chloride is more porous than in its absence (Hirato, et al, 1987; Lu, et al, 2000). However, the underlying reason for these experimental observations is still unknown.

In this thesis, a systematic study is done to clarify the mechanism of chalcopyrite leaching in acidic chloride solution. First, leaching experiments were done to investigate the factors affecting the redox potential dependence of chalcopyrite leaching. Second, electrochemical experiments, including anodic polarization and electrochemical impedance spectroscopy, were carried out to study the anodic dissolution of chalcopyrite. Based on experimental data, a new reaction model was proposed to explain the experimental observations and solve the remaining issues in the published works by other authors.

Through an understanding about the chloride effect and redox potential dependence of chalcopyrite leaching, a good leaching system for chalcopyrite can be developed. This is a significant academic contribution for the copper extractive metallurgy. The outcome of this research help to sustain the global supply of copper.

1.2 Statement of problem

The experimental observations showed that high leaching rate of chalcopyrite was obtained at low redox potential, and in chloride solutions. However, the mechanism for these experimental observations remains unclear. This study therefore aims to understand the mechanism of redox potential dependence of chalcopyrite leaching and the promotion effects of chloride ions.

1.3 Outline of the dissertation

This dissertation is composed of seven chapters. The key contents of each chapter are outlined as follows:

Chapter 1 gives the general introduction including overview of study, statement of the problem and outline of dissertation.

Chapter 2 give a literature review on chalcopyrite leaching.

Chapter 3 investigated the effects of temperature and solution composition on the redox potential dependence of chalcopyrite leaching.

Chapter 4 studied the effects of solution composition on the anodic dissolution of chalcopyrite.

Chapter 5 presents the effects of solution composition on the electrochemical impedance spectroscopy of chalcopyrite electrodes.

Chapter 6 describes the proposed mechanism of chalcopyrite leaching based on the experimental results.

Chapter 7 gives the summary, implications and conclusion of the dissertation.

1.4 References

A. Baba, A., I. Ayinla, K., A. Adekola, F., K. Ghosh, M., S. Ayanda, O., B. Bale, R., R. Sheik, A., R. Pradhan, S., 2012. A Review on Novel Techniques for Chalcopyrite Ore Processing. MINING 1, 1–16. https://doi.org/10.5923/j.mining.20120101.01

Aguirre, C.L., Toro, N., Carvajal, N., Watling, H., Aguirre, C., 2016. Leaching of chalcopyrite (CuFeS2) with an imidazolium-based ionic liquid in the presence of chloride. Minerals Engineering 99, 60–66. https://doi.org/10.1016/j.mineng.2016.09.016

Deepak, D., Das, K., 1981. Bioleaching of copper from a low-grade chalcopyrite ore. Journal of Chemical Technology and Biotechnology 31, 358–362. https://doi.org/10.1002/jctb.503310149

Fagan-Endres, M.A., Cilliers, J.J., Sederman, A.J., Harrison, S.T.L., 2017. Spatial variations in leaching of a low-grade, low-porosity chalcopyrite ore identified using X-ray μCT. Minerals Engineering 105, 63–68. https://doi.org/10.1016/j.mineng.2017.01.010

Gericke, M., Govender, Y., Pinches, A., 2010. Tank bioleaching of low-grade chalcopyrite concentrates using redox control. Hydrometallurgy, 18th International Biohydrometallurgy Symposium, IBS2009, Bariloche-Argentina, 13-17 September 2009 104, 414–419. https://doi.org/10.1016/j.hydromet.2010.02.024

Ghosh, A., Pandey, B.D., 2015. Bioleaching of low grade granitic chalcopyrite ore by hyperthermophiles: Elucidation of kinetics-mechanism. Metall. Res. Technol. 112, 506. https://doi.org/10.1051/metal/2015031

Hirato, T., Majima, H., Awakura, Y., 1987. The leaching of chalcopyrite with ferric sulfate. MTB 18, 489–496. https://doi.org/10.1007/BF02654260

Li, J., Kawashima, N., Kaplun, K., Absolon, V.J., Gerson, A.R., 2010. Chalcopyrite leaching: The rate controlling factors. Geochimica et Cosmochimica Acta 74, 2881–2893. https://doi.org/10.1016/j.gca.2010.02.029

Lu, Z.Y., Jeffrey, M.I., Lawson, F., 2000. The effect of chloride ions on the dissolution of chalcopyrite in acidic solutions. Hydrometallurgy 56, 189–202. https://doi.org/10.1016/S0304-386X(00)00075-X

Mikhlin, Y.L., Tomashevich, Y.V., Asanov, I.P., Okotrub, A.V., Varnek, V.A., Vyalikh, D.V., 2004. Spectroscopic and electrochemical characterization of the surface layers of chalcopyrite (CuFeS2) reacted in acidic solutions. Applied Surface Science 225, 395–409. https://doi.org/10.1016/j.apsusc.2003.10.030

Muñoz-Ribadeneira, F.J., Gomberg, H.J., 1971. Leaching of Chalcopyrite (CuFeS2) with Sodium Chloride Sulfuric Acid Solutions. Nuclear Technology 11, 367–371. https://doi.org/10.13182/NT71-A30870

Plumb, J.J., McSweeney, N.J., Franzmann, P.D., 2008. Growth and activity of pure and mixed bioleaching strains on low grade chalcopyrite ore. Minerals Engineering, Selected papers from Bio and Hydrometallurgy '07, Falmouth, UK, May 2007 21, 93–99. https://doi.org/10.1016/j.mineng.2007.09.007

Sohn, H.-S., 2019. 동스크랩의 리사이클링. 자원리싸이클링 28, 3–14. https://doi.org/10.7844/KIRR.2019.28.3.3

Third, K.A., Cord-Ruwisch, R., Watling, H.R., 2000. The role of iron-oxidizing bacteria in stimulation or inhibition of chalcopyrite bioleaching. Hydrometallurgy 57, 225–233. https://doi.org/10.1016/S0304-386X(00)00115-8

Tshilombo, A.F., Petersen, J., Dixon, D.G., 2002. The influence of applied potentials and temperature on the electrochemical response of chalcopyrite during bacterial leaching. Minerals Engineering 15, 809–813. https://doi.org/10.1016/S0892-6875(02)00122-X

Wang, S., 2005. Copper leaching from chalcopyrite concentrates. JOM 57, 48–51. https://doi.org/10.1007/s11837-005-0252-5

Watling, H.R., 2013. Chalcopyrite hydrometallurgy at atmospheric pressure: 1. Review of acidic sulfate, sulfate–chloride and sulfate–nitrate process options 18.

Yoo, K., Kim, S., Lee, J., Ito, M., Tsunekawa, M., Hiroyoshi, N., 2010. Effect of chloride ions on leaching rate of chalcopyrite - ScienceDirect. Minerals Engineering 23 (2010) 471–477. https://doi.org/doi:10.1016/j.mineng.2009.11.007

CHAPTER 2: LITTERATURE REVIEW

2.1 Copper extractive metallurgy

Pyrometallurgy is the major route for extracting copper from its primary sulfide minerals (Yoo et al., 2007; Lim et al., 2019; Sohn, 2019). With the exhaustion of high-grade copper deposits, however, the exploitation of vast low-grade copper ores has become the norm and will be problematic to conventional pyro-metallurgical operations because of the lower quality of concentrates and the presence of high amounts of impurities like arsenic (i.e., 'dirty' concentrates) (Baba et al., 2012; Watling, 2013). Because of these, hydrometallurgical approaches to extract copper are currently being explored as an alternative processing strategy for low-grade ores and 'dirty' concentrates (Hiroyoshi et al., 1997, Sandstrom et al., 2005). For several decades, the research for pollution free hydrometallurgy processes has been accelerating (M. Bonan et al., 1981).

2.2 Leaching reaction of chalcopyrite

One of the biggest challenges in copper hydrometallurgy is how to establish the leaching method suitable for chalcopyrite ($CuFeS_2$), the primary and most abundant sulfide mineral of copper (Dutrizac, 1981; Hiroyoshi et al., 1998). For this, it is important to understand the leaching mechanism and the factors affecting the leaching rate of chalcopyrite. The dissolution of chalcopyrite proceeds via an electrochemical mechanism (Hiroyoshi et al., 2004; Nicol et al., 2017), a process whereby distinct anodic and cathodic reactions occur almost simultaneously on the surface of the mineral via the transfer of electrons between distinct anodic and cathodic sites through the crystal lattice (Tabelin et al., 2017a; Williamson and Rimstidt, 1994). This type of electrochemical dissolution has been well studied for other sulfide minerals like marmatite ([Zn, Fe]S), pyrite (FeS_2) and arsenopyrite (FeAsS) (Igarashi et al., 2020; Li et al., 2019a, 2019b; Meng et al., 2019; Park et al., 2019, 2018a; Seng et al., 2019a, 2019b; Tabelin et al., 2019, 2018, 2013, 2012; Tomiyama et al., 2019, 2020). Chalcopyrite leaching is typically done under strongly acidic conditions (pH < 2) to limit the precipitations not only of extracted copper ions (i.e., Cu^{2+}) but also of the primary oxidant (i.e., Fe^{3+}) essential for the reaction as explained below

$$CuFeS_2 + 4\ Fe^{3+} = Cu^{2+} + 5\ Fe^{2+} + 2\ S^0 \quad (2\text{-}1)$$

2.3 Effect of chloride ions

2.3.1 The promotion effect of chloride ions

The effect of chloride ions in the leaching rate of chalcopyrite has been well reported. Dutrizac (1980) compared chalcopyrite leaching rate in two media, one was 0.2 M FeCl3 in 0.3 M HCl, and another one was 0.2 M $Fe_2(SO_4)_3$ in 0.3 M H_2SO_4, at 98 ^oC, using 0.78 g Transvaal chalcopyrite. The results showed that the leaching rate of chalcopyrite in ferric chloride solution was higher than that in ferric sulfate solution. For example, when 100/r (r is particle size) equals 8 μ^{-1}, the chalcopyrite leaching rate in chloride solution (18 mg/hour) was about four times higher than that in sulfate solution (4 mg/hour).

In agree with Dutrizac result, Yoo et al (2010) did leaching experiments at 80 ^{o}C using 4.5 g chalcopyrite in 150 ml of 0.1 M H_2SO_4 and/or 0.1 M HCl. The authors reported that leaching rate of chalcopyrite followed this order: HCl > mixture of HCl and H_2SO_4 > H_2SO_4.

In 2000, Z. Y. Lu et al compared the copper extraction (%) from chalcopyrite in the absence and presence of 1.0 M NaCl, at 95 ^{o}C using 32 g chalcopyrite with d_{50} of 4μm in 800 ml of 0.8 M H_2SO_4. The results showed that in the absence of NaCl, the copper extraction was 30 % after 8 hours, while in the presence of 1.0 M NaCl, the copper extraction was about 95% after only 6 hours.

M. Skrobian et al., (2005) did leaching experiment at 80 ^{o}C, in solution containing HCl 0.5 M, $CuCl_2$ 0.75 M and different concentration of NaCl. The result indicated that the amount if metal ion extracted from chalcopyrite increased with increasing NaCl concentration. For example, after 300 minutes, the iron extraction was 15, 18, and 26 % with the NaCl addition of 200, 250, and 300 g/L respectively.

The above published data indicated that the leaching rate of chalcopyrite was higher in the presence of chloride ions than in its absence. The remaining question is that how much chloride concentration is enough to obtain highest leaching rate.

2.3.2 The effect of chloride ions concentration

Palmer et al. (1981) studied the dissolution of 270 x 400 mesh chalcopyrite in a solution

containing 0.2 M $FeCl_3$, 0.2 M HCl and reported that the rate of dissolution increased with increasing chloride concentration for values up to one molar but became independent of this parameter for higher concentration.

T. Hirato et al. (1987) investigated the effect of NaCl concentration from 0 to 4 M, at 70 ^{o} C in solution containing 0.1 M CuCl2, 0.2 M HCl. The results showed that the leaching rate increased about 6 times with increasing NaCl concentration from 0 to 2 M, nevertheless, a rise in NaCl concentration from 3 to 4 M did not result in a further increase in leaching rate.

Lu et al. (2000) reported that the copper extraction from chalcopyrite in 0.8 M H_2SO_4 at 95 ^{o} C was almost unchanged when increasing NaCl concentration from 0.5 to 2 M.

PH-M Kinnuen and JA Puhakka (2004) studied the ferric sulfate leaching of chalcopyrite concentrate in batch experiment at 90 ^{o} C and reported that after 2 weeks, the copper yield were approximately 60, 80 and 100 % with the addition of 0, 1 and 5 g dm^{-3} Cl^{-}, respectively; however continuing to increase in chloride concentration to 10 g dm^{-3} (0.28 M) did not further improve the leaching rate.

Although there is difference in experimental conditions, and the different range of NaCl concentration was used, there general conclusion is that the presence of chloride ion can enhance the leaching rate of chalcopyrite, however, high concentration of chloride ions do not always further increase the chalcopyrite leaching rate.

2.3.3 The morphology of elemental sulfur

It was reported that the chloride ions change the morphology of chalcopyrite surface.
T. Hitaro et al (1987) studied the leaching of chalcopyrite with 1 M $CuCl_2$ in 0.2 M HCl solution. The surface and cross section of chalcopyrite specimens after 100 hours and 480 hours leaching were shown. The product formed on the surface of chalcopyrite after 480 hours leaching was identified as elemental sulfur by X-ray analysis. The micrographs clearly showed that the sulfur layer is porous. The interface between the unreacted chalcopyrite and elemental sulfur was roughened by prolonged leaching, leading to an increase in the effective reaction surface area, and hence accelerate the leaching rate of chalcopyrite after 300 hours leaching. After 800 hours, leaching was repeated using a fresh, re-prepared leaching solution. The observed leaching rate

was much greater than in the initial stage, and almost as fast as the final stage. This result suggested that the formation of the porous elemental sulfur layer roughened the chalcopyrite surface and hence, increased the effective surface area, consequently, increased leaching rate at later stage.

Z. Y. Lu et al (2000) based on SEM image, reported that in the absence of chloride, the leached chalcopyrite is completely coated by an amorphous or cryptocrystalline film of sulfur, acting as a protective coating on the mineral particles. Once present, this coating may hinder the leaching process or even stop leaching completely. In the presence of chloride, sulfur layer is crystalline and porous. The chloride ions thus modify the morphology of the deposited sulfur.

The above published data implied that a porous elemental sulfur layer was formed on the chalcopyrite surface in the presence of chloride ions. However, the mechanism how the chloride ions changed the morphology of elemental sulfur is still unknown.

2.3.4 Other candidates for passivation layer

PH-M Kinnunen and JA Puhakka (2004), in the study on chloride-promoted leaching of chalcopyrite concentrate by biologically-produced ferric sulfate, reported that a decreased potential of 60 mV in the presence of Cl- indicated the accumulation of partially oxidized forms of dissolved sulfur compounds such as thiosulfate and polythionate instead of elemental sulfur and, thus, a decrease in sulfur passivation.

M. Lundstrom et al. (2005) studied chalcopyrite dissolution in cupric chloride solution and reported that, with $[Cu^{2+}] > 9$ g/L, the reaction rate increased with increasing Cu^{2+} concentration, and the reaction was controlled by the diffusion of Cu^{2+} through the reaction product layer. With $[Cu^{2+}] > 9$ g/ L and temperature from 70 to 90 degree, the dissolution rate increased with a rise in pH values from pH 1 to pH 3. The low dissolution rates low pH values were due to the rapid formation of a sulfur-rich reaction product layer that impedes the dissolution of chalcopyrite, supported by the detection of high surface concentrations of sulfur from SEM-EDS analysis. In the meanwhile, the higher dissolution rates at high pH values was most likely due to the slower formation of the porous iron rich reaction product layer, suggested as goethite and iron hydroxides, supported by the visual observation and the calculated Fe/O ratio fall between 1:2 and 1:3.

Eduardo Luis Recalde Chiluiza and Patricio Navarro Donoso (2016) studied the chalcopyrite leaching in acidic chloride solution without sulfates and found that the formation of hydrogen sulfide (H_2S) at room temperature and atmospheric pressure is a possible precursor of passivating species that prevent chalcopyrite dissolution.

2.3.5 The formation of Cu (I) species

M. L. O′Malley and K. C. Liddell (1987) studied chalcopyrite leaching in aqueous $FeCl_3$, HCl and NaCl and found the relationship between copper extraction rate, redox potential and Cu(I) concentration. At the initial stage of leaching (less than 25 hours), the redox potential was high due to high Fe (III) to Fe (II) concentration ratio. The total copper extraction increase steadily, mainly from an increase in Cu (II) concentration and there was essentially no Cu (I) in solution. As the leaching prolonged (after 25 hours), Fe (III) were consumed and Fe (II) was produced, the redox potential decreased. The total copper extraction dramatically increased, simultaneously with a sharp increase in Cu (I) concentration. In the early stage, the solution potential was too high for the reduction of Cu (II) to Cu (I) to take place; whereas at later stage, the solution potential dropped sharply, reaching a value low enough that reduction of Cu (II) become possible. The effects of total chloride ion concentration on Cu (I) concentration during leaching of chalcopyrite was also investigated. At low redox potential (after 25 hours leaching), the Cu (I) concentration increased with increasing chloride ion concentration from 0 to 3 M.

Lin et al (1991), through the E_h—log a_{Cl^-} diagram for the Cu(I)/Cu(II)—CI—H_2O system, confirmed the formation of Cu(I) species at high chloride concentration. At low chloride concentration (a_{Cl-} < 10^{-3}), cupric ions and copper metal were the main copper species. At higher chloride concentration (a_{Cl-} > 10^{-3}), cuprous ion species such as CuCl, $CuCl_2^-$, $CuCl_3^{2-}$, $CuCl_4^{3-}$ were formed as chloro-cuprate (I) ions. With increasing chloride concentration, cuprous species became more stable over a wider potential range.

It is clear that the Cu (I) species are formed and more stable at higher chloride ion concentration and low redox potential. However, the mechanism how Cu (I) affect the solution redox potential, as well as how Cu (I) contribute to the leaching rate of chalcopyrite still remain unclear.

2.3.6 The role of Cu (I) species

Hiroyoshi et al. (2002 – 2007) proposed a reaction model, which suggests that a zone of rapid leaching of chalcopyrite exists between the critical potential (E_c, the equilibrium redox potential for the reduction of $CuFeS_2$ to Cu_2S) and the oxidation potential (E_{ox}, the equilibrium redox potential for the oxidation of Cu_2S), that is $E_{ox} < E < E_c$. Based on this model, Yoo et al. (2010) investigated the effect of chloride ions on the leaching rate of chalcopyrite. From the thermodynamic calculations, the authors found that with an increase in the chloride concentration, the concentration of Cu (I) ions increased; and the contribution of Cu (I) ions to the critical potential, E_c is greater than that of Cu (II) ions. Thus, the formation of Cu (I) ions in a chloride solution increased E_c value, thus expanded the rapid leaching zone, and improve the overall leaching rate. In this work by Yoo et al., there are many parameters were assumed to be constant during thermodynamic calculation, which does not represent an actual leaching system. Therefore, further study is required to clarify the role of Cu (I) ions.

2.4 Redox potential dependence for chalcopyrite leaching

2.4.1 The role of Fe^{2+}

From the generally reported chalcopyrite leaching reaction, Fe^{3+} are oxidant and considered to be effective for leaching chalcopyrite, while Fe^{2+} contributes to leaching only as a source of Fe^{3+}. N. Hiroyoshi et al. (1997) was the earliest author discovered the role of ferrous ions. Under aerobic condition, the amount of copper extracted increased with increasing Fe^{2+} concentration. By addition of Fe^{2+}, the consumption of both proton and dissolved oxygen increased, indicating that ferrous ions enhance the leaching reaction of chalcopyrite with proton and dissolve oxygen:

$$CuFeS_2 + O_2 + 4H+ = Cu^{2+} + Fe^{2+} + 2S^0 + 2H_2O \quad (2\text{-}2)$$

After 7 days leaching in air, the copper extraction with 0.04 M Fe^{2+} was four times higher than copper extraction with 0.20 M Fe^{3+}. In a later paper, N. Hiroyoshi et al., (1998) reported that the copper extraction was 150 g m^{-3} with addition of 0.1 M Fe^{3+} and 1400 g m^{-3} with addition of 0.1 M Fe^{2+}. A similar result was obtained by Third et al (2001), who reported that chalcopyrite leach consistently faster (up to four times) in presence of 0.1 M Fe^{2+} than in presence of 0.1 M Fe^{3+}. These results suggested that Fe^{2+} is a promoter for chalcopyrite leaching. The solution redox potential of chalcopyrite leaching depends on concentration ratio between Fe^{3+} and Fe^{2+} , following Nernst equation (Hiroyoshi et al., 2007, 2004, 2002, 2001; Kametani and Aoki, 1985; Sandstrom et al., 2005; Third et al., 2001). The promotion effect of Fe^{2+} suggested that leaching rate was enhanced at low redox potential.

2.4.2 High leaching rate was obtained at low redox potential

Hiroshi Kametani and Aiko Aoki (1985) did one the earliest study on effect of suspension potential (Pt s SCE) on the oxidation rate of chalcopyrite in a sulfuric acid solution. In this study, $KMnO_4$ was used as oxidant and the chalcopyrite leaching rate was proportional to the rate of $KMnO_4$ consumption. At potential below 0.37 V, the speed of reaction increased with increasing potential. When the potential range 0.40 to 0.43 was reached, the rate become very fast, the oxidation was complete within 2 hours (consumed about 11 g of $KMnO_4$). The rate of oxidation for 0.45 V is greatest, which approaches completion within 100 minutes. Further increase in suspension potential resulted in relative slow increase in rate. At 0.47 V, the oxidation was incomplete even after 40 hours of reaction. At 0.60 V and 0.65 V, the oxidation approached completion after 50 hours (and consumed about 25 g of $KMnO_4$)

In 2000, A. Ahmadi et al. compared different methods to leach high grade chalcopyrite flotation concentrates in a stirred bioreactor. The results showed that the metal recovery increased in this order: chemical leaching < electrochemical leaching < bioleaching < electrochemical bioleaching. The main reason for increasing copper recovery by electrochemical bioleaching is the control of redox potential between 400 and 425 mV vs Ag/AgCl. According to the authors, under this condition, the precipitation of iron oxy-hydroxides on the surface of chalcopyrite, which can act as a diffusion barrier and prevents chalcopyrite dissolution, is significantly reduced. This leads to a higher electrochemical reduction of chalcopyrite and its improved dissolution.

E. M. Cordoba et al. (2008) investigated the effect of initial redox potential on leaching of chalcopyrite with ferric ions at 68 ^{o} C, for 13 days. With $E_{initial} \geq 500$ mV, the copper extraction was less than 30%. With $E_{initial} \leq 400$ mV, more than 80 % Cu extraction was achieved during the first 5 days of leaching; during this time, the redox potential values were lower than 450 mV. For times longer than 5 days, the potential rose to 500 mV, and chalcopyrite dissolution stop.

M. Gericke et al. (2010) did bioleaching experiment of low grade chalcopyrite concentrate at 45 ^{o} C, and reported an optimum “redox window” between 410 and 440 mV vs Ag/AgCl. Within this redox potential window, the copper recovery was higher than 80%. Outside this redox potential window, i.e., at redox potential higher than 450 V, the Cu recovery was less than 45%.

From above published data, it is generally accepted that high chalcopyrite leaching rate can be achieved at low redox potential.

2.4.3 Controlling leaching at low redox potentials yields high copper recovery

Many studies have tried to control the leaching of chalcopyrite at low redox potentials and achieved high copper recovery.

Third et al., (2001) controlled redox potential in bacterial leaching by limitation of supplied oxygen. In the case of continuous aeration, the redox potential increased with time due to the oxidation of ferrous ions. As a result, passivation occurred at the redox potential > 420 mV vs Ag/AgCl. By limiting the supplied oxygen, the redox potential was controlled at 380 mV vs Ag/AgCl and yielded the final copper recovery of 52 – 61 %, which was twice that achieved with continuous supply of oxygen (< 30% extraction).

M. Gericke et al. (2010) did three-stage tank bioleaching of chalcopyrite and controlled the redox potential at each stage. At 70 ^{o} C, the high copper extraction of ≥ 88 % were obtained at all stages despite of the high redox potentials were used (≥ 560 mV vs Ag/AgCl). At 45 ^{o} C, the redox potential showed an effect on the copper extraction. In stage one, when reducing the redox potential from 640 to 420 mV, the soluble copper concentration increased from 7 g/L to 13 g/L, or copper recovery increased from 52 to 87 %. In stage 2, a decline in the redox potential from 570 to 420 mV resulted in an increase the Cu extraction from 91 to 97 %. These results suggested that a low redox potential around 420 mV give much higher leaching rate than high redox potentials.

2.5 References

A. Baba, A., I. Ayinla, K., A. Adekola, F., K. Ghosh, M., S. Ayanda, O., B. Bale, R., R. Sheik, A., R. Pradhan, S., 2012. A Review on Novel Techniques for Chalcopyrite Ore Processing. International Journal of Mining Engineering and Mineral Processing 1, 1–16. https://doi.org/10.5923/j.mining.20120101.01

Dutrizac, J.E., 1981. The dissolution of chalcopyrite in ferric sulfate and ferric chloride media. METALLURGICAL TRANSACTIONS B 8.

Hirato, T., Majima, H., Awakura, Y., 1987. The leaching of chalcopyrite with cupric chloride. Metallurgical Transactions B 18, 31–39. https://doi.org/10.1007/BF02658429

Hiroyoshi, N., Hirota, M., Hirajima, T., Tsunekawa, M., 1997. A case of ferrous sulfate addition enhancing chalcopyrite leaching. Hydrometallurgy 47, 37–45. https://doi.org/10.1016/S0304-386X(97)00032-7

Hiroyoshi, N., Kuroiwa, S., Miki, H., Tsunekawa, M., Hirajima, T., 2004. Synergistic effect of cupric and ferrous ions on active-passive behavior in anodic dissolution of chalcopyrite in sulfuric acid solutions. Hydrometallurgy 74, 103–116. https://doi.org/10.1016/j.hydromet.2004.01.003

Hiroyoshi, N., 英人前田, 一三木, 剛平島, 昌美恒川, 1998. Ferrous Promoted Chalcopyrite Leaching- Ferric formation and its effects on the leaching -. 資源と素材 114, 795–800. https://doi.org/10.2473/shigentosozai.114.795

Kinnunen, P.H.-M., Puhakka, J.A., 2004. Chloride-promoted leaching of chalcopyrite concentrate by biologically-produced ferric sulfate. Journal of Chemical Technology & Biotechnology 79, 830–834. https://doi.org/10.1002/jctb.1051

Lim, Y.H., Kim, S.H., Lee, H.I., Jung, K.B., Yoo, K., 2019. Leaching of Copper from Chalcopyrite Using 50 L Pressure Oxidation Autoclave. ksmer 56, 326–333. https://doi.org/10.32390/ksmer.2019.56.4.326

Lu, Z.Y., Jeffrey, M.I., Lawson, F., 2000. The effect of chloride ions on the dissolution of chalcopyrite in acidic solutions. Hydrometallurgy 56, 189–202. https://doi.org/10.1016/S0304-386X(00)00075-X

Lundström, M., Aromaa, J., Forsén, O., Hyvärinen, O., Barker, M.H., 2005. Leaching of chalcopyrite in cupric chloride solution. Hydrometallurgy 77, 89–95. https://doi.org/10.1016/j.hydromet.2004.10.013

Meng, X., Zhao, H., Sun, M., Zhang, Yisheng, Zhang, Yanjun, Lv, X., Kim, H., Vainshtein, M., Wang, S., Qiu, G., 2019. The role of cupric ions in the oxidative dissolution process of marmatite: A dependence on Cu2+ concentration. Science of The Total Environment 675, 213–223. https://doi.org/10.1016/j.scitotenv.2019.04.227

Nicol, M., Miki, H., Zhang, S., 2017. The anodic behaviour of chalcopyrite in chloride solutions: Voltammetry. Hydrometallurgy 171, 198–205. https://doi.org/10.1016/j.hydromet.2017.05.016

Palmer, B.R., Nebo, C.O., Rau, M.F., Fuerstenau, M.C., 1981. Rate phenomena involved in the dissolution of chalcopyrite in chloride bearing lixiviants. Metallurgical Transactions B 12, 595–601. https://doi.org/10.1007/BF02654332

Park, I., Tabelin, C.B., Jeon, S., Li, X., Seno, K., Ito, M., Hiroyoshi, N., 2019. A review of recent strategies for acid mine drainage prevention and mine tailings recycling. Chemosphere 219, 588–606. https://doi.org/10.1016/j.chemosphere.2018.11.053

Sandstrom, A., Shchukarev, A., Jan, P., 2005. XPS characterisation of chalcopyrite chemically and bio-leached at high and low redox potential. Minerals Engineering 18 (2005) 505–515.

Seng, S., Tabelin, C.B., Kojima, M., Hiroyoshi, N., Ito, M., 2019a. Galvanic Microencapsulation (GME) Using Zero-Valent Aluminum and Zero-Valent Iron to Suppress Pyrite Oxidation. Mater. Trans. 60, 277–286. https://doi.org/10.2320/matertrans.M-M2018851

Seng, S., Tabelin, C.B., Makino, Y., Chea, M., Phengsaart, T., Park, I., Hiroyoshi, N., Ito, M., 2019b. Improvement of flotation and suppression of pyrite oxidation using phosphate-enhanced galvanic microencapsulation (GME) in a ball mill with steel ball media. Minerals Engineering 143, 105931. https://doi.org/10.1016/j.mineng.2019.105931

Skrobian, M., Havlik, T., Ukasik, M., 2005. Effect of NaCl concentration and particle size on chalcopyrite leaching in cupric chloride solution. Hydrometallurgy 77, 109–114. https://doi.org/10.1016/j.hydromet.2004.10.015

Sohn, H.-S., 2019. 동스크랩의 리사이클링. 자원리싸이클링 28, 3–14. https://doi.org/10.7844/KIRR.2019.28.3.3

Tabelin, C.B., Corpuz, R.D., Igarashi, T., Villacorte-Tabelin, M., Ito, M., Hiroyoshi, N., 2019. Hematite-catalysed scorodite formation as a novel arsenic immobilisation strategy under ambient conditions. Chemosphere 233, 946–953. https://doi.org/10.1016/j.chemosphere.2019.06.020

Tabelin, C.B., Igarashi, T., Villacorte-Tabelin, M., Park, I., Opiso, E.M., Ito, M., Hiroyoshi, N., 2018. Arsenic, selenium, boron, lead, cadmium, copper, and zinc in naturally contaminated rocks: A review of their sources, modes of enrichment, mechanisms of release, and mitigation strategies. Science of The Total Environment 645, 1522–1553. https://doi.org/10.1016/j.scitotenv.2018.07.103

Tabelin, C.B., Igarashi, T., Yoneda, T., 2012. Mobilization and speciation of arsenic from hydrothermally altered rock containing calcite and pyrite under anoxic conditions. Applied Geochemistry 27, 2300–2314. https://doi.org/10.1016/j.apgeochem.2012.07.020

Tabelin, C.B., Igarashi, T., Yoneda, T., Tamamura, S., 2013. Utilization of natural and artificial adsorbents in the mitigation of arsenic leached from hydrothermally altered rock. Engineering Geology 156, 58–67. https://doi.org/10.1016/j.enggeo.2013.02.001

Tabelin, C.B., Veerawattananun, S., Ito, M., Hiroyoshi, N., Igarashi, T., 2017. Pyrite oxidation in the presence of hematite and alumina: II. Effects on the cathodic and anodic half-cell reactions. Science of The Total Environment 581–582, 126–135. https://doi.org/10.1016/j.scitotenv.2016.12.050

Tomiyama, S., Igarashi, T., Tabelin, C.B., Tangviroon, P., Ii, H., 2019. Acid mine drainage sources and hydrogeochemistry at the Yatani mine, Yamagata, Japan: A geochemical and isotopic study. Journal of Contaminant Hydrology 225, 103502. https://doi.org/10.1016/j.jconhyd.2019.103502

Watling, H.R., 2013. Chalcopyrite hydrometallurgy at atmospheric pressure: 1. Review of acidic sulfate, sulfate–chloride and sulfate–nitrate process options. Hydrometallurgy 140, 163–180. https://doi.org/10.1016/j.hydromet.2013.09.013

Williamson, M.A., Rimstidt, J.D., 1994. The kinetics and electrochemical rate-determining step of aqueous pyrite oxidation. Geochimica et Cosmochimica Acta 58, 5443–5454. https://doi.org/10.1016/0016-7037(94)90241-0

Yoo, K., Kim, S., Lee, J., Ito, M., Tsunekawa, M., Hiroyoshi, N., 2010. Effect of chloride ions on leaching rate of chalcopyrite - ScienceDirect. Minerals Engineering 23 (2010) 471–477. https://doi.org/doi:10.1016/j.mineng.2009.11.007

Yoo, K., Lee, J., Hiroyoshi, N., Alorro, R., Tsunekawa, M., 2007. The Effect of Redox Potential on the Leaching of Chalcopyrite in Chloride Media, in: Proceedings of the

Sixth International Copper-Cobre Conference, Vol. IV: The John E. Dutrizac International Symposium on Copper Hydrometallurgy. Presented at the Sixth International Copper-Cobre Conference, The John E. Dutrizac International Symposium on Copper Hydrometallurgy, Canadian Institute of Mining, Metallurgy and Petroleum, pp. 259–267.

CHAPTER 3: EFFECTS OF TEMPERATURE AND SOLUTION COMPOSITION ON THE REDOX POTENTIAL DEPENCE OF CHALCOPYRITE DISSOLUTION

3.1 Introduction

In acid solutions containing ferric ions, chalcopyrite is dissolved according to

$$CuFeS_2 + 4\ Fe^{3+} = Cu^{2+} + 5\ Fe^{2+} + 2\ S^o \quad (3\text{-}1)$$

Previous studies have shown that the leaching rate of chalcopyrite in acid solutions strongly depended on the redox potential of the system (Velásquez-Yévenes et al., 2010; Yévenes et al., 2010; Nicol et al., 2010), determined by the concentration ratio of Fe^{3+} to Fe^{2+} (Hiroyoshi et al., 2007, 2004, 2002, 2001; Kametani and Aoki, 1985; Sandstrom et al., 2005; Third et al., 2001). It is also well-known that the rate of chalcopyrite dissolution in sulfate media depended on the redox potential; that is, the highest leaching rate is obtained at a specific value of redox potential, which has been termed as a peak or an optimum redox potential (Hiroyoshi et al., 2008; Zhao et al., 2015). Kametani and Aoki (1985) conducted one of the earliest studies to elucidate the redox potential-dependent leaching behavior of chalcopyrite and reported the fastest leaching rate at 0.470V V (vs. Ag/AgCl). Similarly, Pinches et al. (2001) suggested a value of peak redox potential around 0.470V V (vs. Ag/AgCl) in the absence of bacteria, and a significantly higher value in their presence (0.575V–0.625V V vs. Ag/AgCl for *Leptospirillum* and 0.425V–0.475 mV vs. Ag/AgCl for *Acidithiobacillus ferrooxidans*). Ahmadi et al. (2010) used the electro-chemical bioleaching method and found the peak redox potential at around recommended a range of 0.400–0.425 V vs. Ag/AgCl. Third et al., (2001) found that high copper recovery can be obtained at a constant redox potential of 0.380 V vs. Ag/AgCl, and redox potential higher than 0.420 V vs. Ag/AgCl would inhibit chalcopyrite dissolution. Although different values of the peak redox potential have been reported, which is most probably due to differences in experimental conditions, the general agreement is that the leaching rate is higher at lower redox potentials.

To explain the why faster chalcopyrite leaching rates are achieved at low redox potentials, Hiroyoshi et al., (1997 – 2008) proposed a reaction model assuming the formation of Cu_2S as an intermediate phase. At lower redox potentials, chalcopyrite is reduced by Fe^{2+} in the presence of cupric ions to form Cu_2S (Eq. 3-2). The Cu_2S-intermediate phase is then oxidized by Fe^{3+} (Eq. 3-3) and/or dissolved oxygen (Eq. 3-4) to release Cu^{2+}. The overall reaction is same as generally reported reaction (Eq. 3-1).

$$CuFeS_2 + 3\ Cu^{2+} + 3\ Fe^{2+} = 2\ Cu_2S + 4\ Fe^{3+} \quad (3\text{-}2)$$

$$Cu_2S + 4\ Fe^{3+} = 2\ Cu^{2+} + S + 4\ Fe^{2+} \quad (3\text{-}3)$$

$$Cu_2S + 4\ H^{+} + O_2 = 2\ Cu^{2+} + S + 2\ H_2O \quad (3\text{-}4)$$

The oxidation rate of this Cu_2S-intermediate phase is higher than that of chalcopyrite, which causes rapid copper extraction at low redox potentials. Based on this model, Hiroyoshi et al. (2008) conducted an electrochemical study to investigate the effects of various parameters on the optimum redox potential (E_{op}) and provided an empirical equation to predict the E_{op} for chalcopyrite leaching in sulfate media as a function of Cu^{2+} and Fe^{2+} concentrations as follows:

$$E_{op} = 0.691 + 0.030 \log [Cu^{2+}] + 0.013 \log [Fe^{2+}] \quad (3\text{-}5)$$

More recently, Yoo et al., (2010, 2007) reported that the redox potential dependence of chalcopyrite leaching rate in HCl solutions was not only very similar to that observed in H_2SO_4 solutions but also exhibited the peak redox potential. One interesting difference in these two acidic media was that the maximum rate (i.e., peak rate) was higher in HCl than in H_2SO_4. These results suggest that the redox potential-controlled leaching of chalcopyrite in HCl solutions is potentially attractive for extracting copper from low-grade copper sulfide ores and 'dirty' concentrates. To develop the redox-controlled leaching system, it is crucial to know the value of the peak redox potential under a given condition. Unfortunately, very few studies have been done to investigate the redox potential dependence of chalcopyrite leaching in HCl solutions, and the factors affecting the peak redox potential in HCl media are still not well understood.

This chapter investigated the effects of temperature and solution composition on the redox potential-dependent chalcopyrite leaching in acidic ferric chloride solutions using a specially designed leaching experimental setup. Based on the results, the effects of temperature and solution composition on the peak redox potential (E_p) and peak leaching rate (R_p) were discussed and an empirical equation to predict the value of E_p as a function of Cu^{2+} concentration is proposed.

3.2 Materials and methods

3.2.1 Materials

A chalcopyrite specimen obtained from Copper Queen Mine, Arizona, USA was used. The specimen was dry-ground with a vibratory disc mill (RS 100, Retsch Inc., Germany) and dry-

sieved to obtain a –53+38 μm fraction. To remove the oxidized layer and fine particles on the surface of chalcopyrite, the ground sample was washed using a modified washing based on the technique developed by McKibben and Barnes (1986). This involves ultrasonic cleaning in ethanol, washing in 0.1 M HNO_3, multiple rinsing in deionized water, and dewatering in a vacuum desiccator (Park et al., 2020, 2018; Tabelin et al., 2017d) . The XRF results showed that the sample is mainly composed of Cu (30 wt%), Fe (34 wt%) and S (22 wt%), including Si (8.2 wt%), Ca (3.7 wt%), Zn (0.8 wt%) in minor to moderate amounts. The XRD pattern confirmed that the sample is mainly composed of chalcopyrite with minor amounts of quartz, sphalerite and montmorillonite.

3.2.2 Methods

The leaching experiment setup was shown in Fig. 3-1. First, 3 g of chalcopyrite sample and 12 ml of a solution containing a predetermined concentration of HCl was added to the reactor, and the suspension was agitated by magnetic stirring (2.3 × 0.5 φ cm stirring bar and a stirring speed of 400 rpm). The ORP electrode, which is a combination Pt electrode with KCl-saturated Ag/AgCl reference electrode, was inserted into the solution. This ORP electrode was then connected to a potentiometer and a data logger to measure and record the values of redox potential continuously. The reactor was sealed by a silicon rubber with a gas inlet/outlet tube. Ultrapure nitrogen gas (99.999%) was then introduced simultaneously to the solution to remove dissolved oxygen while the reactor was heated to the desired temperature, using a double-jacketed glass reactor connected to a thermostat recirculating water bath. After 1 hour and confirming that the redox potential remains constant, 3 ml of a solution containing predetermined concentrations of HCl, $FeCl_3$, and $CuCl_2$ were added to start the reaction. The amount of extracted copper was calculated from the measured redox potential as detailed later. After finishing the experiments, the leachate was collected by filtering the suspension through a 0.2 μm syringe-driven membrane filter (LMS Co. Ltd., Japan), and the filtrates containing dissolved Cu and Fe were analyzed by inductively coupled plasma atomic emission spectroscopy (ICP-AES) (ICPE-9820, Shimadzu Corporation, Japan).

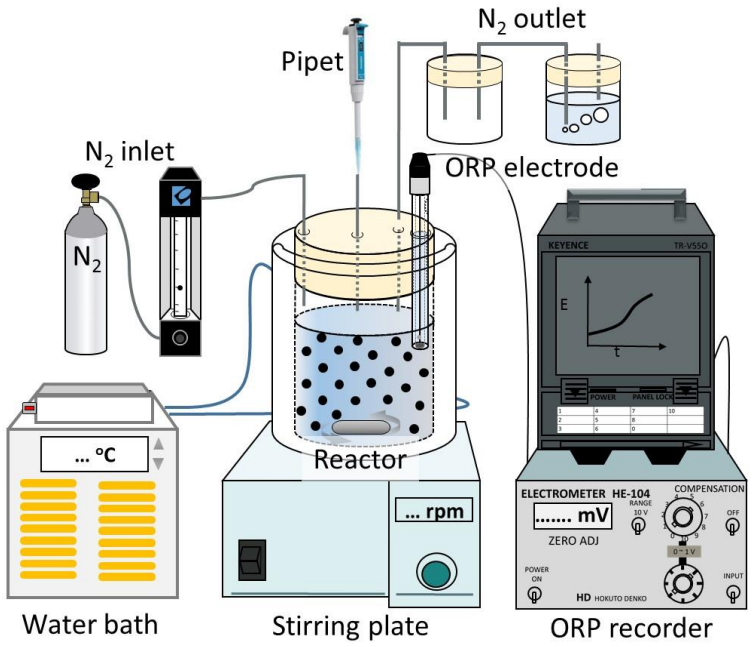


Fig. 3-1. A schematic diagram of the leaching experimental set up.

3.3 Results and discussions

3.3.1 An example of the results and calculation method

The overall reaction of chalcopyrite leaching in acidic ferric chloride solution is described in Eq. 3-1. The redox potential of leaching solution, E (V vs. Ag/AgCl), is expressed by the Nernst equation for Fe^{3+}/Fe^{2+} redox pair (Eq. 3-6).

$$E = E^{0\prime} + \frac{RT}{F} ln \frac{[Fe^{3+}]}{[Fe^{2+}]} \quad (3\text{-}6)$$

Where R is the gas constant (8.3145 J K^{-1} mol^{-1}), T is the absolute temperature (K), F is the Faraday constant (96485 C mol^{-1}), $[Fe^{3+}]$ is the Fe^{3+} concentration in molarity, $[Fe^{2+}]$ is the Fe^{2+} concentration in molarity, and $E^{0\prime}$ is the formal redox potential for Fe^{3+}/Fe^{2+} redox pair (V). In acidic chloride solutions, not only Fe^{3+}/Fe^{2+} redox couple but other redox couples like Cu^{2+}/Cu^{+} is also present, but the effects of Cu^{2+}/Cu^{+} can be neglected in our experimental system and the calculation method because of the following reason: these redox couples present in the aqueous phase and this allows rapid electron exchange between them. In this case, the following reaction (Eq. 3-7) is in equilibrium (Miki and Nicol, 2008, 2011), and values of redox potentials for Fe^{3+}/Fe^{2+} pair and Cu^{2+}/Cu^{+} pair are the same as described in Eq. 3-8. Because of this, regardless the presence of Cu^{2+}/Cu^{+} redox pair, the concentration ratio of Fe^{3+} to Fe^{2+} can be determined from the measured values of redox potential, E, and the amount of Fe^{3+} consumption, needed for calculating copper extraction from chalcopyrite, can be evaluated from the change in

the E value.

$$Cu^{+} + Fe^{3+} = Cu^{2+} + Fe^{2+} \quad (3\text{-}7)$$

$$E = E_{Fe}^{0\prime} + \frac{RT}{F} ln \frac{[Fe^{3+}]}{[Fe^{2+}]} = E_{Cu}^{0\prime} + \frac{RT}{F} ln \frac{[Cu^{2+}]}{[Cu^{+}]} \quad (3\text{-}8)$$

During the leaching experiments, Fe^{3+} are consumed while Fe^{2+} are formed according to Eq. 3-1, resulting in a decrease in the redox potential. Copper extraction amount and rate can be calculated from the measured redox potential. The detail calculation method is explained below, using a representative experimental result.

Calculations used the values of the formal electrode potential ($E^{0'}$) determined by measuring the redox potential of a standard solution (0.1 M HCl with 0.01 M Fe^{3+}, Fe^{2+} and Cu^{2+}) at different temperature (0.586 V, 0.546 V, and 0.531V at 343 K, 313 K, 298 K, respectively). The $E^{0'}$ values depend on solution composition and shift from that of standard solution, but the shift was within 0.01V under the experimental condition used in this study, and its effect can be negligible in the calculation results such as the relation between copper extraction rate and redox potential, appeared later.

Fig. 3-2 A shows the changes in redox potential in the leaching experiments done at 343 K in 0.1 kmol m^{-3} HCl solution with initial Fe^{3+} concentration, $[Fe^{3+}]_0$, of 0.01 kmol m^{-3} and initial Cu^{2+} concentration, $[Cu^{2+}]_0$, of 0.01 kmol m^{-3}. Assuming the reaction in Eq. 3-1, when x kmol m^{-3} of Cu^{2+} is extracted, 4 x kmol m^{-3} of Fe^{3+} are consumed and 5 x kmol m^{-3} of Fe^{2+} are formed and the redox potential is given by

$$E = E^{0\prime} + \frac{\mathrm{RT}}{\mathrm{F}} \ln \frac{[\mathrm{Fe}^{3+}]_0 - 4x}{[\mathrm{Fe}^{2+}]_0 + 5x} \quad (3\text{-}9)$$

The above equation can be rearranged to

$$x = \frac{[\mathrm{Fe}^{3+}]_0 - [\mathrm{Fe}^{2+}]_0 \exp\frac{(E - E^{0\prime})\mathrm{F}}{\mathrm{RT}}}{4 + 5 \exp\frac{(E - E^{0\prime})\mathrm{F}}{\mathrm{RT}}} \quad (3\text{-}10)$$

Using this equation, the amount of copper extraction, x, can be calculated from the value of measured redox potential, E. The value of $[\mathrm{Fe}^{3+}]_0$ is decided from the amount of $FeCl_3$ added in the experiments, and $[\mathrm{Fe}^{2+}]_0$ is calculated by substituting the measured value of redox potential at time 0 (when Fe^{3+} and Cu^{2+} solution was added) to E in the Nernst equation (Eq. 3-9) assuming x = 0. Fig. 3-2 B shows the copper extraction, x, calculated from the data set of redox potential, E, shown in Fig.3-2 A.

The rate of copper extracted from chalcopyrite (r, kmol s^{-1} g^{-1}) was calculated from the increments of copper extraction (Δx) and time (Δt) using

$$r = \frac{\Delta X}{\Delta t} \frac{V_s}{M} \quad (3\text{-}11)$$

Where, V_s is solution volume ($15 \times 10^{-6}\ m^3$) and M is the weight of the chalcopyrite sample

added (3 g). Fig. 3-2 C shows the copper extraction rate, *r*, calculated from the data set shown in Fig. 3-2 B.

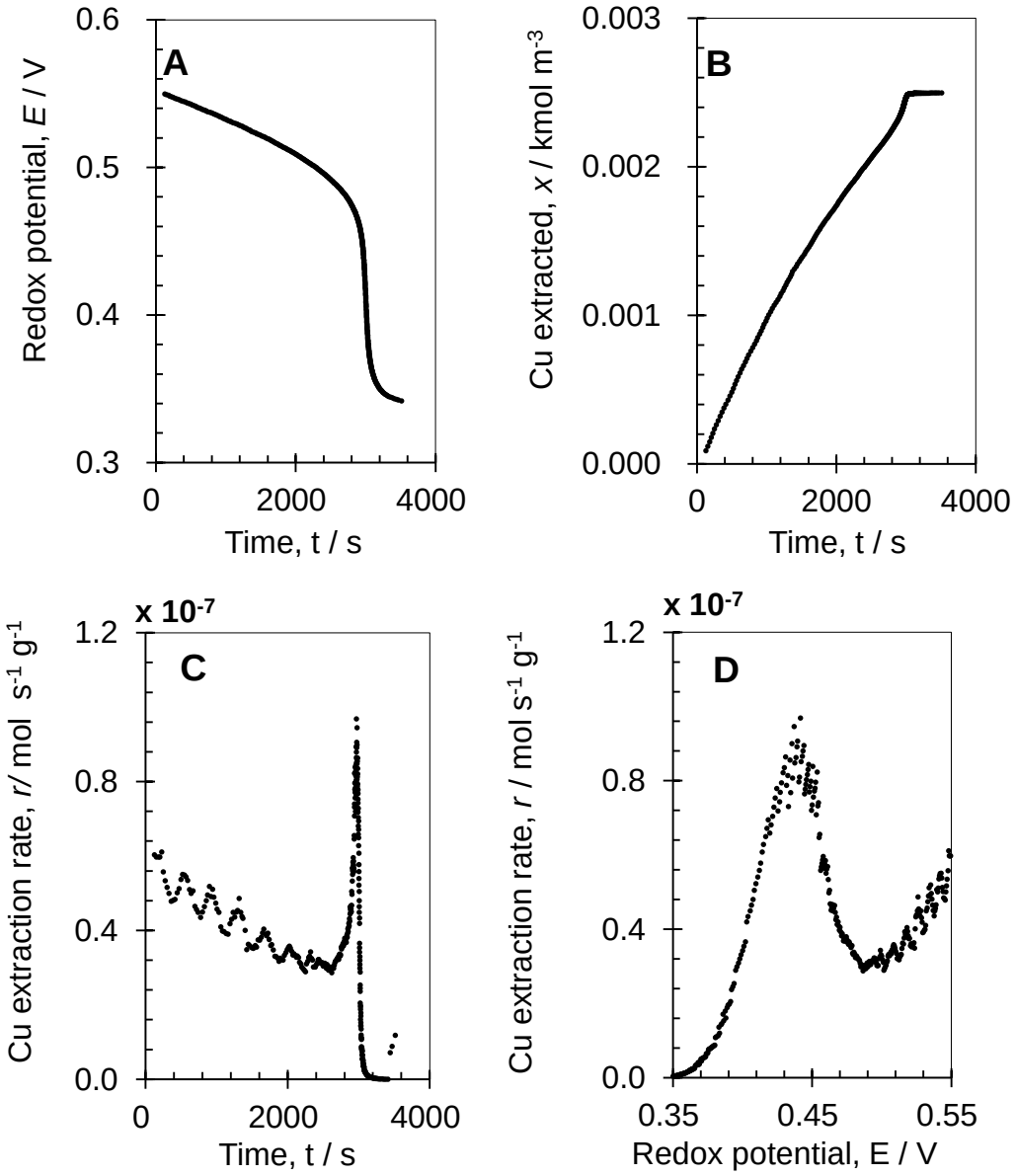


Fig. 3-2. An example of experimental data and calculated results: A redox potential vs. leaching time, B copper extracted amount vs. leaching time, C copper extraction rate vs. leaching time, and D copper extraction rate vs. redox potential. (Conditions: temperature of 343 K, initial Fe^{3+} concentration of 0.01 kmol m^{-3}, initial Cu^{2+} concentration of 0.01 kmol m^{-3}, solid-to-liquid ratio of 0.3 g $CuFeS_2$/15 ml, and agitation speed of 400 rpm).

By combining the measured redox potential, *E*, shown in Fig. 3-2 A and copper extraction rate, r, shown in Fig. 3-2 C, the relationship between the copper extraction rate and the redox potential

can be plotted as shown in Fig. 3-2 D. In this figure, the peak behavior of chalcopyrite leaching was observed. At low redox potentials, the leaching rate increased with increasing redox potential and reached a peak (i.e., peak rate) while at higher redox potentials, the leaching rate decreased with increasing redox potential. The peak rate, r_p, was observed at around 0.442 V (vs. Ag/AgCl) and the redox potential value that gives the peak rate is defined as peak redox potential, E_p, in this paper.

3.3.2 Effects of temperature

To examine the effects of temperature on the redox potential dependence of chalcopyrite leaching, experiments were carried out at various temperatures (298, 313, and 343K). The concentration of HCl was 0.1 kmol m^{-3}, and initial concentrations of both ferric and cupric ions were 0.01 kmol m^{-3}.

Fig. 3-3 A shows the relationship between the copper extraction rate and redox potential at different temperatures. At all temperatures evaluated, a peak redox potential was observed in the copper extraction rate vs. redox potential plots and the peak rate increased with increasing temperature. As illustrated in Fig. 3-3 B, the temperature dependence of the peak rate could be expressed using the Arrhenius-type equation (Eq. 3-12). From Fig. 3-3 B, the value of E_a is estimated at ~85 kJ/mol.

$$r_p = A \exp\left(-\frac{E_a}{RT}\right) \tag{3-12}$$

Where A is a constant, and E_a is the activation energy.

Fig. 3-3 C shows the relationship between peak redox potential, E_p and temperature. The values of E_p were almost the same at different temperatures, indicating that E_p is independent of the leaching temperature.

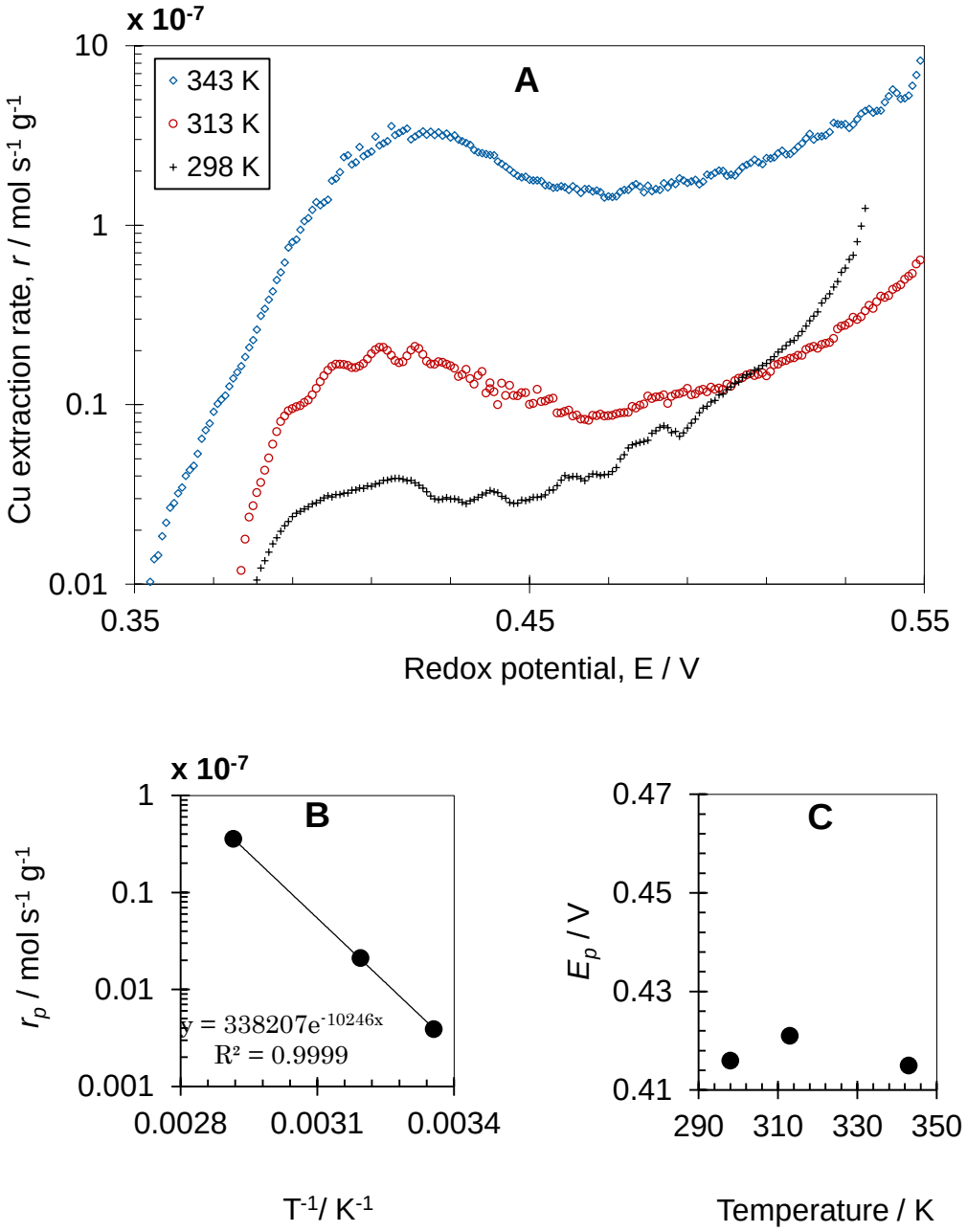
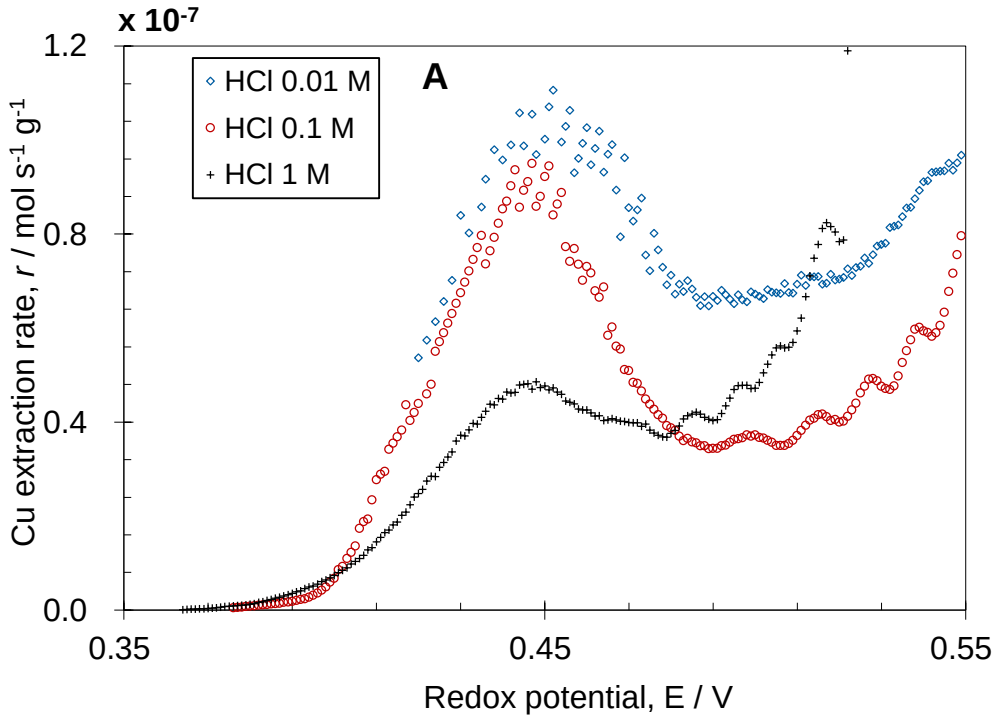


Fig. 3-3. Effects of temperature on the redox potential dependence of chalcopyrite leaching: A copper extraction rate as function of redox potential, B the peak rate as a function of leaching temperature, and C the peak redox potential as a function of leaching temperature. (Conditions: HCl concentration of 0.1 kmol m^{-3}, initial Fe^{3+} concentration of 0.01 kmol m^{-3}, initial Cu^{2+} concentration of 0.01 kmol m^{-3}, solid-to-liquid ratio of 0.3 g $CuFeS_2$/15 ml, and agitation speed of 400 rpm).

3.3.3 Effects of HCl concentration

To examine the effects of HCl concentration on the redox potential dependence of chalcopyrite leaching, experiments were carried out with various HCl concentrations at 343 K. The initial concentrations of ferric and cupric ions were 0.01 kmol m^{-3}.

Fig. 3-4 A shows the copper extraction rate vs. redox potential plot obtained at different HCl concentrations. The results showed that there is a significant effect of HCl concentration on the leaching rate. As shown in Fig. 3-4 B, the peak rate decreased with increasing HCl concentration. Fig. 3-4 C showed the relationship between peak redox potential, E_p and HCl concentration. The results showed that E_p did not change significantly when HCl concentration varied, indicating that the value of E_p is not affected by HCl concentration.



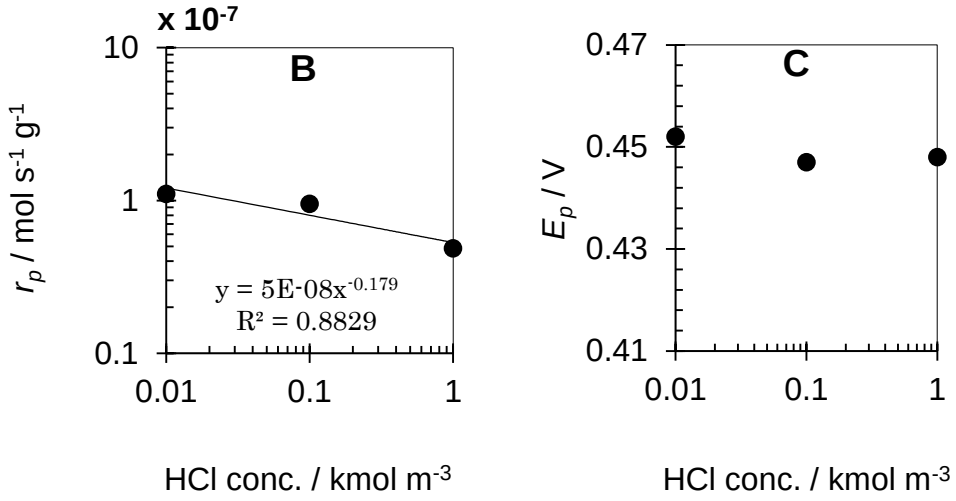


Fig. 3-4. Effects of HCl concentration on the redox potential dependence of chalcopyrite leaching: A copper extraction rate as function of redox potential, B the peak rate as functions of HCl concentration, and C the peak redox potential as functions of HCl concentration. (Conditions: temperature of 343 K, initial Fe^{3+} concentration of 0.01 kmol m^{-3}, initial Cu^{2+} concentration of 0.01 kmol m^{-3}, solid-to-liquid ratio of 0.3 g $CuFeS_2$/15 ml, and agitation speed of 400 rpm).

3.3.4 Effects of ferric ion concentration

The effects of Fe^{3+} concentration on the redox potential dependence of chalcopyrite leaching were investigated by varying the initial concentrations of Fe^{3+} at 343K. The concentration of HCl was 0.1 kmol m^{-3} and the initial concentration of Cu^{2+} was 0.01 kmol m^{-3}.

Fig. 3-5 A shows the copper extraction rate vs. redox potential plot obtained with different initial Fe^{3+} concentrations. The leaching rate increased with decreasing initial Fe^{3+} concentration.

Fig. 3-5 C shows the relationship between the peak redox potential, E_p, and initial Fe^{3+} concentration. The results showed that the E_p did not change significantly when the initial Fe^{3+} concentration was varied. During the experiments, Fe^{3+} was reduced to Fe^{2+} according to Eq. 3-1. Considering this, the results in Fig. 3-5 C indicates that the peak redox potential is independent of both Fe^{3+} and Fe^{2+} concentrations.

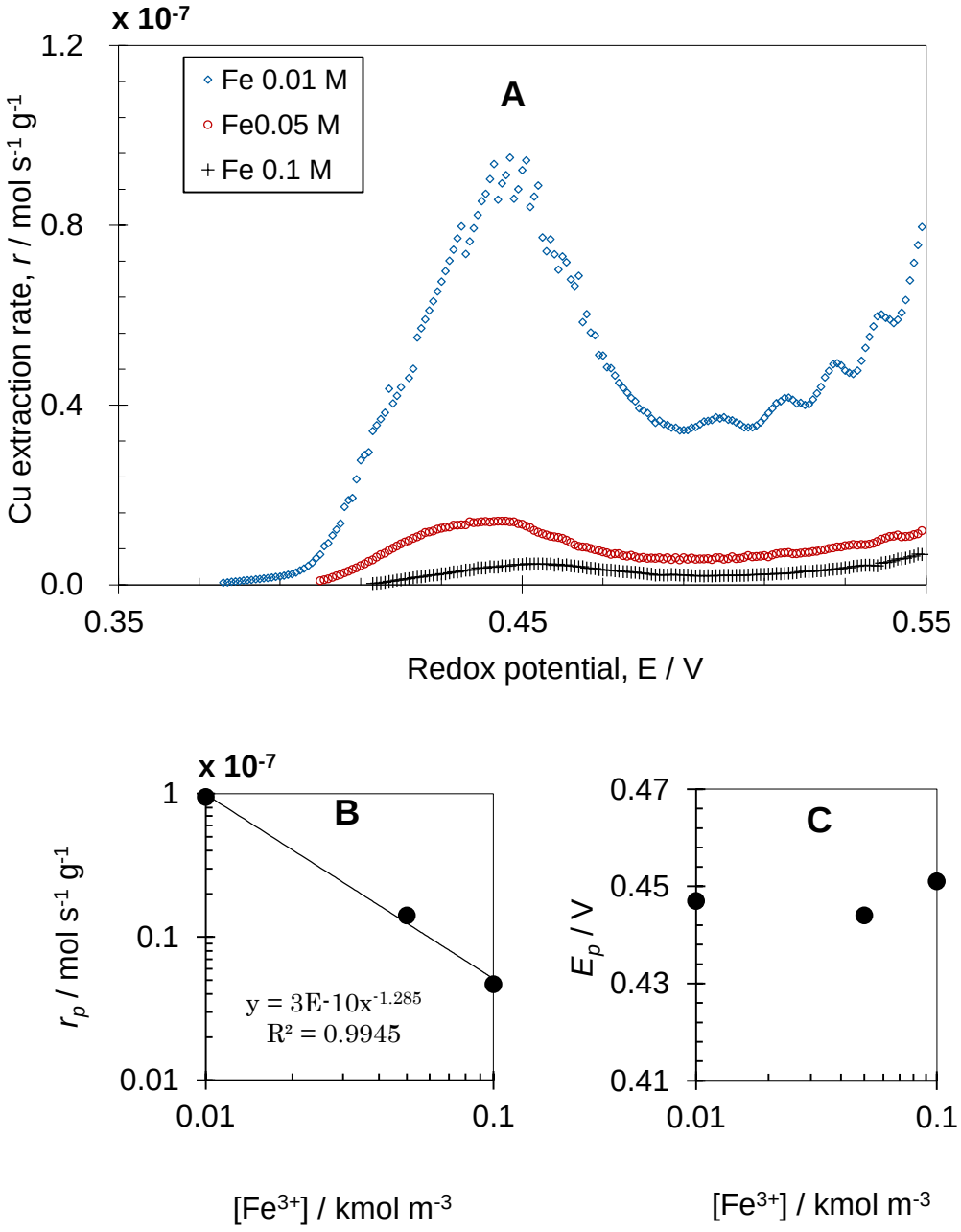


Fig. 3-5. Effects of ferric ion concentration on the redox potential dependence of chalcopyrite leaching: **A** copper extraction rate as a function of redox potential, **B** the peak rate as functions of Fe^{3+} concentration, and **C** the peak redox potential as functions of Fe^{3+} concentration. (Conditions: temperature of 343 K, HCl concentration of 0.1 kmol m^{-3}, initial Cu^{2+} concentration of 0.01 kmol m^{-3}, a solid-to-liquid ratio of 0.3g $CuFeS_2$/15 ml, and agitation speed of 400 rpm).

3.3.5 Effects of cupric ion concentration

To examine the effects of Cu^{2+} concentration on the redox potential dependence of chalcopyrite leaching, experiments were carried out by varying the initial concentrations of Cu^{2+} at 343K. The concentration of HCl was 0.1 kmol m^{-3} and the initial concentration of Fe^{3+} was 0.01 kmol m^{-3}. Fig. 3-6 shows the effects of Cu^{2+} concentration on the redox potential dependence of chalcopyrite leaching. On the copper extraction rate vs. redox potential plot (Fig. 3-6 A), a shift of peak position was observed when Cu^{2+} concentration was varied. Moreover, the peak copper extraction rates were almost constant with different Cu^{2+} concentration (Fig. 3-6 B) while the peak redox potential increased with increasing Cu^{2+} concentration (Fig. 3-6 C). The slope of the trend line in E_p vs. Cu^{2+} concentration plot (Fig. 3-6 C) is 0.012 V/ decade. During the experiments, Cu^{2+} concentration increased with time due to the extraction of copper from chalcopyrite. Because of this, when the redox potential reached E_p, the concentration of Cu^{2+} in the solution was different from the initial concentration. To account for this difference, Cu^{2+} concentration was calculated by summing up the initial dosage and extracted amounts of Cu^{2+}. Considering this, the values of E_p are plotted against the Cu^{2+} concentration when redox potential reached E_p (Fig. 3-7). In this figure, the plot can be fitted with a straight line with a slope of 0.015 V/decade.

As described above, the peak redox potential is independent of temperature as well as the concentrations of HCl, Fe^{3+}, and Fe^{2+}. The only factor that influenced the peak redox potential was Cu^{2+} concentration. From the results shown in Fig. 3-7, the value of peak redox potential for chalcopyrite leaching in acidic ferric chloride solutions can be expressed as a function of Cu^{2+} concentration (Eq. 3-13).

$$E_p = 0.470 + 0.015\,\mathrm{Log}[Cu^{2+}] \quad (3\text{-}13)$$

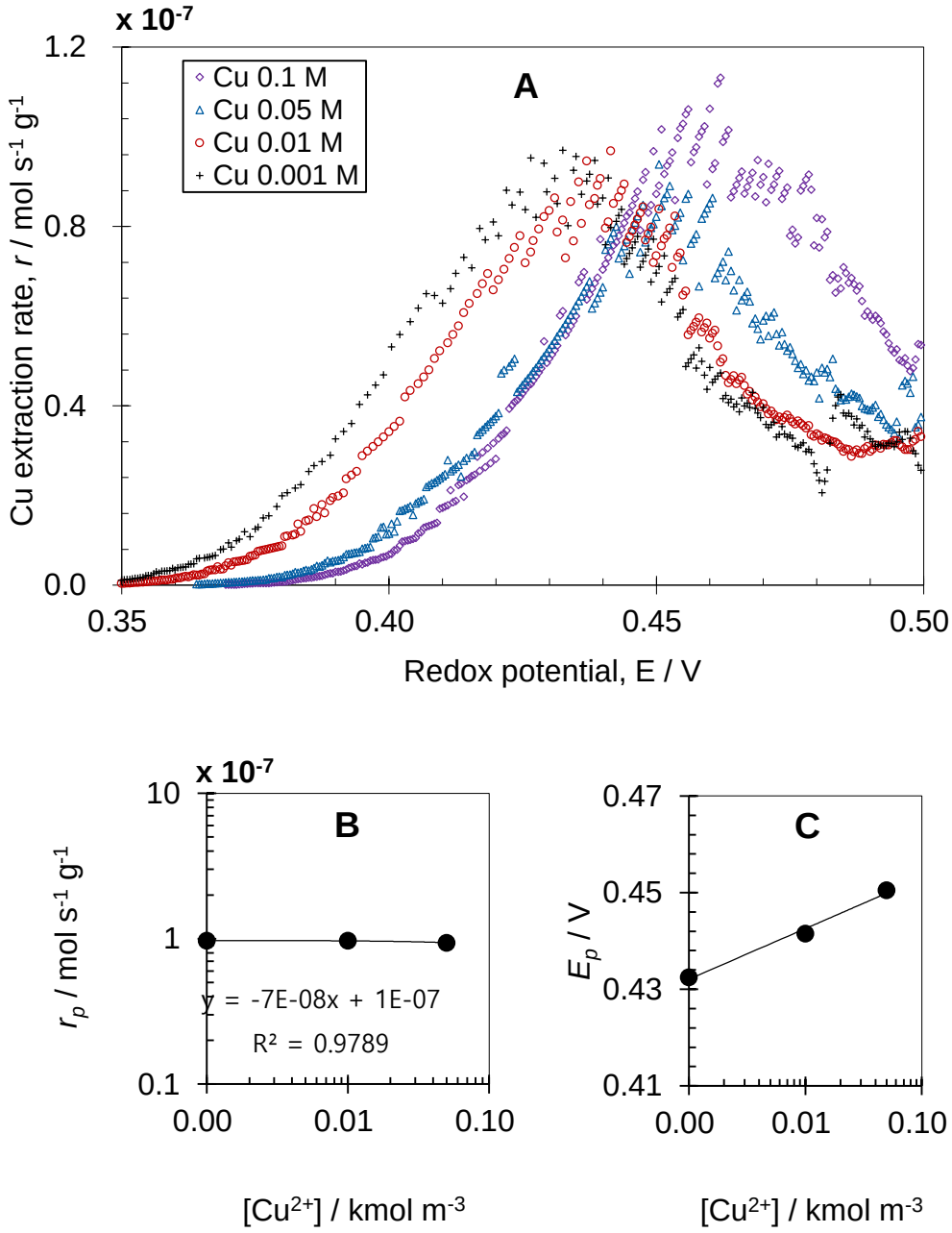


Fig. 3-6. Effects of cupric ion concentration on the redox potential dependence of chalcopyrite leaching: **A** copper extraction rate as a function of redox potential, **B** the peak rate as functions of Cu^{2+} concentration, and **C** the peak redox potential as functions of Cu^{2+} concentration. (Conditions: temperature of 343 K, HCl concentration of 0.1 kmol m^{-3}, initial Fe^{3+} concentration of 0.01 kmol m^{-3}, a solid-to-liquid ratio of 0.3 g $CuFeS_2$/15 ml, and agitation speed of 400 rpm).

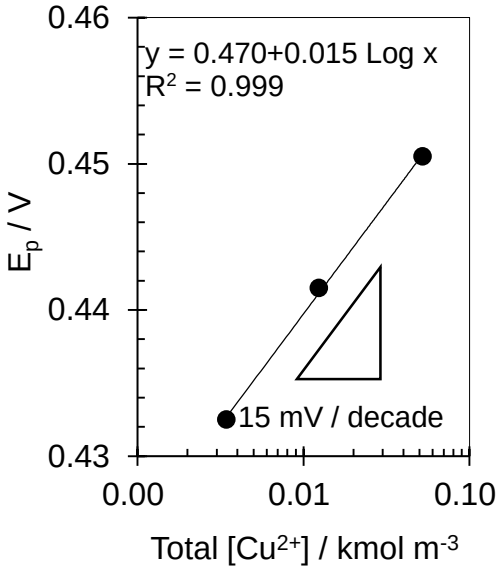


Fig. 3-7. Relationship between total Cu^{2+} concentration and peak redox potential (E_p) (Conditions: temperature of 343K, HCl concentration of 0.1 kmol m^{-3}, initial Fe^{3+} concentration of 0.01 kmol m^{-3}, a solid-to-liquid ratio of 0.3 g $CuFeS_2$/15 ml, and agitation speed of 400 rpm).

3.4 Summary

The redox potential dependence of chalcopyrite leaching in acidic ferric chloride solutions was investigated using a specially designed batch leaching setup under different temperatures with varying concentrations of Fe^{3+}, Cu^{2+}, and HCl. From the redox potential data recorded as a function of time, the amount of extracted copper was calculated, and copper extraction rate vs. redox potential curve was plotted.

In the copper extraction rate vs. redox potential curve, a peak behavior was observed; that is, the copper extraction rate increased with increasing redox potential, reaching a maximum value (peak rate) at a certain redox potential (peak redox potential). After this peak, the rate decreased with increasing redox potential. The peak rate (r_p) increased with increasing temperature; however, it decreased with increasing HCl and Fe^{3+} concentrations. Meanwhile, r_p was not significantly affected by Cu^{2+} concentration. The peak redox potential (E_p) was less dependent on temperature and the concentrations of HCl, Fe^{3+} and Fe^{2+}. A major factor affecting E_p was Cu^{2+} concentration; that is, E_p increased with increasing Cu^{2+} concentration, as shown in the following empirical equation:

$$E_p = 0.470 + 0.015\,\mathrm{Log}[Cu^{2+}]$$

3.5 References

Ahmadi, A., Schaffie, M., Manafi, Z., Ranjbar, M., 2010. Electrochemical bioleaching of high-grade chalcopyrite flotation concentrates in a stirred bioreactor. Hydrometallurgy 104, 99–105. https://doi.org/10.1016/j.hydromet.2010.05.001

Hiroyoshi, N., Arai, M., Miki, H., Tsunekawa, M., Hirajima, T., 2002. A new reaction model for the catalytic effect of silver ions on chalcopyrite leaching in sulfuric acid solutions. Hydrometallurgy 63, 257–267. https://doi.org/10.1016/S0304-386X(01)00228-6

Hiroyoshi, N., Kitagawa, H., Tsunekawa, M., 2008. Effect of solution composition on the optimum redox potential for chalcopyrite leaching in sulfuric acid solutions. Hydrometallurgy Volume 91, Issues 1–4, March 2008, Pages 144-149.

Hiroyoshi, N., Kuroiwa, S., Miki, H., Tsunekawa, M., Hirajima, T., 2007. Effects of coexisting metal ions on the redox potential dependence of chalcopyrite leaching in sulfuric acid solutions. Hydrometallurgy 87, 1–10. https://doi.org/10.1016/j.hydromet.2006.07.006

Hiroyoshi, N., Kuroiwa, S., Miki, H., Tsunekawa, M., Hirajima, T., 2004. Synergistic effect of cupric and ferrous ions on active-passive behavior in anodic dissolution of chalcopyrite in sulfuric acid solutions. Hydrometallurgy 74, 103–116. https://doi.org/10.1016/j.hydromet.2004.01.003

Hiroyoshi, N., Miki, H., Hirajima, T., Tsunekawa, M., 2001. Enhancement of chalcopyrite leaching by ferrous ions in acidic ferric sulfate solutions. Hydrometallurgy 60, 185–197. https://doi.org/10.1016/S0304-386X(00)00155-9

Hiroyoshi, N., Miki, H., Hirajima, T., Tsunekawa, M., 2000. A model for ferrous-promoted chalcopyrite leaching Hydrometallurgy 57 (2000) 31–38.

Hiroyoshi, N., 英人前田, 一三木, 剛平島, 昌美恒川, 1998. Ferrous Promoted Chalcopyrite Leaching- Ferric formation and its effects on the leaching -. 資源と素材 114, 795–800. https://doi.org/10.2473/shigentosozai.114.795

Kametani, H., Aoki, A., 1985. Effect of suspension potential on the oxidation rate of copper concentrate in a sulfuric acid solution. MTB 16, 695–705. https://doi.org/10.1007/BF02667506

Nicol, M., Miki, H., Velásquez-Yévenes, L., 2010. The dissolution of chalcopyrite in chloride solutions: Part 3. Mechanisms. Hydrometallurgy 103, 86–95. https://doi.org/10.1016/j.hydromet.2010.03.003

Sandstrom, A., Shchukarev, A., Jan, P., 2005. XPS characterisation of chalcopyrite chemically and bio-leached at high and low redox potential. Minerals Engineering 18 (2005) 505–515.

Third, K.A., Cord-Ruwisch, R., Watling, H.R., 2001. Control of the redox potential by oxygen limitation improves bacterial leaching of chalcopyrite.

Velásquez-Yévenes, L., Nicol, M., Miki, H., 2010. The dissolution of chalcopyrite in chloride solutions: Part 1. The effect of solution potential. Hydrometallurgy 103, 108–113. https://doi.org/10.1016/j.hydromet.2010.03.001

Yoo, K., Lee, J., Hiroyoshi, N., Alorro, R., Tsunekawa, M., 2007. The Effect of Redox Potential on the Leaching of Chalcopyrite in Chloride Media, in: Proceedings of the Sixth International Copper-Cobre Conference, Vol. IV: The John E. Dutrizac International Symposium on Copper Hydrometallurgy. Presented at the Sixth International Copper-Cobre Conference, The John E. Dutrizac International Symposium on Copper Hydrometallurgy, Canadian Institute of Mining, Metallurgy and Petroleum, pp. 259–267.

Zhao, H., Wang, J., Yang, C., Hu, M., Gan, X., Tao, L., Qin, W., Qiu, G., 2015. Effect of redox potential on bioleaching of chalcopyrite by moderately thermophilic bacteria: An emphasis on solution compositions. Hydrometallurgy 151, 141–150. https://doi.org/10.1016/j.hydromet.2014.11.009

CHAPTER 4: EFFECTS OF SOLUTION COMPOSITION ON THE ANODIC DISSOLUTION OF CHALCOPYRITE ELECTRODE

4.1 Introduction

In acid solutions containing ferric ions, chalcopyrite is dissolved according to

$$CuFeS_2 + 4\ Fe^{3+} = Cu^{2+} + 5\ Fe^{2+} + 2\ S^o \quad (4\text{-}1)$$

In chapter 3, the effects of solution composition and temperature on chalcopyrite leaching in acidic chloride solutions were investigated by a specially designed leaching experiment. The results revealed that chalcopyrite leaching rate strongly depended on the redox potential, determined by the concentration ratio of ferric ions to ferrous ions. A peak behavior was observed on the copper extraction rate versus redox potential plot, i.e., at low redox potential, the rate increased with a rise in the redox potential, followed by a decrease in leaching rate at higher redox potentials. A similar peak behavior was reported for chalcopyrite leaching in acidic sulfate solutions (Yoo *et al.*, 2010), suggesting that leaching mechanism of chalcopyrite is essentially common in both chloride and sulfate solutions.

From the electrochemical viewpoint, the overall reaction of chalcopyrite dissolution (Eq. 4-1) is divided into the following half-cell reactions (Hiroyoshi *et al.*, 2004):

$$CuFeS_2 = Cu^{2+} + Fe^{2+} + 2\ S^o + 4e^- \quad (4\text{-}2)$$

$$4\ Fe^{3+} + 4\ e^- = 4\ Fe^{2+} \quad (4\text{-}3)$$

Eq. (4-2) represents the anodic dissolution of chalcopyrite, and Eq. (4-3) is the cathodic reduction of ferric to ferrous ions. Many researchers have attempted to elucidate the leaching mechanism of chalcopyrite through an understanding about the anodic dissolution (Gómez *et al.*, 1996; Elsherief, 2002; Hiroyoshi *et al.*, 2004; Lazaro and Nicol, 2006).

Hiroyoshi et al. (2004) investigated the effects of solution composition on the anodic dissolution of chalcopyrite electrode (Eq. 4-2) in sulfuric acid solutions. In the absence of cuprous and/or ferrous ions in solution, the peak behavior did not appear on the anodic polarization curve (current density versus redox potential plot). When cupric and ferrous ions coexist in the solution, a peak current density was observed on the anode polarization curve. This peak current density corresponded to the peak chalcopyrite leaching rate. This result suggested that coexisting cupric and ferrous ions plays an important role in chalcopyrite leaching in acidic sulfate solutions. Based on the results, a reaction model for chalcopyrite dissolution in sulfuric acid solutions was

proposed.

Assuming the basic mechanism of chalcopyrite dissolution is common for both sulfate and chloride solutions, it is expected that the peak current density in the anodic polarization curve for a chalcopyrite electrode would be also observed in acidic chloride solutions containing both cupric and ferrous ions. To confirm this, in this chapter, the effects of solution composition on the anodic dissolution of chalcopyrite in acidic chloride solutions were investigated.

4.2 Materials and methods

4.2.1 Materials

Chalcopyrite electrode was prepared by the following procedure. A regular shape specimen was cut from an ore lump of chalcopyrite and polished to a thickness of about 5 mm. The specimen was ultrasonically washed in ultrapure water and dehydrated with acetone. A thin layer of gold was sputter-contact and copper wire was connected to the gold layer with a conducting silver paste. Then the specimen was embedded in non-conducting resin to expose only one side of the chalcopyrite. Before each experiment, a fresh electrode surface was prepared by polishing with silica-carbon paper and fine polishing on a glass plate with 5 to 1 μm alumina suspension. The surface was ultrasonically washed in ultrapure water to remove excess alumina powders. After each experiment, the electrode surface area was determined using a microscope and image analyzer.

For preparing the electrolyte, ultrapure water and reagent grade chemicals were used. Unless stated otherwise, the electrolyte was 0.1 kmol m^{-3} HCl containing various concentrations of cupric chloride and ferrous chloride. In some series of experiments, HCl solutions containing sodium chloride or cuprous chloride was also used as electrolyte.

4.2.2 Methods

Electrochemical measurements were performed using a computer-controlled electrochemical measurement system (Analytical SI 1280B, Solartron) on a conventional three-electrode cell consisting of a saturated Ag/AgCl reference electrode, a platinum counter electrode, and a chalcopyrite working electrode at 298 K (25 degrees Celsius) in a nitrogen atmosphere. The cell

was filled with 140 cm^3 of electrolyte and the electrolyte was agitated using a magnetic stirrer (agitation speed, 300 rpm) during the measurements (Fig. 4-1).

After immersing electrodes into the electrolyte, the rest potential of the chalcopyrite electrode was measured as a function of time. When the rate of the rest potential change became less than 5 mV min^{-1}, the rest potential measurement was stopped.

A 10 mV of DC bias against the rest potential was applied to the chalcopyrite electrode and the chrono-amperometry measurement was run, measuring the current as a function of time at a constant applied potential. The measurement was terminated when the rate of the current change became less than 5% of the total current in 1 min. Then, the potential increased another 10 mV and the measurement was repeated. Anodic – polarization curves were obtained by plotting the final current density against the applied potential.

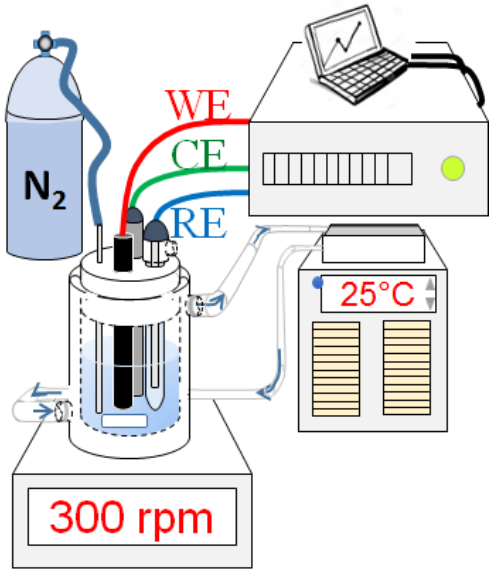


Fig. 4-1. Electrochemical experiment setup

4.3 Results and discussions

4.3.1 Effects of cupric and ferrous ions on anodic polarization curves for chalcopyrite electrode in acidic chloride solutions

Fig. 4-2 shows the effects of cupric and ferrous ions on the anodic-polarization curve for the chalcopyrite electrode in 0.1 kmol m^{-3} HCl solutions containing known concentrations of cupric and ferrous ions at 298 K in a nitrogen atmosphere. Without cupric and ferrous ions, anodic

current increased monotonically with increasing the applied potential. The anodic current observed here corresponds to the rate of anodic dissolution of chalcopyrite (Eq. 4-2), and the result suggests that in the absence of cupric and ferrous ions the chalcopyrite dissolution rate increases monotonically with increasing the redox potential.

The polarization curve in the presence of 0.05 kmol m^{-3} cupric ions shows that anodic current was almost same as that without both cupric and ferrous ions. With 0.05 kmol m^{-3} ferrous ions, a larger current was observed, likely caused by the oxidation of ferrous ions on the working electrode surface, according to

$$Fe^{2+} = Fe^{3+} + e^{-} \tag{4-4}$$

In three cases described above (anodic polarization curves without cupric and ferrous ions, with only cupric ions, and with only ferrous ions), anodic current increased monotonically with increasing the applied potential. As shown in Fig. 4-2, however, when both cupric and ferrous ions were added, the shape of the polarization curve changed drastically, and a peak was observed in the polarization curve. With increasing the potential, anodic current increased to reach its peak at around 0.45 V. At higher redox potentials, the current decreased with increasing the potential. The peak current observed in the presence of both cupric and ferrous ions was much larger than the current observed in other cases.

The current observed in the presence of both cupric and ferrous ions is the sum of the currents generated by anodic dissolution of chalcopyrite (Eq. 4-2) and the oxidation of ferrous ions (Eq. 4-4). Because of this, it is difficult to determine the current due to chalcopyrite dissolution only from the anodic polarization curve, while the peak behavior observed in anodic polarization curve in the presence of both cupric and ferrous ions is very similar to that observed in copper extraction rate versus redox potential plot obtained by leaching experiments in chapter 2. Considering this, it is reasonable to conclude that coexisting cupric and ferrous ions causes the enhanced anodic dissolution of chalcopyrite (Eq. 4-2) at redox potentials around 0.45 V, and this is the reason of faster copper extraction at the potential region near 0.45 V in leaching experiments.

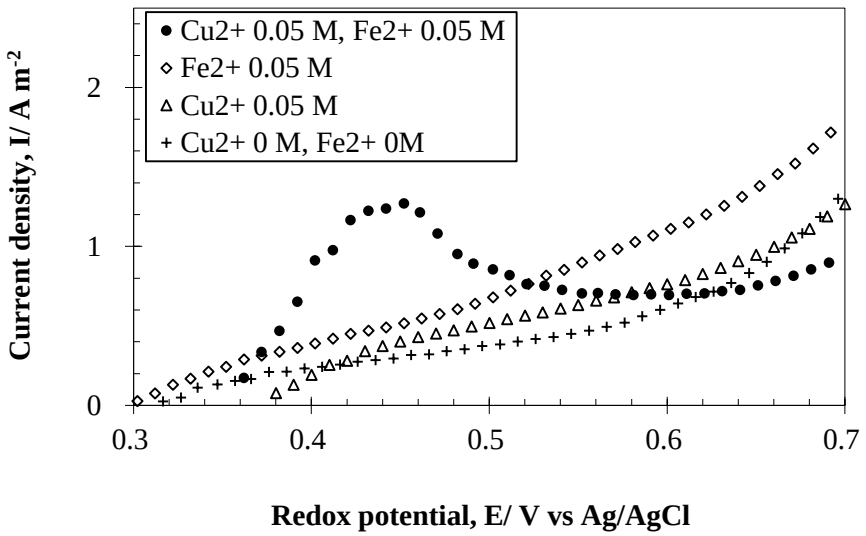


Fig. 4-2. Effects of cupric and ferrous ions on anodic-polarization curves for the chalcopyrite electrode. (Condition: HCl concentration of 0.1 kmol m^{-3} at 298 K in a nitrogen atmosphere, stirring speed 300 rpm.)

4.3.2 Comparison of the anodic polarization curves in sulfate and chloride solutions

Fig. 4-3 shows the anodic polarization curves for chalcopyrite electrode in a sulfate solution (0.1 kmol m^{-3} H_2SO_4 containing 0.1 kmol m^{-3} $FeSO_4$ and 0.1 kmol m^{-3} $CuSO_4$) and a chloride solution (0.1 kmol m^{-3} HCl containing 0.1 kmol m^{-3} $FeCl_2$ and 0.1 kmol m^{-3} $CuCl_2$). In both cases, shape of the polarization curves were qualitatively similar: a current peak was observed in the polarization curve. This may implies that dissolution mechanism (or elementary reactions involved in the anodic dissolution of chalcopyrite) is common for both chloride and sulfate systems. From a quantitative view point, however, the anodic polarization curves in these solutions are quite different: higher current density was observed in the chloride solutions than in the sulfate solutions. For example, current density at the peak was about 4.5 A m^{-2} in the chloride solution and this was about four to five times higher than that observed in the sulfate solutions (about 0.8 Am^{-2}) . The peak potentials were also different in both solutions: it was 0.45 V in the sulfate solutions and 0.48 V in chloride solutions. Many researches have reported that copper extraction from chalcopyrite is much faster in acidic chloride solutions than in acidic sulfate solutions. The result shown in Fig. 4-3 confirms that the faster copper extraction is due to the faster anodic dissolution of chalcopyrite in acidic chloride solutions.

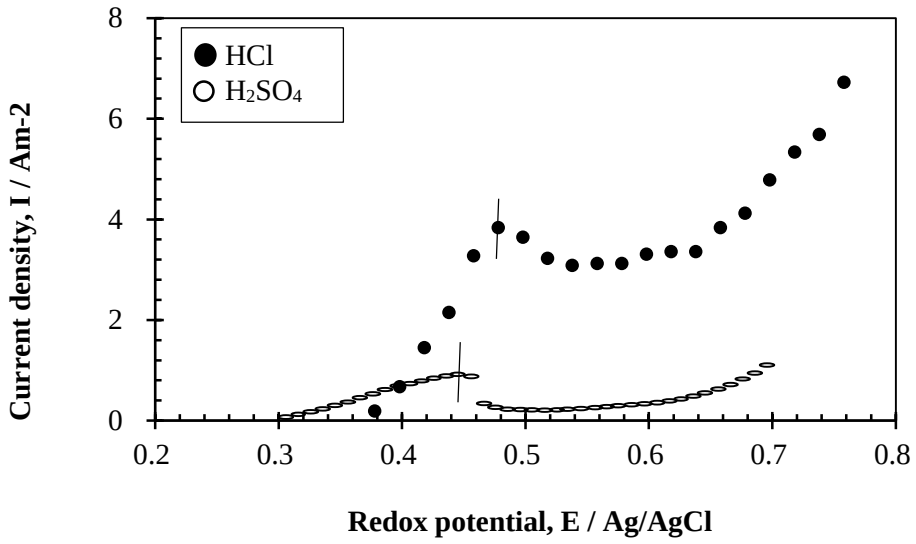


Fig. 4-3. Anodic polarization curves for chalcopyrite electrode in a chloride solution (condition: 0.1 kmol m^{-3} HCl containing 0.1 kmol m^{-3} $FeCl_2$ and 0.1 kmol m^{-3} $CuCl_2$) and a sulfate solution (condition: 0.1 kmol m^{-3} H_2SO_4 containing 0.1 kmol m^{-3} $FeSO_4$ and 0.1 kmol m^{-3} $CuSO_4$). Black dots: in chloride solution, red dots: in sulfate solution.

4.3.3 Effects of chloride ion and proton

To investigate the effect of chloride ions, anodic polarization experiments for chalcopyrite electrode was carried out using the electrolyte containing 0.05 M Cu^{2+}, 0.05 M Fe^{2+}, 0.1 M HCl and varied concentration of NaCl. The results (Fig. 4-4) clearly showed that the current density increased with increasing chloride concentration. This suggested that the chloride ion is a promoter for chalcopyrite dissolution.

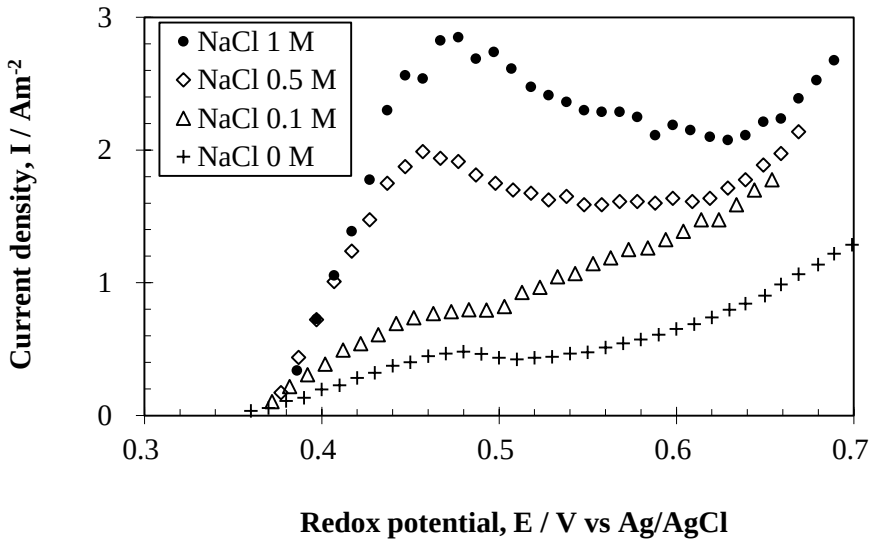


Fig. 4-4. Effects of chloride ions concentration on anodic-polarization curves for the chalcopyrite electrode. (Condition: $[Cu^{2+}] = [Fe^{2+}] = 0.05$ kmol m^{-3}, HCl concentration of 0.1 kmol m^{-3} at 298 K in a nitrogen atmosphere, stirring speed 300 rpm.)

To investigate the effects of proton on the anodic dissolution of chalcopyrite, anodic polarization experiments were carried out using the electrolytes containing 0.05 M Cu^{2+}, 0.05 M Fe^{2+} and varied concentration of HCl and NaCl. By adjusting the ratio of NaCl and HCl added in the solutions, total chloride concentration was kept at 1.3 kmol m^{-3}.

The peak current density increased with decreasing HCl concentration (Fig. 4-5). This result is in line with the leaching experiment result reported in chapter 2, where the leaching rate of chalcopyrite increased with decreasing the HCl concentration. Because the concentration of chloride ions was constant in the experiments, the results shown in Fig. 4-5 indicates that proton is a suppressor for chalcopyrite dissolution.

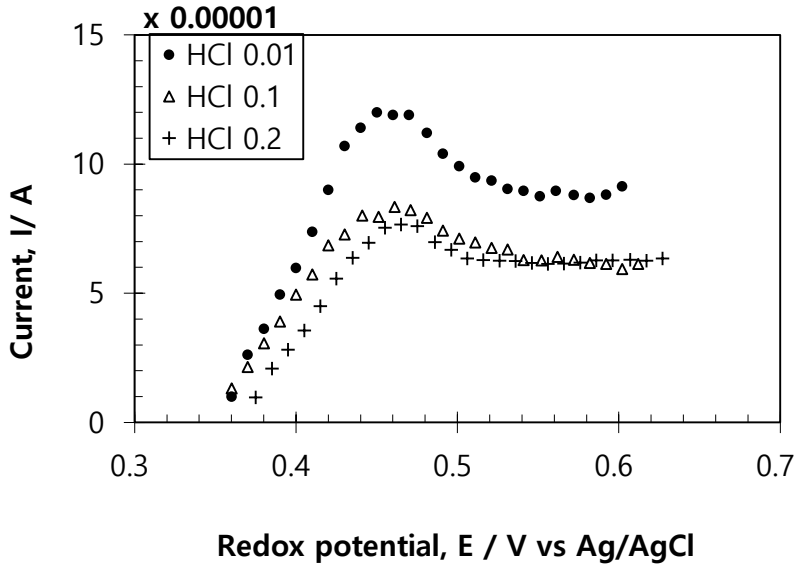


Fig. 4-5. Effects of HCl concentration on anodic polarization curves for the chalcopyrite electrode. (Condition: $[Cu^{2+}] = [Fe^{2+}] = 0.05$ kmol m^{-3}, at 298 K in a nitrogen atmosphere, stirring speed 300 rpm.)

4.3.4 Effect of cuprous ion concentration

The experimental results shown above indicates that when both Cu^{2+} and Fe^{2+} are present in solution, a peak current was appeared, and that this peak current increased with increasing chloride ion concentration. From thermodynamic point of view, when both Cu^{2+} and Fe^{2+} ions are present in solution, they react to form Cu^{+} ions (Eq. 4-5).

$$Cu^{2+} + Fe^{2+} = Cu^{+} + Fe^{3+} \quad (3\text{-}5)$$

Fig. 4-6 shows results of thermodynamic calculation (Eh – log a_{Cl^-} diagram for Cu^{2+}/Cu^{+}-Cl^{-} - H_2O system) using Geochemist's Workbench® with MINTEQ database. As shown in this figure, when activity of chloride ions increases, cuprous chloride complexes like $CuCl_2^-$ and $CuCl_3^{2-}$ are formed, and their stable region is expanded to higher redox potentials. This suggested that Cu^{+} ions might play an important role in the chalcopyrite leaching.

The effects of Cu^{+} ions on the anodic dissolution of chalcopyrite were examined using solution containing 0.1 kmol m^{-3} HCl with 0.001 kmol m^{-3} CuCl. As shown in Fig. 4-7, in the presence of Cu^{+}, a peak appeared at around 0.4 V vs Ag/AgCl on the anodic polarization curve. This peak position is far from the oxidation potential of Cu^{+} to form Cu^{2+} (around 0.2 V vs Ag/AgCl), determined from a cyclic voltammogram shown in Fig. 4-8. This confirms that the peak observed

on the anodic polarization curve in Fig. 4-7 is not due to Cu^{+} oxidation and it corresponds to the peak for the anodic dissolution of chalcopyrite.

Considering the promotion effect of Cu^{+} ions, the effects of coexistence Cu^{2+} and Fe^{2+} ions, as well as chloride ions could be explained as follows. The high leaching rate achieved at low redox potential in the presence of both Cu^{2+} and Fe^{2+} ions was due to the formation of promoter Cu^{+} ions. The stability of Cu^{+} ions at high chloride ions concentration resulted in a faster chalcopyrite leaching rate at higher chloride ions concentration.

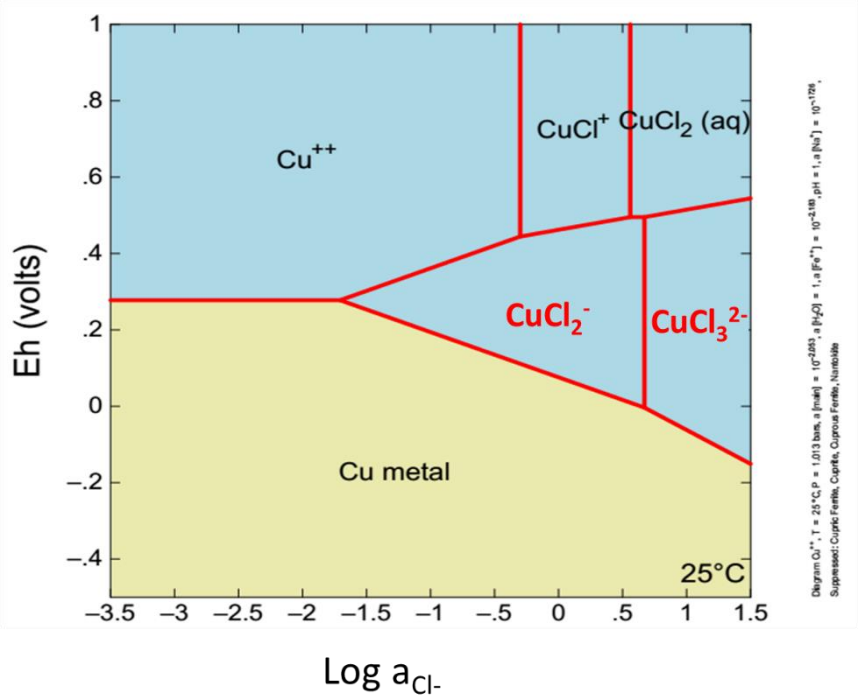


Fig. 4-6. The Eh-log a_{Cl^-} diagram for the Cu^{+}/Cu^{2+}-Cl^{-} - H_2O system

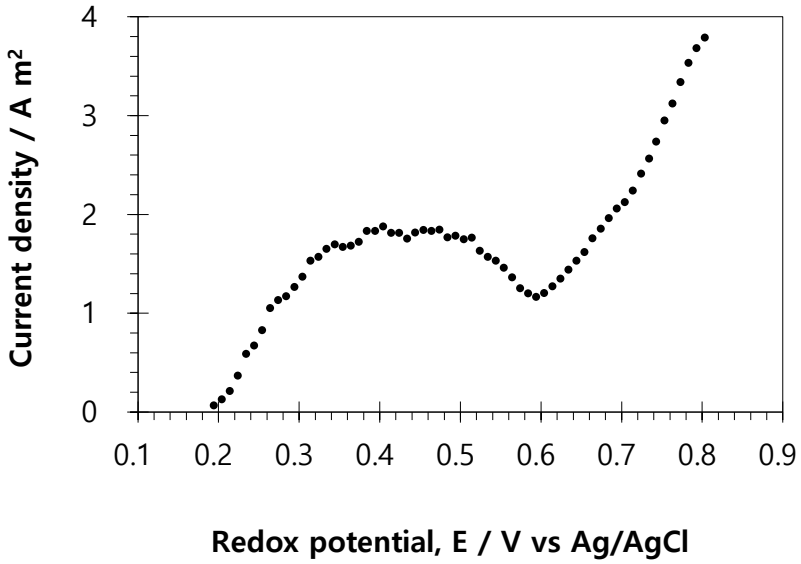


Fig. 4-7. Effects of cuprous ions on anodic polarization curves for the chalcopyrite electrode. (Condition: HCl concentration of 0.1 kmol m^{-3} at 298 K in a nitrogen atmosphere, stirring speed 300 rpm.)

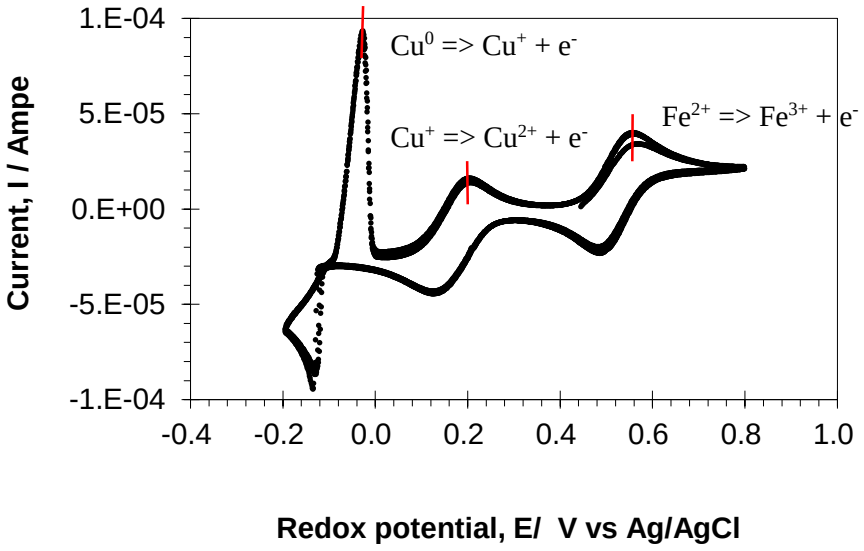


Fig. 4-8. A cyclic voltammogram obtained using a platinum electrode in the electrolyte containing 0.1 kmol m^{-3} HCl, 0.05 kmol m^{-3} Cu^{2+} and 0.05 kmol m^{-3} Fe^{2+} at 298 K in a nitrogen atmosphere.

4.4 Summary

The effects of solution compositions on the anodic dissolution of chalcopyrite were investigated, using a conventional three electrode system, with chalcopyrite as working electrode, at 298 K under nitrogen atmosphere.

The results indicated that in the absence of Cu^{2+} and/or Fe^{2+}, the current density increased monotonically with increasing applied redox potential. Only in the presence of both Cu^{2+} and Fe^{2+} in solution, the peak behavior was observed in anodic polarization curve, which was similar to the peak leaching rate, reported in leaching experiments. At low redox potential region (< 0.50 V), the current density in the presence of Cu^{2+} and Fe^{2+} were much higher than that in the absence of these ions. This result indicated that coexistence of Cu^{2+} and Fe^{2+} promoted the dissolution of chalcopyrite at low redox potentials.

The effects of chloride ions on the anodic dissolution of chalcopyrite in the presence of both Cu^{2+} and Fe^{2+} were investigated. In the solutions containing 0.1 M HCl, 0.05 M Cu^{2+}, 0.05 M Fe^{2+}, and various concentration of NaCl, current density increased with increasing NaCl concentration. It indicated that chloride ions were promoter for the dissolution of chalcopyrite.

The effects of Cu^{+} ions on the anodic dissolution of chalcopyrite were examined using solution containing 0.1 M HCl with 0.001 M CuCl. The result showed that Cu^{+} ions promoted the chalcopyrite dissolution rate at low redox potentials and the peak behavior appeared on the anodic polarization curve even with only Cu^{+} ions present in solution.

Considering the promotion effect of Cu^{+} ions, the effects of coexistence Cu^{2+} and Fe^{2+} ions, as well as chloride ions were explained. The high leaching rate achieved at low redox potential in the presence of both Cu^{2+} and Fe^{2+} ions was due to the formation of promoter Cu^{+} ions as a reaction product between Cu^{2+} and Fe^{2+}. The promotion effect of chloride ions was caused by the stability of Cu^{+} ions at high chloride ion concentration by the formation of cuprous chloride complexes.

4.5 References

Dutrizac, J.E., 1981. The dissolution of chalcopyrite in ferric sulfate and ferric chloride media. MTB 12, 371–378. https://doi.org/10.1007/BF02654471

Elsherief, A.E., 2002. The influence of cathodic reduction, Fe2+ and Cu2+ ions on the electrochemical dissolution of chalcopyrite in acidic solution. Minerals Engineering 15, 215–223. https://doi.org/10.1016/S0892-6875(01)00208-4

Gómez, C., Figueroa, M., Muñoz, J., Blázquez, M.L., Ballester, A., 1996. Electrochemistry of chalcopyrite. Hydrometallurgy 43, 331–344. https://doi.org/10.1016/0304-386X(96)00010-2

Hiroyoshi, N., Kuroiwa, S., Miki, H., Tsunekawa, M., Hirajima, T., 2004. Synergistic effect of cupric and ferrous ions on active-passive behavior in anodic dissolution of chalcopyrite in sulfuric acid solutions. Hydrometallurgy 74, 103–116. https://doi.org/10.1016/j.hydromet.2004.01.003

Lazaro, I., Nicol, M.J., 2006. A rotating ring–disk study of the initial stages of the anodic dissolution of chalcopyrite in acidic solutions. J Appl Electrochem 36, 425–431. https://doi.org/10.1007/s10800-005-9089-4

McMillan, R.S., MacKinnon, D.J., Dutrizac, J.E., 1982. Anodic dissolution of n-type and p-type chalcopyrite. J Appl Electrochem 12, 743–757. https://doi.org/10.1007/BF00617495

Yoo, K., Kim, S., Lee, J., Ito, M., Tsunekawa, M., Hiroyoshi, N., 2010. Effect of chloride ions on leaching rate of chalcopyrite - ScienceDirect. Minerals Engineering 23 (2010) 471–477. https://doi.org/doi:10.1016/j.mineng.2009.11.007

CHAPTER 5: ELECTROCHEMICAL IMPEDANCE SPECTROSCOPY FOR CHALCOPYRITE ELECTRODE DURING ANODIC DISSOLUTION IN ACIDIC CHLORIDE SOLUTIONS

5.1 Introduction

Electrochemical impedance spectroscopy (EIS) is a non-destructive method to study kinetic and mechanism of reactions happening on the material surface. This technique has been widely applied in studies of concrete (Song, 2000), proton exchange membrane (PEM) fuel cell (Yuan *et al.*, 2007), lithium ion battery (Momma *et al.*, 2012), coating failure (Lillard *et al.*, 1995), and corrosion behavior of coated steel (Liu *et al.*, 2003). Recently, EIS has found its application in mineral processing (Ferdosi, Ametov and Harmer, 2011), especial in the study of sulfide minerals, such as enargite (Pauporté and Schuhmann, 1996), pyrrhotite (Ekmekçi *et al.*, 2010), and arsenopyrite (Deng and Gu, 2018).

Chalcopyrite itself presents as an attractive research topic of EIS. As early as 1998, Velásquez *et al.*, studied EIS analysis of chalcopyrite electrodes in alkaline solution. Also in alkaline solutions, Velásquez *et al.*, (2005) analyzed electrochemically modified electrode surfaces of natural chalcopyrite and pyrite. In later years, Liu and Li, (2011, 2010) compared the electrochemical behaviors of pyrite and chalcopyrite in a NaCl solution at room temperature and under differential stress. Rafsanjani-Abbasi and Davoodi, (2016) investigated electrochemical characterization of natural chalcopyrite dissolution in sulfuric acid solution in presence of peroxydisulfate. Using a modified carbon paste electrode, Arena *et al.*, (2016) simulated the main stages of chalcopyrite leaching and bioleaching in ferrous ions solution by EIS study.

It can be seen that there is limited EIS study on chalcopyrite leaching in acidic solution, using natural chalcopyrite electrode without surface modification, except the work published by Hiroyoshi et al. (2004). The authors applied EIS to study the mechanism of anodic dissolution of chalcopyrite electrode in sulfuric acid solutions and reported that this technique can be used to evaluate the passivation of chalcopyrite during anodic dissolution.

In this chapter, EIS is applied to investigate chalcopyrite electrode during anodic polarization in chloride solutions and the effects of coexisting cupric and ferrous ions on the passivation of chalcopyrite was discussed based on the results.

5.2 Materials and methods

5.2.1 Materials

Chalcopyrite electrode was prepared by the following procedure. A regular shape specimen was cut from an ore lump of chalcopyrite and polished to a thickness of about 5 mm. The specimen was ultrasonically washed in ultrapure water and dehydrated with acetone. A thin layer of gold was sputter-contact and copper wire was connected to the gold layer with a conducting silver paste. Then the specimen was embedded in non-conducting resin to expose only one side of the chalcopyrite. Before each experiment, a fresh electrode surface was prepared by polishing with silica-carbon paper and fine polishing on a glass plate with 5 to 1 μm alumina suspension. The surface was ultrasonically washed in ultrapure water to remove excess alumina powders. After each experiment, the electrode surface area was determined using a crystal microscope.

The electrolyte was 0.1 kmol m^{-3} HCl containing known concentrations of cupric and ferrous chloride, prepared using ultrapure water and reagent grade chemicals.

5.2.2 Methods

Electrochemical measurements were performed using a computer-controlled electrochemical measurement system (Analytical SI 1280B, Solartron) on a conventional three-electrode cell consisting of a saturated Ag/AgCl reference electrode, a platinum counter electrode, and a chalcopyrite working electrode at 298 K in a nitrogen atmosphere. The cell was filled with 140 cm^3 of electrolyte and the electrolyte was agitated using a magnetic stirrer during the measurements.

After immersing electrodes into the electrolyte, the rest potential of the chalcopyrite electrode was measured as a function of time. When the rate of the rest potential change became less than 5 mV min^{-1}, the rest potential measurement was stopped and an AC impedance spectrum was measured (DC bias, 0 mV; AC amplitude, 5 mV; AC frequency, 20000 Hz to 0.1 Hz). After finishing the AC impedance spectrum measurement, 10 mV of DC bias against the rest potential was applied to the chalcopyrite electrode and the anodic current was measured as a function of time. When the rate of the current change became less than 5% of the total current in 1 min, the

current measurement was stopped and the AC impedance spectrum were measured. Anodic polarization measurements and AC impedance measurements were repeated alternately with 10 mV step increases in the DC bias. The equivalent circuit model fitting for the AC impedance was carried out using the computer-software Zview (Solartron Co.Ltd).

5.3 Results and discussions

5.3.1 EIS for chalcopyrite electrode in the absence of both cupric and ferrous ions

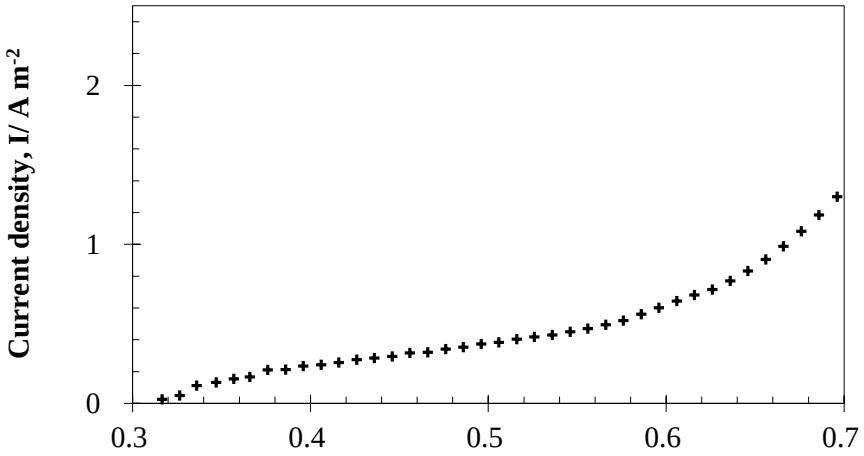


Fig. 5-1. Anodic-polarization curves for the chalcopyrite electrode in the absence of cupric and ferrous ions. (Condition: HCl concentration of 0.1 kmol m^{-3} at 298 K in a nitrogen atmosphere, stirring speed 300 rpm.)

The result from anodic polarization experiment showed that in the absence of cupric and ferrous ions in the solution, the current density was very low (< 1 A m^{-2}) and it increased monotonically with increasing applied redox potential. Electrochemical impedance spectroscopy (EIS) was applied for the chalcopyrite electrode during the anodic polarization experiments at each applied DC potentials to understand the change on the chalcopyrite surface during anodic dissolution.

5.3.1.1 EIS data

Figs. 5-1 and 5-2 show the magnitude of impedance, |Z|, and the value of phase angle, θ, as a function of frequency, f, respectively. The data show that the magnitude of impedance increased

with decreasing frequency, and there is a peak in phase angle versus frequency plot. Generally impedance of an electrochemical system or electrode is expressed using an equivalent circuit composed of electric elements such as resistor, R, and capacitor, C. The impedance of a resistor, $Z_R = R$ is independent from frequency, while the impedance of a capacitor, $Z_C = - j/\omega C$ ($\omega = 2\pi f$, angle frequency) is dependent on frequency. The observed dependence of impedance on frequency in Figs. 5-1 and 5-2 suggests that the equivalent circuit contains capacitors.

Fig. 5-3 shows several example of the complex plane plot of impedance data at different applied potentials. At all applied redox potentials, the data was plotted as a part of compressed (flat) semi-circle connected with an inclined straight line. The compressed semi-circle appeared at high frequencies and the connected straight line appeared at low frequencies. With increasing applied DC potential, the diameter of semi-circle increased.

A semi-circle on the complex plane plot appeared when a parallel circuit of resistor, R, and capacitor, C, is contained in the equivalent circuit. The semi-circle is compressed to be a flat semi-circle when electrode surface or product formed on the electrode surface is rough and uniform. In this case, the impedance data can be fitted with an R-CPE equivalent circuit, using constant phase element, CPE, instead of the capacitance, C in the R-C parallel circuit. In these cases, the value of resistance, R in R-C (or R-CPE) parallel circuit corresponds to horizontal diameter of semi-circle on the complex plane plot.

The presence of semi-circle or R-C (CPE) parallel circuit on the complex plane plot corresponds to the formation of a solid product layer on the surface of chalcopyrite electrode. The increase in the diameter of the semi-circle with increasing applied redox potential would imply the growth of this product layer at higher redox potential.

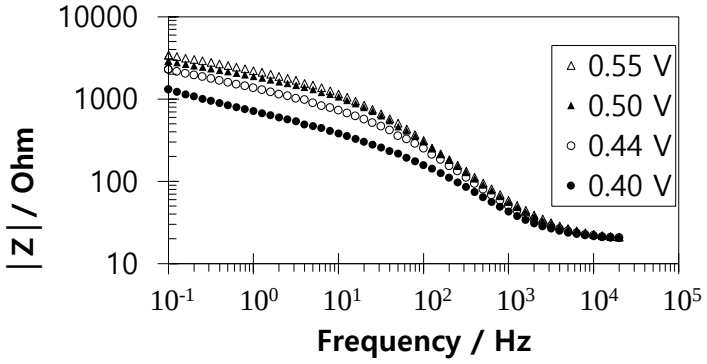


Fig. 5-2. The Bode plot, magnitude of impedance as a function of frequency (Condition: 140 ml electrolyte containing HCl 0.1 M, at 25 ºC, under N2 atmosphere).

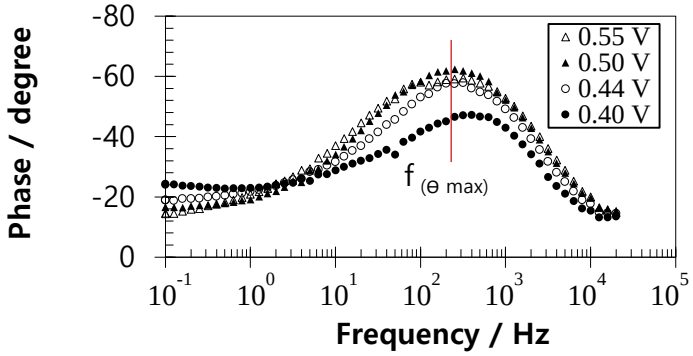


Fig. 5-3. The Bole plot, phase angle as a function of frequency. (Condition: 140 ml electrolyte containing HCl 0.1 M, at 25 ºC, under N2 atmosphere)

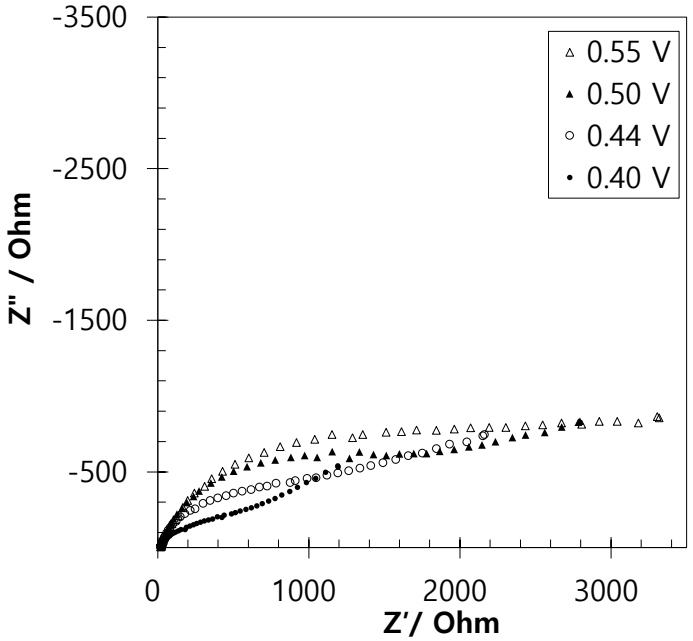


Fig. 5-4. The complex plane plot (Condition: 140 ml electrolyte containing HCl 0.1 M, at 25 º C under N2 atmosphere)

5.3.1.2 Fitting of EIS data

As described above, in the absence of both Cu^{2+} and Fe^{2+}, the complex plane plot composed of a compressed semi-circle at high frequencies connected with an inclined straight line at low frequencies. Usually, the semi-circle can be fitted using a parallel R-C circuit and the compressed semi-circle can be fitted using a parallel of R-CPE circuit, where constant phase element CPE is

a none-idea case of capacitor C. An inclined line usually corresponds to a diffusion process, and it can be fitted using a Warburg impedance or a constant phase element CPE, where the CPE presents for the high frequencies portion of Warburg impedance.

Considering the above, the equivalent circuit as shown in Fig. 5-4 was used to fit the experimental data, where R_s represented the portion of the solution resistance, parallel circuit of CPE2//R_{ct} represented the portion of the compress semi-circle, and the CPE1 represented the portion of straight line on the complex plane plot.

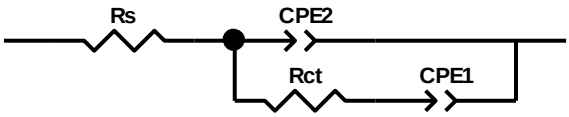


Fig. 5-5. Equivalent circuit in the case of without Cu^{2+} and Fe^{2+} in solution

Fig. 5-5 showed the fitting result for the solution resistance, R_s. The fitting result indicated that the solution resistance was almost constant at all applied redox potential.

Fig. 5-7 showed the fitting result for the constant phase element CPE1-T and CPE2-T. The CPE1-T was related to the straight line portion (diffusion effect). The CPE2-T was related to the compress semi-circle portion (formation of product layer), and its value corresponded to the capacitance of the product layer. The value of CPE2-T remained almost unchanged at all applied redox potential, indicating that the material of product layer was unchanged.

Fig. 5-8 showed the fitting result of charge transfer resistance, R_{ct}, as a function of applied redox potential. At low redox potentials (< 0.42 V), the value of R_{ct} was small and did not change significantly. At high redox potentials (> 0.42 V), the value of R_{ct} increased dramatically with increasing applied redox potential. This may be due to the increase in the thickness of the product layer formed on electrode surface during anodic polarization.

It have been reported that elemental sulfur is formed as a reaction product of chalcopyrite oxidation, and that it covers on the surface of chalcopyrite, acting as a passive layer. The EIS data shown in this section is well matched with the reported results, and the parallel R-CPE circuit in the equivalent circuit correspond to the passive elemental sulfur layer, which hindered the anodic dissolution of chalcopyrite.

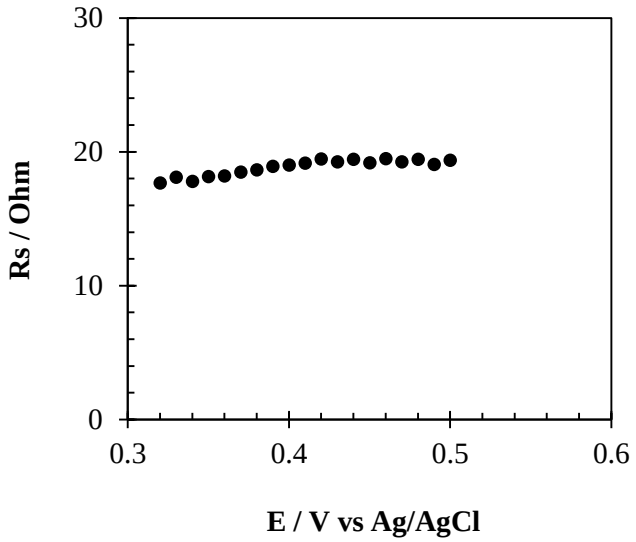


Fig. 5-6. Fitting result of solution resistance (Condition: 140 ml electrolyte containing HCl 0.1 M, at 25 ^{o}C, under N_2 atmosphere)

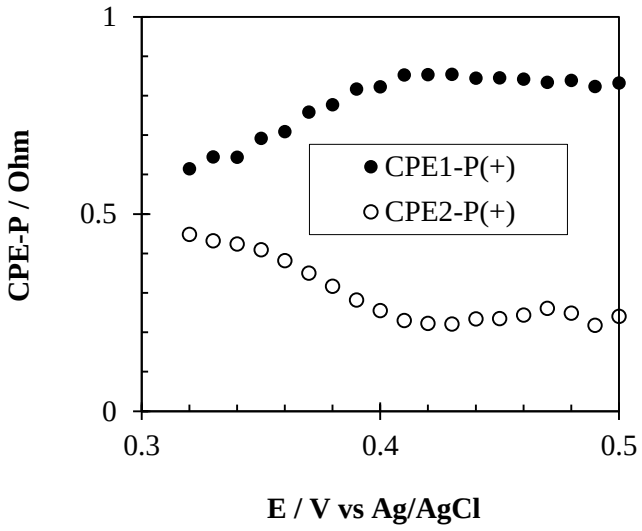


Fig. 5-7. Fitting result of constant phase element, CPE-P (Condition: 140 ml electrolyte containing HCl 0.1 M, at 25 ^{o}C, under N2 atmosphere)

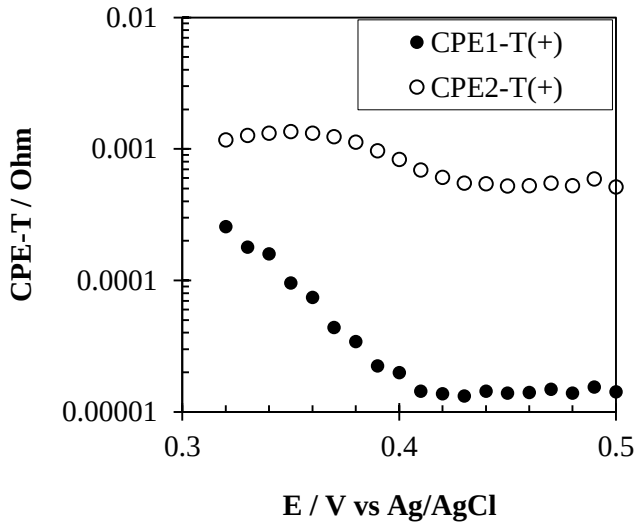


Fig. 5-8. Fitting result of constant phase element, CPE-T (Condition: 140 ml electrolyte containing HCl 0.1 M, at 25 ºC, under N2 atmosphere)

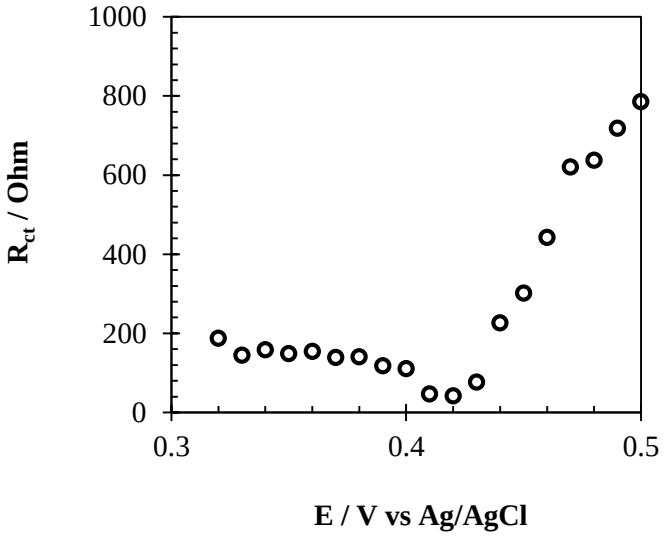


Fig. 5-9. Fitting result of charge transfer resistance, R (Condition: 140 ml electrolyte containing HCl 0.1 M, at 25 ºC, under N2 atmosphere)

5.3.2 EIS for chalcopyrite electrode in the presence of both cupric and ferrous ions

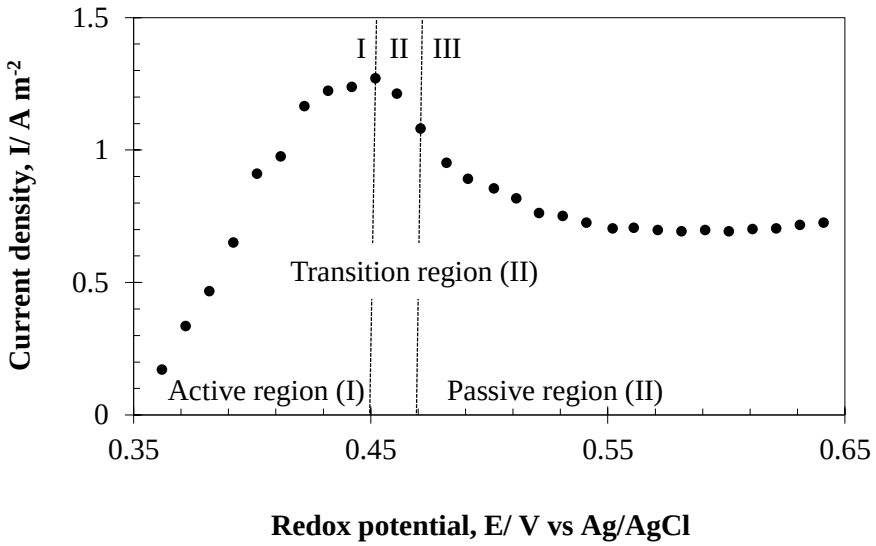


Fig. 5-10. Anodic-polarization curves for the chalcopyrite electrode in the presence of 0.05 M cupric and ferrous ions. (Condition: HCl concentration of 0.1 kmol m^{-3} at 298 K in a nitrogen atmosphere, stirring speed 300 rpm.)

An active-passive behavior was observed on the anodic polarization curve of chalcopyrite electrode in the presence of cupric and ferrous ions in the solution (Fig. 5.10). At the active region I (E < 0.45 V), the current density increased dramatically with increasing applied redox potential. In the transition region II (0.46 V), the current density began to decline. In the passive region III (E > 0.46 V), the current density decreased with further increasing in applied redox potentials. Electrochemical impedance spectroscopy (EIS) was applied for the chalcopyrite electrode during the anodic polarization experiments at each applied DC potentials to understand the change on the chalcopyrite surface at each regions.

5.3.2.1 EIS data

5.3.2.1.1 EIS data at active region I (E < 0.45 V)

As shown in Fig. 5-11, at low redox potentials (< 0.45 V), a part of compressed semi-circle appeared on the complex plane plot. The diameter of the compressed semi-circle slightly increased with increasing applied redox potential.

Fig. 5-12 and Fig. 5-13 showed the magnitude of impedance and the phase angle as the function of frequency, respectively. As shown in Fig. 5-12, the magnitude of impedance depended on frequency, i.e. it increased with decreasing frequency. In Fig. 5-12, a peak present on phase angle versus frequency plot. This peak is denoted as $f_{(\Theta \max)}$, frequency where the phase angle is max. The peak position ($f_{(\Theta \max)}$) was shifted when redox potential changed. The peak position ($f_{(\Theta \max)}$) in Fig. 5-12 is different from that observed in the absence of cupric and ferrous ions (Fig. 5-3), suggesting that passive layer was not formed in the presence of cupric and ferrous ions at low redox potentials. The shift of the peak position observed in Fig. 5-12 suggest there is a change on the chalcopyrite electrode surface at low redox potentials.

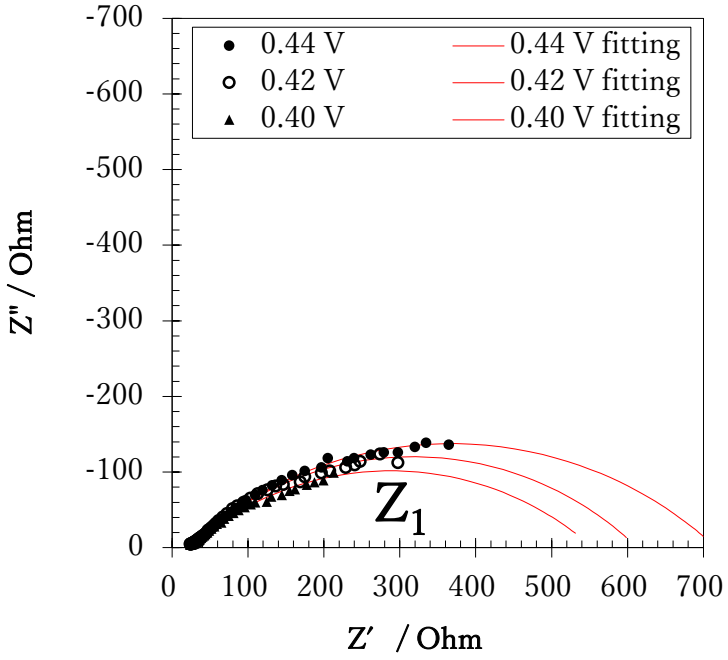


Fig. 5-11. The complex plane plot at active region I (E < 0.45 V) (Condition: 140 ml electrolyte containing Cu^{2+} 0.05 M Fe^{2+} 0.05 M in HCl 0.1 M, at 25 ^{o}C, under N2 atmosphere).

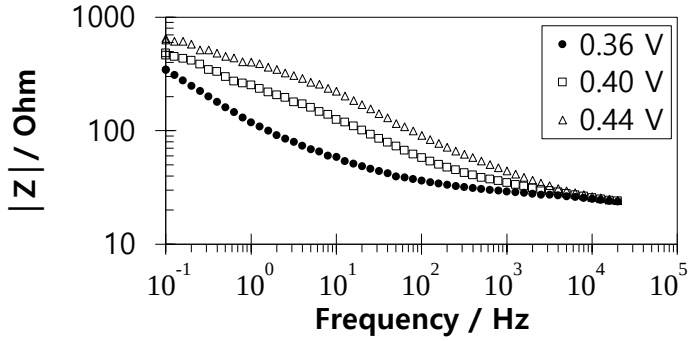


Fig. 5-12. The Bode plot, magnitude of impedance as a function of frequency at active region I (E < 0.45 V) (Condition: 140 ml electrolyte containing Cu^{2+} 0.05 M Fe^{2+} 0.05 M in HCl 0.1 M, at 25 ^{o}C, under N2 atmosphere).

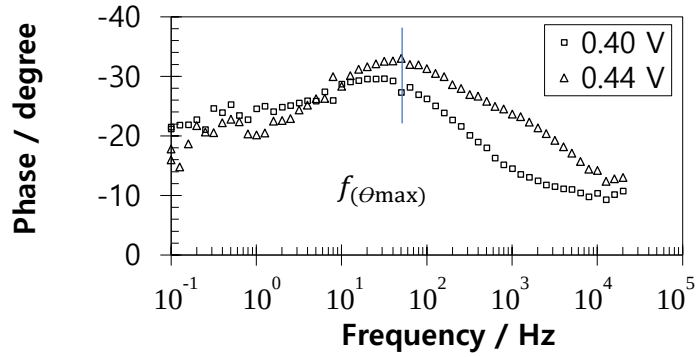


Fig. 5-13. The Bode plot, phase angle as a function of frequency at active region I (E < 0.45 V) (Condition: 140 ml electrolyte containing Cu^{2+} 0.05 M Fe^{2+} 0.05 M in HCl 0.1 M, at 25 ^{o}C, under N2 atmosphere).

5.3.2.1.2 EIS data at transition region II (E = 0.46 V)

At transition region II in the anodic polarization curve, the current density started to decline at 0.46 V. The EIS data at this applied voltage showed that in addition to the first semi-circle (Z1) at low frequencies portion, a second semi-circle (Z2) appeared at high frequency portion of the complex plane plot (Fig. 5-14). The phase angle versus frequency plot in Fig. 5-15 showed that there are two peaks of $f_{(\Theta\ max)}$, the first peak is at approximately 100 Hz, similar to the peak of $f_{(\Theta\ max)}$ in active region I, the second peak is at approximately 1000 Hz. These two results (Fig. 5-14 and Fig. 5-15) indicated that a new product layer was formed on the chalcopyrite electrode surface at the transition region II.

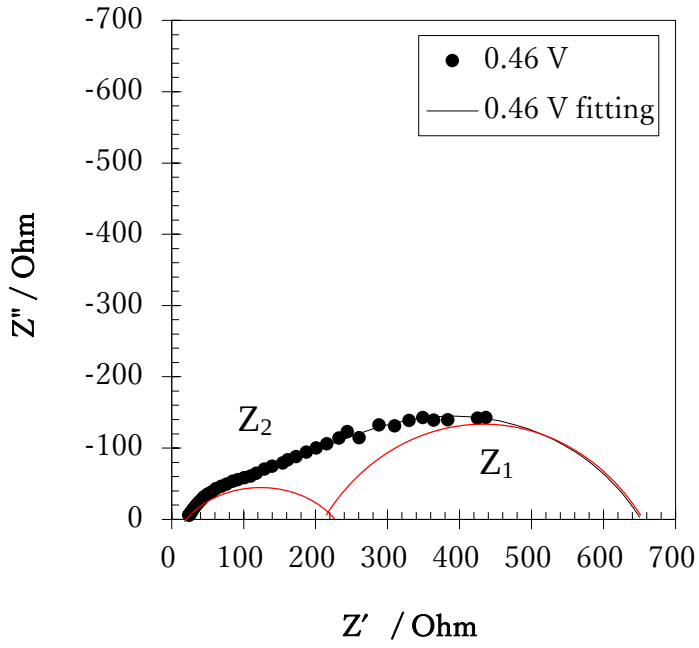


Fig. 5-14. The complex plane plot at transition region II (E = 0.46 V) (Condition: 140 ml electrolyte containing Cu^{2+} 0.05 M Fe^{2+} 0.05 M in HCl 0.1 M, at 25 ^{o}C, under N2 atmosphere).

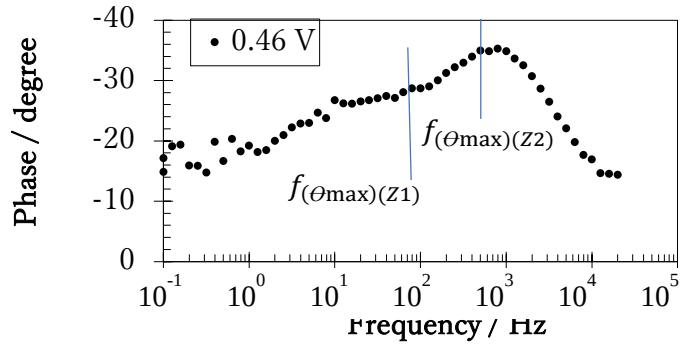


Fig. 5-15. The Bode plot, phase angle as a function of frequency at transition region II (E = 0.46 V) (Condition: 140 ml electrolyte containing Cu^{2+} 0.05 M Fe^{2+} 0.05 M in HCl 0.1 M, at 25 ^{o} C, under N2 atmosphere).

5.3.2.1.3 EIS data at passive region III (E > 0.46 V)

In the passive region III (E > 0.46 V), the compressed semi-circle Z1 disappeared and the compressed semi-circle Z2 became dominant on the complex plane plot (Fig. 5-16). Similar to the impedance data without Cu^{2+} and Fe^{2+} in the solution, the diameter of the semi-circle Z2 increased with increasing applied redox potential. The presence of semi-circle on complex plane

plot indicated that there was a product layer was formed on the surface of chalcopyrite electrode. The increase in diameter of semi-circle indicates that product layer grows when the potential increased.

Fig. 5-17 showed the magnitude of impedance as a function of frequency. At high frequencies (10 Hz – 20,000 Hz), the impedance decreased with increasing frequencies. At low frequencies (0.1 Hz – 10 Hz), the impedance became less dependence on frequency.

Fig. 5-18 showed the value phase angle as a function of frequency. There was only one peak ($f_{(\theta max)}$) at approximately 1000 Hz, corresponding to the second peak observed in EIS data at transition zone at 0.46 V. This peak was also at the same position as $f_{(\theta max)}$ peak observed the case without cupric and ferrous ions (Fig. 5-3). These results suggest that even in the presence of cupric and ferrous ions, at higher redox potentials, a passive layer was formed, and this layer is same as that formed in the absence of cupric and ferrous ions.

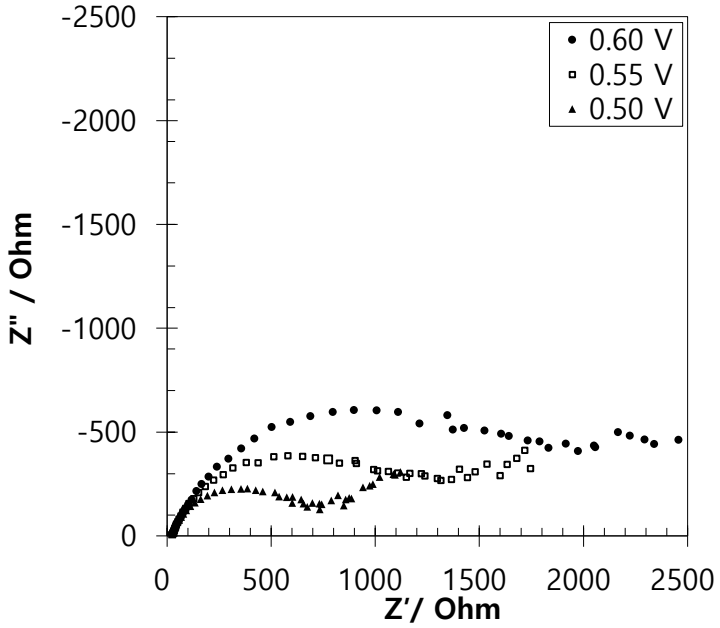


Fig. 5-16. The complex plane plot at passive region II (E > 0.46 V) (Condition: 140 ml electrolyte containing Cu^{2+} 0.05 M Fe^{2+} 0.05 M in HCl 0.1 M, at 25 ^{o}C, under N2 atmosphere)

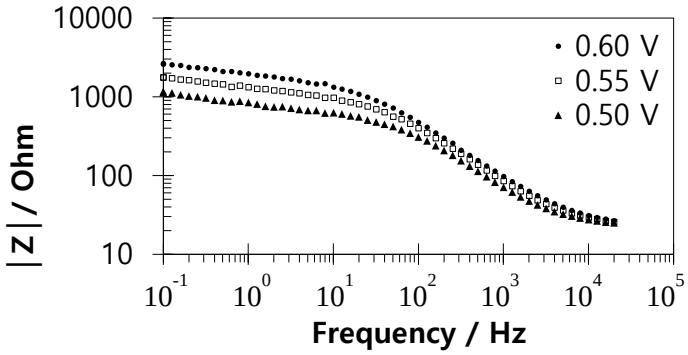


Fig. 5-17. The Bode plot, magnitude of impedance as a function of frequency at passive region II (E > 0.46 V) (Condition: 140 ml electrolyte containing Cu^{2+} 0.05 M Fe^{2+} 0.05 M in HCl 0.1 M, at 25 ^{o}C, under N2 atmosphere).

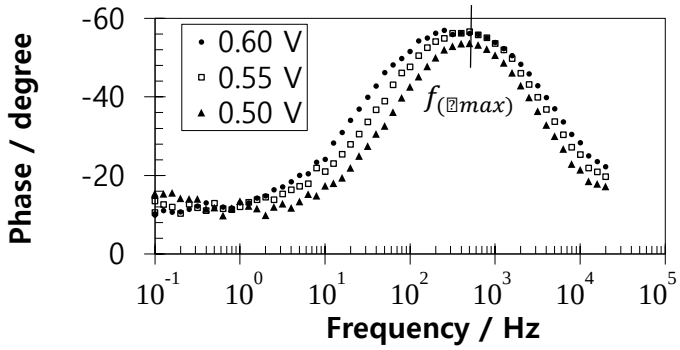


Fig. 5-18. The Bode plot, phase angle as a function of frequency at passive region II (E > 0.45 V) (Condition: 140 ml electrolyte containing Cu^{2+} 0.05 M Fe^{2+} 0.05 M in HCl 0.1 M, at 25 ^{o}C, under N2 atmosphere)

5.3.2.2 Fitting of EIS data

The parallel R-CPE circuit in series with solution resistance (Rs) was used to fit the EIS data at active region I and passive region III (Fig. 5-19 and Fig. 5-21). The EIS data at transition region II was fitted using a circuit including solution resistance (Rs) in series with two parallel R-CPE circuits, also in series (Fig. 5-20).

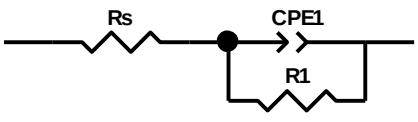


Fig. 5-19. Equivalent circuit used for fitting the impedance data at active region I (E =< 0.45 V)

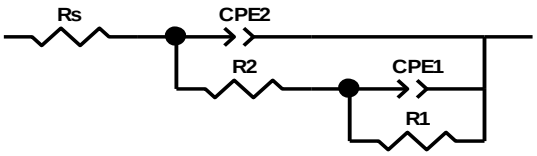


Fig. 5-20. Equivalent circuit used for fitting the impedance data at transition region II (E = 0.46 V).

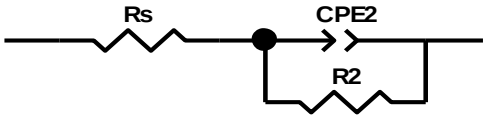


Fig. 5-21. Equivalent circuit used for fitting the impedance data at passive region II (E > 0.46 V).

Fig. 5-22 showed the fitting result of constant phase element CPE-T value. The value of CPE-T can be considered as the value of capacitance. It is important to note that the impedance of capacitance, Z_C, is inverse proportional to capacitance, C ($Z_C = -j/\omega C$). The lower capacitance gives the higher impedance value, meaning that the electrons (or electric charges) are more difficult to pass through the circuit with lower capacitance value. The value of capacitance, C is high in the active region I (E =< 0.45 V), and is 2 order higher than that in the passive region II (E > 0.46 V). These results indicated that the product layer covering the chalcopyrite surface at active region I is kind of conducting material while the product layer covering the chalcopyrite surface at passive region II is kind of insulating material.

Fig. 5-23 showed the fitting result of charge transfer resistance, R_{ct}. The value of R_{ct} equals the diameter of the semi-circle and it can be assumed to be proportional to the thickness of the product layer. In active region I, the value of resistance is small (< 700 Ohm) and did not change significantly with changing redox potential, suggesting that a thin product layer was formed on chalcopyrite surface at low redox potentials. In the passive region III, the R_{ct} value increased significantly with increasing applied redox potential and reached 2000 Ω at 0.60 V, suggesting a growth in thickness of the product layer at high redox potentials.

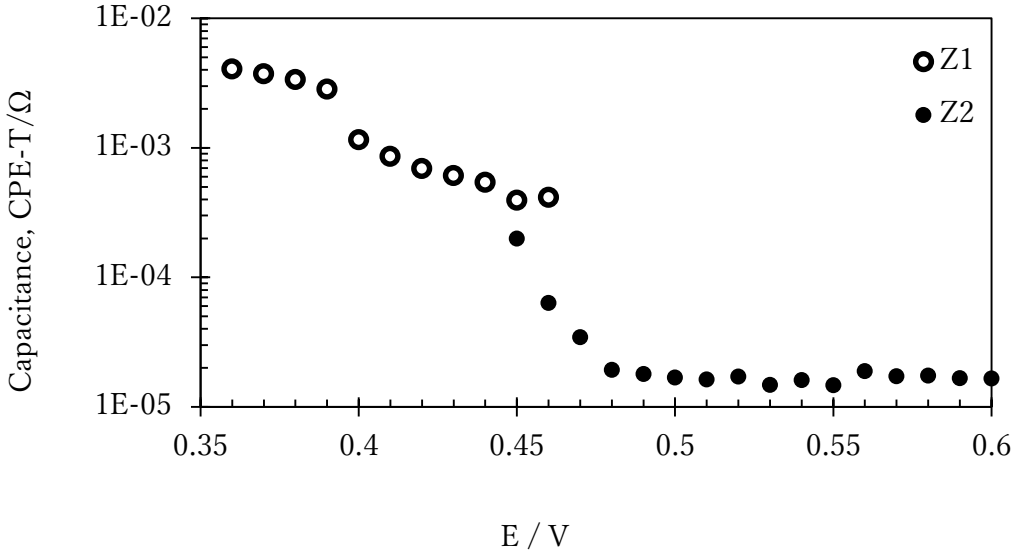


Fig. 5-22. Fitting result of constant phase element, CPE-T (Condition: 140 ml electrolyte containing Cu^{2+} 0.05 M Fe^{2+} 0.05 M in HCl 0.1 M, at 25 °C, under N2 atmosphere)

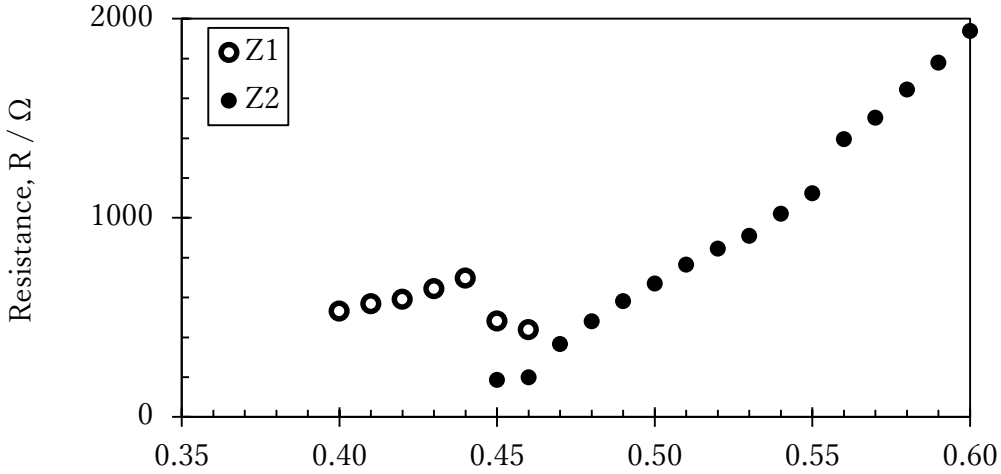


Fig. 5-23. Fitting result of charge transfer resistance, R (Condition: 140 ml electrolyte containing Cu^{2+} 0.05 M Fe^{2+} 0.05 M in HCl 0.1 M, at 25 °C, under N2 atmosphere)

5.4 Summary

Electrochemical impedance of chalcopyrite electrode during anodic polarization was investigated in acidic chloride solutions. The impedance data for the electrode in the absence of Cu^{2+} and Fe^{2+} in the solution can be fitted with a parallel R-CPE circuit, suggesting that a high resistance passive layer was formed on chalcopyrite surface. The results in the presence of both Cu^{2+} and Fe^{2+} showed that the passive layer was also formed at high redox potential (> 0.45 V), while it was not formed at low redox potential (< 0.45 V).

5.5 References

Arena, F.A., Suegama, P.H., Bevilaqua, D., dos Santos, A.L.A., Fugivara, C.S., Benedetti, A.V., 2016. Simulating the main stages of chalcopyrite leaching and bioleaching in ferrous ions solution: An electrochemical impedance study with a modified carbon paste electrode. Minerals Engineering 92, 229–241. https://doi.org/10.1016/j.mineng.2016.03.025

Bayoudh, S., Othmane, A., Ponsonnet, L., Ben Ouada, H., 2008. Electrical detection and characterization of bacterial adhesion using electrochemical impedance spectroscopy-based flow chamber. Colloids and Surfaces A: Physicochemical and Engineering Aspects 318, 291–300. https://doi.org/10.1016/j.colsurfa.2008.01.005

Deng, S., Gu, G., 2018. An electrochemical impedance spectroscopy study of arsenopyrite oxidation in the presence of Sulfobacillus thermosulfidooxidans. Electrochimica Acta 287, 106–114. https://doi.org/10.1016/j.electacta.2018.08.051

Ekmekçi, Z., Becker, M., Tekes, E.B., Bradshaw, D., 2010. An impedance study of the adsorption of CuSO4 and SIBX on pyrrhotite samples of different provenances. Minerals Engineering 23, 903–907. https://doi.org/10.1016/j.mineng.2010.02.007

Ferdosi, Y.J., Ametov, I., Harmer, S., 2011. Monitoring surfaces of mineral particles using electrochemical impedance spectroscopy. Chemeca 2011: Engineering a Better World: Sydney Hilton Hotel, NSW, Australia, 18-21 September 2011 1873.

Lillard, R.S., Kruger, J., Tait, W.S., Moran, P.J., 1995. Using Local Electrochemical Impedance Spectroscopy to Examine Coating Failure. CORROSION 51, 251–259. https://doi.org/10.5006/1.3293590

Liu, C., Bi, Q., Leyland, A., Matthews, A., 2003. An electrochemical impedance spectroscopy study of the corrosion behaviour of PVD coated steels in 0.5 N NaCl aqueous solution: Part II.: EIS interpretation of corrosion behaviour. Corrosion Science 45, 1257–1273. https://doi.org/10.1016/S0010-938X(02)00214-7

Liu, Q., Li, H., 2011. Electrochemical behaviour of chalcopyrite (CuFeS2) in FeCl3 solution at room temperature under differential stress. International Journal of Mineral Processing 98, 82–88. https://doi.org/10.1016/j.minpro.2010.10.010

Liu, Q., Li, H., 2010. A comparison of the electrochemical behaviors of pyrite and chalcopyrite in a NaCl solution at room temperature and under differential stress. Minerals Engineering 23, 691–697. https://doi.org/10.1016/j.mineng.2010.04.005

Momma, T., Matsunaga, M., Mukoyama, D., Osaka, T., 2012. Ac impedance analysis of lithium ion battery under temperature control. Journal of Power Sources 216, 304–307.

https://doi.org/10.1016/j.jpowsour.2012.05.095

Pauporté, Th., Schuhmann, D., 1996. An electrochemical study of natural enargite under conditions relating to those used in flotation of sulphide minerals. Colloids and Surfaces A: Physicochemical and Engineering Aspects 111, 1–19. https://doi.org/10.1016/0927-7757(95)03498-6

Rafsanjani-Abbasi, A., Davoodi, A., 2016. Electrochemical Characterization of Natural Chalcopyrite Dissolution in Sulfuric Acid Solution in Presence of Peroxydisulfate. Electrochimica Acta 212, 921–928. https://doi.org/10.1016/j.electacta.2016.07.061

Song, G., 2000a. Equivalent circuit model for AC electrochemical impedance spectroscopy of concrete. Cement and Concrete Research 30, 1723–1730. https://doi.org/10.1016/S0008-8846(00)00400-2

Velásquez, P., Gómez, H., Leinen, D., Ramos-Barrado, J.R., 1998. Electrochemical impedance spectroscopy analysis of chalcopyrite CuFeS2 electrodes. Colloids and Surfaces A: Physicochemical and Engineering Aspects 140, 177–182. https://doi.org/10.1016/S0927-7757(97)00276-8

Velásquez, P., Leinen, D., Pascual, J., Ramos-Barrado, J.R., Grez, P., Gómez, H., Schrebler, R., Del Río, R., Córdova, R., 2005. A Chemical, Morphological, and Electrochemical (XPS, SEM/EDX, CV, and EIS) Analysis of Electrochemically Modified Electrode Surfaces of Natural Chalcopyrite (CuFeS2) and Pyrite (FeS2) in Alkaline Solutions. J. Phys. Chem. B 109, 4977–4988. https://doi.org/10.1021/jp048273u

Yuan, X., Wang, H., Colinsun, J., Zhang, J., 2007. AC impedance technique in PEM fuel cell diagnosis—A review. International Journal of Hydrogen Energy 32, 4365–4380. https://doi.org/10.1016/j.ijhydene.2007.05.036

CHAPTER 6: MECHANISM OF CHALCOPYRITE LEACHING IN ACIDIC CHLORIDE SOLUTIONS

6.1 Introduction

In chapter 3, a specially designed batch leaching experiments were carried out and it was found that chalcopyrite leaching in acidic chloride solutions strongly depends on the redox potential determined by the concentration ratio of ferric ions to ferrous ions: A peak behavior was observed in the leaching rate versus the redox potential plot, i.e, the leaching rate increased with increasing redox potential reaching a local maximum (i.e., the peak rate) at a certain redox potential (i.e., the peak redox potential).

In chapter 4, anodic polarization experiments for a chalcopyrite electrode were conducted using a conventional three-electrode system in chloride solutions containing Fe^{2+} and/or Cu^{2+}, and it was found that a peak behavior, similar to that reported in the leaching experiments in chapter 2, was observed in the polarization curve when Cu^{2+} and Fe^{2+} coexisted in the solutions. The anodic current increase with redox potential to reach maximum at a certain potential, then it decreased at higher potentials, and the peak current increased with increasing Cl^- concentration and decreased with increasing H^+ concentration. Even without Cu^{2+} and Fe^{2+}, the peak behavior was observed when Cu+ was added to the solutions. These results suggested that Cu^{2+}, Fe^{2+}, Cu^+, H^+, and Cl^- play important roles in the chalcopyrite leaching.

In chapter 5, electrochemical impedance spectroscopy (EIS) was conducted for a chalcopyrite electrode at varied applied potentials in HCl solutions containing Fe^{2+} and Cu^{2+}, and the impedance date were analyzed by an equivalent-circuit fitting technique. The results suggested that a passive layer may be formed on the surface of chalcopyrite at high redox potentials, while the passive layer is not formed at lower redox potentials.

The above results can be briefly summarized as follows: (1) at high redox potentials, where Fe^{3+} is dominant rather than Fe^{2+}, chalcopyrite surface is covered with a passive product layer, which hinders anodic dissolution of chalcopyrite and causes a slow leaching kinetics, (2) at low redox potential, Fe^{2+} concentration increases and they react with Cu^{2+} to form Cu^+ chloride complexes, causing the disappearance of the passive layer and a faster leaching kinetics. To interpret these results, in this chapter, a new reaction model is proposed by modifying a reaction model proposed

by Hiroyoshi et al., which is developed to interpret the redox potential dependent chalcopyrite leaching in acidic sulfate solutions.

6.2 A brief review on the reaction model reported in previous studies

A series of research done by Hiroyoshi and coauthors (Hiroyoshi *et al.*, 1998, 2000, 2001, 2004, 2007, 2008) had developed a reaction model to interpret the redox potential dependence of chalcopyrite leaching in sulfuric acid solutions containing Fe^{3+}, Fe^{2+} and Cu^{2+}. The model is composed of two-stage reactions: in 1st stage an intermediate Cu_2S is formed from $CuFeS_2$ according to Eq. 6-1, and in 2nd stage intermediate CuS is subsequently oxidized by Fe^{3+} according to Eq. 6-2.

$$CuFeS_2 + 3\ Cu^{2+} + 3\ Fe^{2+} = 2\ Cu_2S + 4\ Fe^{3+} \quad (6\text{-}1)$$

$$Cu_2S + 4\ Fe^{3+} = 2\ Cu^{2+} + S + 4\ Fe^{2+} \quad (6\text{-}2)$$

Reaction (6-1) is a reduction of chalcopyrite with Fe^{2+} as a reductant (electron donner) and the intermediate Cu_2S forms only at low redox potentials, where Fe^{2+} is dominant. The intermediate Cu_2S is more rapidly oxidized than chalcopyrite and this causes the enhanced copper extraction at low potentials in the presence of Cu^{2+} and Fe^{2+}. The model proposed by Hiroyoshi was proven to be correct by the other studies under various leaching conditions (Miki *et al.*, 2001; Yoo *et al.*, 2007; Córdoba *et al.*, 2008; Gericke *et al*, 2010b; Ghahremaninezhad *et al.*, 2015)

This model can explain the redox potential dependence of chalcopyrite leaching in acidic sulfate solutions as well as the role of Fe^{2+} and Cu^{2+} in the leaching. To apply this model to interpret the mechanism of chalcopyrite in acidic chloride solutions, however, modification is needed, because the reactions in the model proposed by Hiroyoshi et al. does not involve H^+, Cl^-, and Cu^+ and their roles and effects cannot be interpreted.

Another unsolved problem associated with the previous model is “place of reactions”, which was criticized by (Viramontes-Gamboa *et al* 2007; Nicol *et al*, 2010). The model does not describe the places where Cu_2S formation and Cu_2S dissolution occurs. Cu_2S is formed by a reduction of chalcopyrite with Fe^{2+} as reductant (electron donner), while Cu_2S is dissolved by the oxidation with Fe^{3+} as an oxidant (electron accepter). Because these reactions uses Fe^{3+}/Fe^{2+} redox pair as electron donner and accepter, both reactions are unlikely to occur on one solid particle of chalcopyrite, which is a semi-conductor. These reactions may occur at electrically isolated places.

Considering the above, in the present study, the author proposed a modified mechanism that can overcome the inconsistent in Hiroyoshi's model.

6.3 Overview of modified reaction model proposed in this study

In the modified reaction model proposed here, the intermediate Cu_2S formation is divided into three steps (or sub-reactions) as follow:

6.3.1 The 1st stage (formation of intermediate Cu_2S)

Step 1: $CuFeS_2 + 4\ H^+ = Cu^{2+} + Fe^{2+} + 2\ H_2S$ (6-3)

Step 2: $4\ Cu^{2+} + 4\ Fe^{2+} = 4\ Cu^{+} + 4\ Fe^{3+}$ (6-4)

Step 3: $4\ Cu^{+} + 2\ H_2S = 2\ Cu_2S + 4\ H^+$ (6-5)

Net-reaction: $CuFeS_2 + 3\ Cu^{2+} + 3\ Fe^{2+} = 2\ Cu_2S + 4\ Fe^{3+}$

Fig. 6-1 shows the schematic representation of these reactions. In Step 1, chalcopyrite is decomposed by H^+ and Cu^{2+}, Fe^{2+} and H_2S is released in solution phase near chalcopyrite surface. Step 2 is the reduction of Cu^{2+} with Fe^{2+} as electron donner. As product of this reduction reaction Cu^+ and Fe^{3+} are formed in the solution phase. Finally, in Step 3, Cu^+ react with H_2S to form Cu_2S and this is precipitated on chalcopyrite surface. Net-reaction (overall reaction of Steps 1-3) is same as Eq.6-1 used in the reaction model proposed by Hiroyoshi et al. Important points of the above modification are (1) H^+ is involved inn step 1 and step 3, (2) Cu^+ is involved in Step 2 and Step 3, and (3) redox reaction involving electron exchange between reactants is Step 2 occurred in solution phase. As detailed later, these features allow to explain the roles of H^+ and Cu^+ in chalcopyrite leaching and their effects on copper extraction from this mineral.

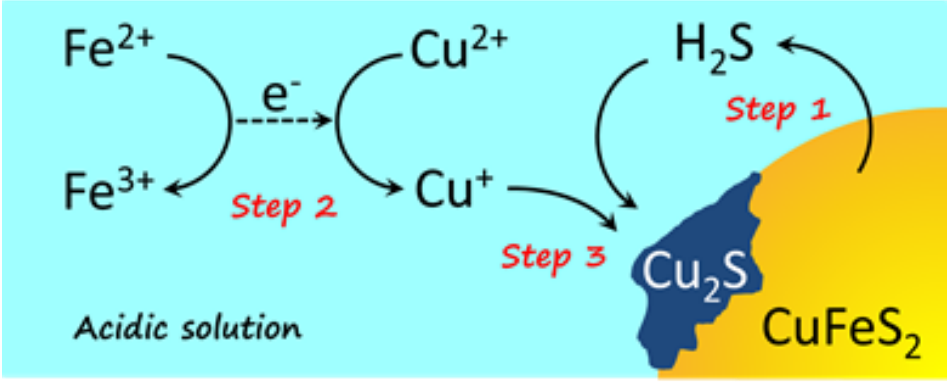


Fig. 6-1. Formation of intermediate Cu_2S in the proposed model.

In the proposed model, the dissolution of Cu_2S is also divided into two steps as follows,

6.3.2 The 2nd stage (dissolution of intermediate Cu_2S)

Step 1: $Cu_2S + 2\ Fe^{3+} = Cu^{2+} + CuS + 2\ Fe^{2+}$ (Fast) (6-6)

Step 2: $CuS + 2\ Fe^{3+} = Cu^{2+} + 2\ S + 2\ Fe^{2+}$ (Slow) (6-7)

Net-reaction: $Cu_2S + 4\ Fe^{3+} = 2\ Cu^{2+} + 2\ S + 4\ Fe^{2+}$

Step 1 is oxidation of Cu_2S to CuS and Cu^{2+} with Fe^{3+} as an oxidant (Eq. 6-6). In step 2, CuS is further oxidized to form Cu^{2+} and an elemental sulfur (Eq. 6-7). Net-reaction of the sequential oxidation is same as that used in the model proposed by Hiroyoshi et al.

As shown in Fig. 6-2, the dissolution of Cu_2S (and CuS) is considered to be a Galvanic cell reaction: Cu_2S/CuS acts as an anode and electrons generated by the anodic dissolution of Cu_2S/CuS pass through the semi-conductor solid phase and transferred to Fe^{3+} as a final electron accepter on the surface of chalcopyrite as an cathode.

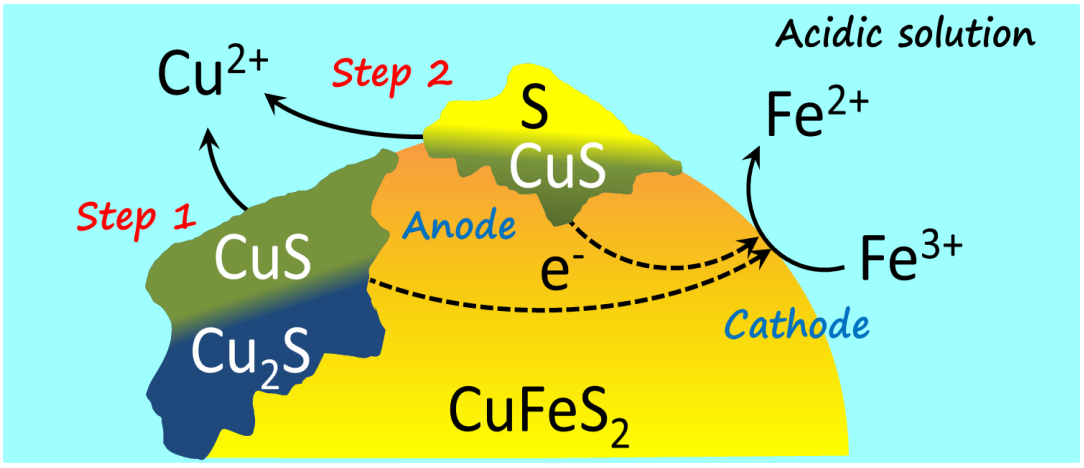


Fig. 6-2. Two-step oxidation of intermediate Cu2S in the proposed model.

6.4 Thermodynamic and kinetic aspects of chalcopyrite leaching in acidic chloride solutions and factors affecting the leaching

In this section, thermodynamic and kinetic aspects of chalcopyrite leaching in acidic chloride

solutions are discussed based on the proposed model and experimental results. Several important factors affecting the leaching are also discussed.

6.4.1 Thermodynamics of intermediate formation

The proposed model assumes that the intermediate is Cu_2S and it is formed by the reaction between Cu^+ and H_2S (Eq. 6-5). Gibbs energy change for this reaction is calculated to be

$$2\ Cu^+ + H_2S = Cu_2S + 2\ H^+ \qquad \Delta G^o = -\ 158.34\ kJ/mol \qquad (6\text{-}8)$$

As the solutions contain not only Cu^+ but also Cu^{2+}, CuS may be also formed, according to

$$Cu^{2+} + H_2S = CuS + 2\ H^+ \qquad \Delta G^o = -\ 91.26\ kJ/mol \qquad (6\text{-}9)$$

The value of Gibbs energy change is more negative for Cu_2S formation (Eq.6-8) than for CuS formation (Eq. 6-9), suggesting that Cu_2S formation is thermodynamically more favorable when Cu^+ and Cu^{2+} activity is same.

6.4.2 Roles and effects of chloride ions

Lin et al., (1991) reported that at high chloride concentration, complex spices of cuprous ions such as CuCl, $CuCl_2^-$, $CuCl_3^{2-}$, $CuCl_4^{3-}$ is formed, and the concentration of cuprous ions species increases with an increase in the concentration of chloride ions. Considering this, in the presence of chloride ions, not only Eq. 6-5, the following reaction may contribute to the formation of intermediate Cu_2S.

$$2\ CuCl_n^{(n-1)-} + H_2S = Cu_2S + 2\ H^+ + 2n\ Cl^- \qquad (6\text{-}10)$$

This reaction may interpret the roles and effects of Cl^- in chalcopyrite leaching: with increasing the concentration of Cl^-, total concertation of Cu^+ species increases and this causes the increase in the amounts of Cu_2S formed on chalcopyrite surface. This would be a reason why Cl^- enhances the anodic current and copper extraction.

6.4.3 Roles and effects of proton

In the reaction model, H^+ is involved in step 1 and step 3 for Cu_2S formation stage. Proton (H^+)

is a reactant in step 1 (decomposition of $CuFeS_2$ to form Cu^{2+}, Fe^{2+}, and H_2S), while H^+ is a product in step 3 (Cu_2S formation from Cu^+ and H_2S). This suggests that H^+ can act as both promoter and suppressor in Cu_2S formation stage. In the absence of H^+, step 1 is stopped and this causes a lack of H_2S, which is need to form Cu_2S. On the other hand, if excessive concentration of H^+ present in the solutions, back reaction of step 3 become dominant and Cu_2S formation is suppressed. The results of anodic polarization experiments showed that anodic dissolution rate decreases with increasing H^+ when HCl concentration is in the range from 0.01 M to 0.2 M. This suggests that suppressive effect of H+ is more dominant in Cu_2S formation stage under the experimental condition.

6.4.4 Thermodynamics of intermediate oxidation

The model assumes that dissolution of intermediate is two-step process as shown in Eqs. 6-6 and 6-7. Because both reactions are oxidation reactions involving Fe^{3+} as an oxidant, thermodynamics of the reactions can be discussed using the following anodic half-cell reactions.

$Cu_2S = CuS + Cu^{2+} + 2\ e^-$ ($E^o_{Cu_2S}$ = 0.508 V vs SHE) (6-11)

$CuS = Cu^{2+} + S + 2\ e^-$ (E^o_{CuS} = 0.617 V vs SHE) (6-12)

As shown in these equations, the standard redox potentials is lower for dissolution of Cu_2S (Eq. 6-11) than for CuS dissolution (Eq. 6-12). This suggests that at very low redox potentials, only Cu_2S dissolution (Eq.6-11) occurs and CuS dissolution (Eq.6-12) does not proceed. At higher potentials, CuS start to dissolve, and elemental sulfur is formed and this covers the surface of the mineral as a passivation layer. The results of EIS study in chapter 5 suggested that a passivation layer formed at redox potential over the peak redox potential. It is reasonable to assume that the passivation layer correspond to elemental sulfur layer formed as a product of CuS oxidation (Eq.6-12). The elemental sulfur layer would hinder the diffusion of copper from mineral surface to solution, resulting in a suppression of copper extraction.

6.4.5 Effect of Cu^{2+} on peak redox potentials

As described in (4), once CuS is start to be oxidized, passivating elemental sulfur layer is formed on the mineral surface, the leaching rate would be suppressed. Considering this, the peak redox potentials observed in leaching and anodic polarization experiments can be identified to be the

oxidation potential of CuS:

$$E_{CuS} = E^{o}_{CuS} + \frac{RT}{2F}\ln a_{Cu^{2+}} = 0.617 + 0.030\log(a_{Cu^{2+}}) \quad (6\text{-}13)$$

Where standard potential for CuS, E^{o}_{CuS} = 0.617 V vs S.H.E., temperature T = 298 K, gas constant R = 8.31447215 J K^{-1} mol^{-1}, Faraday constant F = 96485.339924 C mol^{-1}. Assuming the activity of cupric ions is equal to its molar concentration, Eq. 6-13 can be rearranged to

$$E_{CuS} = 0.617 + 0.030 \log [Cu^{2+}] \quad (6\text{-}14)$$

Discussion here is qualitatively in line with the experimental result: the peak redox potential depends on only Cu^{2+} concentration and it increases with increasing the concentration.

6.5 Summary

Based on the experimental results in previous chapters, a reaction model assuming the formation of an intermediate Cu_2S at low redox potentials were proposed for chalcopyrite leaching in acidic chloride solutions. The intermediate Cu_2S is easier to dissolve than chalcopyrite, thus enhanced the copper extraction rate at low redox potentials. The formation reaction of intermediate Cu_2S involved three steps. Firstly, chalcopyrite reacted with H^+ ions in solution to release Cu^{2+} ions, Fe^{2+} ions, and H_2S into the solution. Then Cu^{2+} and Fe^{2+} ions reacted to form Cu^+ ions. Finally, Cu^+ ions reacted with H_2S to form Cu_2S precipitated on the chalcopyrite surface. The intermediate Cu_2S was oxidatively decomposed to release Cu^{2+} ions and form elemental sulfur. Once elemental sulfur was formed, it acted as a passivation layer suppressing further chalcopyrite dissolution. Using the reaction model, the experimental results observed in the previous chapters were discussed.

6.6 References

Córdoba, E.M., Muñoz, J.A., Blázquez, M.L., González, F., Ballester, A., 2008. Leaching of chalcopyrite with ferric ion. Part II: Effect of redox potential. Hydrometallurgy 93, 88–96. https://doi.org/10.1016/j.hydromet.2008.04.016

Gericke, M., Govender, Y., Pinches, A., 2010. Tank bioleaching of low-grade chalcopyrite concentrates using redox control. Hydrometallurgy 104, 414–419. https://doi.org/10.1016/j.hydromet.2010.02.024

Ghahremaninezhad, A., Radzinski, R., Gheorghiu, T., Dixon, D.G., Asselin, E., 2015. A model for silver ion catalysis of chalcopyrite (CuFeS2) dissolution. Hydrometallurgy 155, 95–104. https://doi.org/10.1016/j.hydromet.2015.04.011

Hiroyoshi, N., Arai, M., Miki, H., Tsunekawa, M., Hirajima, T., 2002. A new reaction model for the catalytic effect of silver ions on chalcopyrite leaching in sulfuric acid solutions. Hydrometallurgy 63, 257–267. https://doi.org/10.1016/S0304-386X(01)00228-6

Hiroyoshi, N., Kitagawa, H., Tsunekawa, M., 2008. Effect of solution composition on the optimum redox potential for chalcopyrite leaching in sulfuric acid solutions. Hydrometallurgy Volume 91, Issues 1–4, March 2008, Pages 144-149.

Hiroyoshi, N., Kuroiwa, S., Miki, H., Tsunekawa, M., Hirajima, T., 2007. Effects of coexisting metal ions on the redox potential dependence of chalcopyrite leaching in sulfuric acid solutions. Hydrometallurgy 87, 1–10. https://doi.org/10.1016/j.hydromet.2006.07.006

Hiroyoshi, N., Kuroiwa, S., Miki, H., Tsunekawa, M., Hirajima, T., 2004. Synergistic effect of cupric and ferrous ions on active-passive behavior in anodic dissolution of chalcopyrite in sulfuric acid solutions. Hydrometallurgy 74, 103–116. https://doi.org/10.1016/j.hydromet.2004.01.003

Hiroyoshi, N., Miki, H., Hirajima, T., Tsunekawa, M., 2001. Enhancement of chalcopyrite leaching by ferrous ions in acidic ferric sulfate solutions. Hydrometallurgy 60, 185–197. https://doi.org/10.1016/S0304-386X(00)00155-9

Hiroyoshi, N., Miki, H., Hirajima, T., Tsunekawa, M., 2000. A model for ferrous-promoted chalcopyrite leaching Hydrometallurgy 57 (2000) 31–38.

Hiroyoshi, N., 英人前田, 一三木, 剛平島, 昌美恒川, 1998. Ferrous Promoted Chalcopyrite Leaching- Ferric formation and its effects on the leaching -. 資源と素材 114, 795–800. https://doi.org/10.2473/shigentosozai.114.795

Miki H., Hiroyoshi N., Hirajima T., Tsunekawa M., 2001. Batch Leaching Behavior of Chalcopyrite in Acidic Ferric Sulfate Solutions-Relationship between solution redox potential and copper extraction. Shigen-to-Sozai 117, 215–220. https://doi.org/10.2473/shigentosozai.117.215

Nicol, M., Miki, H., Velásquez-Yévenes, L., 2010. The dissolution of chalcopyrite in chloride solutions: Part 3. Mechanisms. Hydrometallurgy 103, 86–95. https://doi.org/10.1016/j.hydromet.2010.03.003

Third, K.A., Cord-Ruwisch, R., Watling, H.R., 2001. Control of the redox potential by oxygen limitation improves bacterial leaching of chalcopyrite.

Viramontes-Gamboa, G., Rivera-Vasquez, B.F., Dixon, D.G., 2007c. The Active-Passive Behavior of Chalcopyrite: Comparative Study Between Electrochemical and Leaching Responses. J. Electrochem. Soc. 154, C299. https://doi.org/10.1149/1.2721782

Yoo, K., Lee, J., Hiroyoshi, N., Alorro, R., Tsunekawa, M., 2007. The Effect of Redox Potential on the Leaching of Chalcopyrite in Chloride Media, in: Proceedings of the Sixth International Copper-Cobre Conference, Vol. IV: The John E. Dutrizac International Symposium on Copper Hydrometallurgy. Presented at the Sixth International Copper-Cobre Conference, The John E. Dutrizac International Symposium on Copper Hydrometallurgy, Canadian Institute of Mining, Metallurgy and Petroleum, pp. 259–267.

CHAPTER 7: GENERAL CONCLUSION

Chalcopyrite ($CuFeS_2$) is the most abundant mineral in copper ore bodies, accounting for more than 70% of the world copper reserves. However, with increasing the consumption of copper worldwide, high-grade ores are depleting. To guarantee the sustainable supply of copper, nowadays, low-grade ores are explored, mined, and concentrated with high amounts of impurities that are toxic such as arsenic. The concentrate of chalcopyrite together with arsenic as impurities are then processed for copper metal extraction. The conventional method to extract copper from chalcopyrite concentrate is pyro-metallurgy. However, the pyro-metallurgical process is facing the problem of high running cost and environmental issues related to the release of arsenic through stack emission.

Thus, hydrometallurgy is considered as a promising alternative approach to extract copper from low-grade chalcopyrite concentrate, owning to its low cost and safe removal and handling of arsenic that concomitantly dissolved in aqueous solution. Leaching is the first step of hydrometallurgy, where the metal ions are released (leached) into the solution from the solid particles (minerals). The biggest challenge of copper hydrometallurgy is to overcome the extremely slow leaching rate of chalcopyrite. To propose a good method to improve the chalcopyrite leaching rate, it is important to understand the chalcopyrite leaching mechanism. Therefore, this study aims to clarify the mechanism of chalcopyrite leaching in acidic chloride solution through an understanding of redox potential dependence of chalcopyrite leaching and the effect of chloride ions.

Chapter 1 gave the general introduction including overview of the study, statement of the problem, and outline of dissertation.

Chapter 2 gave a literature review on chalcopyrite leaching.

Chapter 3 investigated the effects of temperature and solution composition on the redox potential dependence of chalcopyrite leaching. The leaching experiments were carried out in acidic ferric chloride solutions using a specially designed batch leaching experimental setup that accurately determined and monitored the redox potential changes with time. Assuming that chalcopyrite oxidation with Fe(III) occurred stoichiometrically, the concentration ratio of Fe(III) to Fe(II) and the relationship between leaching rate versus redox potential were then determined from the redox potential data.

A peak behavior was observed in the copper extraction rate versus the redox potential plot. The leaching rate increased with increasing redox potential reaching a (local) maximum (i.e.,

the peak rate) at a certain redox potential (i.e., the peak redox potential) followed by the gradual decrease in leaching rate at higher redox potentials.

The effects of temperature and solution composition (Cu(II), Fe(III), and Cl^- concentrations) on the peak rate and peak redox potential were investigated. The results showed that the peak rate increased with increasing temperature, and decreased with increasing HCl and Fe(III) concentrations but was not strongly affected by the concentration of Cu(II). In comparison, the peak redox potential was less dependent on the temperature and the concentrations of HCl and Fe(III). Although Cu(II) concentration was not crucial in the peak rate, it was a major factor affecting the peak redox potential, that is, the peak redox potential increased with increasing the cupric ion concentration. Based on these results, an empirical equation for the relationship between the peak redox potential and Cu(II) concentration was derived.

Chapter 4 investigated the effects of solution composition on the anodic polarization curve of chalcopyrite. Anodic polarization experiments were carried out using a conventional three-electrode system, with chalcopyrite as a working electrode, at 298 K under the nitrogen atmosphere.

The results indicated that in the absence of Cu(II) and/or Fe(II), the current density increased monotonically with increasing applied redox potential. Only in the presence of both Cu(II) and Fe(II) in solution, the peak behavior was observed in anodic polarization curve, which was similar to the peak leaching rate, reported in leaching experiments. At low redox potential region (lower than 0.50 V), the current density in the presence of Cu(II) and Fe(II) was much higher than that in the absence of these ions. This result indicated that the coexistence of Cu(II) and Fe(II) promoted the dissolution of chalcopyrite at low redox potentials.

The effects of chloride ions on the anodic dissolution of chalcopyrite in the presence of both Cu(II) and Fe(II) were investigated. In the solutions containing 0.1 M HCl, 0.05 M Cu(II), 0.05 M Fe(II), and various concentration of NaCl, current density increased with increasing NaCl concentration. It indicated that chloride ions were promoters for the dissolution of chalcopyrite. From the thermodynamic point of view, when both Cu(II) and Fe(II) present in solution, they react to form Cu(I). From the result of Geochemist's Workbench® with MINTEQ database, Cu(I) formed cuprous chloride complexes with chloride ions and thus, became more stable at high chloride concentration. It suggested that Cu(I) might play an important role in the chalcopyrite leaching.

The effects of Cu(I) on the anodic dissolution of chalcopyrite were examined using a solution containing 0.1 M HCl with 0.001 M CuCl. The result showed that Cu(I) promoted the chalcopyrite dissolution rate at low redox potentials and the peak behavior appeared on the anodic polarization

curve even with only Cu(I) present in solution. Considering the promotion effect of Cu(I), the effects of coexistence Cu(II) and Fe(II), as well as chloride ions could be explained as follows. The high leaching rate achieved at low redox potential in the presence of both Cu(II) and Fe(II) was due to the formation of promoter Cu(I). The stability of Cu(I) at high chloride ions concentration resulted in a faster chalcopyrite leaching rate at higher chloride ions concentration.

In Chapter 5, the electrochemical impedance spectroscopy (EIS) was conducted to understand different processes happening at the electrode surface. The measurements were done at varied applied potentials on the chalcopyrite electrode in an electrolyte containing 0.05 M Cu(II) and 0.05 M Fe(II) in 0.1 M HCl at 298 K under the nitrogen atmosphere. The results of EIS measurements were plotted in complex plane plots and fitted using equivalent circuits.

At redox potentials lower than 0.45 V, the impedance data were plotted on a straight line of 45 degrees in the complex plane plots and fitted using an equivalent circuit composed of solution resistant (R_s) and constant phase element (CPE) in series. The results suggested that chalcopyrite dissolution at the low redox potential was controlled by a diffusion process.

At redox potentials higher than 0.45 V, the impedance data were plotted on a compressed semi-circle (at high frequencies) connected with a straight line (at low frequencies). The data were fitted with an equivalent circuit containing a parallel circuit of R and CPE, which corresponds to a product layer formed on the surface of the chalcopyrite electrode. With increasing redox potential, the value of R in the parallel circuit increased, suggesting that the product layer grew on chalcopyrite surface and the layer thickness increased with increasing redox potential. This passivation layer hindered the further dissolution of chalcopyrite, resulted in a slow reaction kinetics and leading to a decrease in current density at high redox potential.

In Chapter 6, based on the experimental results in previous chapters, a reaction model assuming the formation of an intermediate Cu_2S at low redox potentials were proposed for chalcopyrite leaching in acidic chloride solutions. The intermediate Cu_2S is easier to dissolve than chalcopyrite, thus enhanced the copper extraction rate at low redox potentials. The formation reaction of intermediate Cu_2S involved three steps. Firstly, chalcopyrite reacted with H^+ in solution to release Cu(II), Fe(II), and H_2S into the solution. Then Cu(II) and Fe(II) reacted to form Cu(I). Finally, Cu(I) reacted with H_2S to form Cu_2S precipitated on the chalcopyrite surface. The intermediate Cu_2S was oxidatively decomposed to release Cu(II) and form elemental sulfur. Once elemental sulfur was formed, it acted as a passivation layer suppressing further chalcopyrite dissolution. Using the reaction model, the experimental results observed in the previous chapters were discussed.

Chapter 7 gave the summary, implications, and conclusion of the dissertation.

Appendix

ELECTROCHEMICAL IMPEDANCE SPECTROSCOPY

Electrochemical impedance spectroscopy (EIS) is a non-destructive method to study kinetic and mechanistic of reactions happening on the electrode surface. The terms resistance and impedance both denote an opposition to the flow of electrons or current. In direct current (DC) circuits, only resistors produce this effect. However, in alternation current (ac) circuits, two other circuit elements, capacitor and inductors, impede the flow of electrons. The inductor will not be considered in this study. Impedance can be expressed as a complex number, where the resistance is the real component and capacitance is the imaginary component.

The total impedance in a circuit is the combined opposition of all its resistors, capacitors to the flow of electrons. Capacitors affect not only the magnitude of an alternating current but also its time-dependent characteristics – or phase. When most of the opposition to the current flow comes from its inductive reactance, a circuit is said to be largely capacitive and the current leads the applied voltage in phase angle.

Electrochemical impedance theory is a well – developed branch of ac theory that describes the response of a circuit to an alternating current or voltage as a function of frequency. In DC theory (a special case of AC theory where the frequency equals 0 Hz), resistant is decided by Ohm' s low:

$$E = I R \qquad \text{(i-1)}$$

Using Ohm' s low, you can apply a DC potential (E) to a circuit, measure the resulting current (I), and compute the resistance (R), or determine any term of the equation if the other two are known. The potential value is measured in volts (V), current in amperes (A), and resistance in ohm (Ω). A resistor is the only element that impedes the flow of electrons in ac circuits.

In AC theory, where the frequency is non-zero, the analogous equation is:

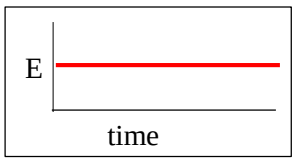
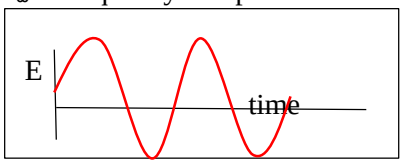
$$E = I Z \qquad \text{(i-2)}$$

As in equation (4-2), E and I are here defined as potential and current, respectively. Z is defined as impedance, the AC equivalent of resistance. Impedance values are also measured in ohm. In addition to resistors, capacitors and inductors impedance the flow of electrons in an AC circuit.

In an electrochemical cell, slow electrode kinetics, slow preceding flow, can be considered

analogous to the resistors, capacitors, and inductors that impede the flow of electrons in an AC circuit.

The main advantage of EIS is that purely electronic model can be used to represent an electrochemical cell. An electrode interface undergoing an electrochemical reaction is typically analogous to an electronic circuit consisting of a specific combination of resistors and capacitors. This analogy is used to establish AC circuit theory to characterize the electrochemical system in terms of its equivalent circuit.

Direct current (DC)	Alternative current (AC)
- Direct current is the one way flow if electrical charge from a positive to a negative charge. - Batteries produce direct current. - Ohm's law: E = E/I R= impedance at the limit of zero frequency. 	- Alternative current is when charges flow back and forth from a source. - Frequency is the number of cycles per second in Hertz. - Impedance: $Z_\omega = E_\omega / I_\omega$ E_ω = frequency – dependent potential. I_ω = frequency – dependent current 

i. Advantages of EIS

- The information content of EIS is much higher than DC techniques or single frequency measurements.
- EIS may be able to distinguish between two or more electrochemical reactions taking place.
- EIS can identify diffusion-limited reactions, e.g., diffusion through a passive film.
- EIS provides information on the capacitive behavior of the system.
- EIS can provide information about the electron transfer rate of reaction.
- EIS techniques use very small excitation amplitudes, often in the range of 5 to 10 mV peak – to peak. Excitation waveforms of this amplitude cause only minimal perturbation

of the electrochemical test system, reducing errors caused by the measurement technique.

ii. Equivalent circuit elements

Circuit element		Impedance equation	Current vs. Voltage
Resistance, R	$\mathbf{R = \rho \frac{d}{A}}$ **(*)**	$\mathbf{Z_R = R + 0\,j}$	$\mathbf{I = \frac{E}{R}}$
Capacitance, C	$\mathbf{C = \frac{\varepsilon_0 \varepsilon_r A}{d}}$ **(**)**	$\mathbf{Z_C = 0 - j/\omega C}$	$\mathbf{I = C \frac{dE}{dt}}$
Constant phase element, CPE		$\mathbf{Z_{CPE} = \frac{1}{T(j\omega)^p}}$	

Where:

ω = 2Πf

f: frequency

For Eq. (**)

d: distance between two plates

A: surface of one plate

ε_0: permittivity of free space (electric constant)

ε_r: dielectric constant (relative electrical permittivity)

Whereas the permittivity of free space is a physical constant, the dielectric constant depends on the material. Notice large difference between the dielectric constant of water and that of an organic coating. The capacitance of a coated substrate changes as it absorbs water. EIS can be used to measure that change.

Material	Dielectric constant (ε_r)
Vacuum	1
Water	80.1 (20 °C)
Organic coating	4 - 8

ii.1 Solution resistance

Solution resistance is often a significant factor in the impedance of an electrochemical cell. A modern three electrode potentiostat compensates for the solution resistance between the counter and reference electrodes. However, any solution resistance between the reference electrode and working electrode must be considered when modelling the electrochemical cell.
The resistance of an ionic solution depends on the ionic concentration, type of ions, temperature, and the geometry of the area in which current is carried. In a bounded area with area, A, and length, I, solution resistivity, ρ, carrying a uniform current, the resistance is defined as,

$$R = \rho \frac{l}{A} \qquad \text{(i-3)}$$

Unfortunately, most electrochemical cells do not have uniform current distribution through a definite electrolyte area. Therefore, calculating the solution resistance from the solution conductivity will not be accurate. Solution resistance is often calculated from the EIS spectra.

The impedance of a resistance has no imaginary component at all. The phase shift is zero degree, that is, the current is in phase with the voltage. Both current and impedance are independent of the frequency.

ii.2 Charge transfer resistance

Resistance in this example is formed by a single, kinetically – controlled electrochemical reaction. In this case, we do not have a mixed potential, but rather a single reaction at equilibrium.
Consider a metal substrate in contact with an electrolyte, the metal can electrolytically dissolve into electrolyte, according to:

$$Me \Leftrightarrow Me^{n+} + n\, e^-$$

Or more generally

$$Red \Leftrightarrow Ox + n\, e^-$$

In the forward reaction in the first equation, electrons enter the metal and metal ions diffuse into the electrolyte. Charges are being transferred. This charge transfer reaction has a certain speed. The speed depends on the kind of reaction, the temperature, the concentration of the reaction products and the potential.

The general relation between the potential and the current (which is directly related with the amount of electrons and so the charge transfer via Faraday law) is:

$$i = i_0 \left(\frac{C_0}{C_0^*} \exp\left(\frac{\alpha n F \eta}{RT}\right) - \frac{C_R}{C_R^*} \exp\left(\frac{-(1-\alpha) n F \eta}{RT}\right) \right)$$

When the concentration in the bulk is the same as at the electrode surface, $C_0 = C_0^*$ and $C_R = C_R^*$. The above equation is simplified to:

$$i = i_0 \left(\exp\left(\frac{\alpha n F \eta}{RT}\right) - \exp\left(\frac{-(1-\alpha) n F \eta}{RT}\right) \right)$$

This equation is called the Butler – Volmer equation. It is applicable when the polarization depends only on the charge-transfer kinetics. Stirring the solution to minimize the diffusion layer thickness can help minimize concentration polarization.

When the over potential, ŋ, is very small and the electrochemical system is at equilibrium, the expression for the charge transfer resistance changes to:

$$R_{ct} = \frac{RT}{nFi_0}$$

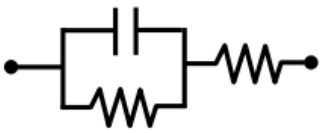
From this equation, the exchange current density can be calculated when Rct is known.

ii.3 Capacitance

Conversely, the impedance of a capacitor has no real component. Its imaginary component is a function of both capacitance and frequency. The current through a capacitor is always 90 degrees out of phase with voltage across it, with current leading the voltage. Because the impedance of a capacitor varies inversely with frequency, at high frequencies a capacitor act as a short circuit – its impedance tends toward zero (meaning that the capacitor does not hinder the flow of electron). At low frequencies (approaching DC), a capacitor acts as an open circuit, and impedance tends toward infinite (meaning that capacitor hinder the flow of electron).

ii.4 Double layer capacitance

An electrical double layer exists on the interface between an electrode and its surrounding electrolyte. The double layer is formed as ions from the solution adsorb on the electrode surface. The charged electrode is separated from the charged ions by an insulating space, often on the order of angstroms. Charges separated by an insulator form a capacitor so a bare metal immersed in an electrolyte will behave like a capacitor.



Randles Cell
(Simplified)

iii. Plot analysis

The Randles cell (Fig. i-1) models the electrochemical impedance of an interface and fits many chemical systems. The circuit components in the Randles cell can be equated with familiar physical phenomena, such as adsorption or film formation. Rs is the ohmic or uncompensated resistance of the solution between working and reference electrode. Rp is the polarization resistance or charge transfer resistance at the electrode/ solution interface. Cdl is the double layer capacitance at the interface.

Fig. i-1. Equivalent circuit for a single electrochemical cell (the Randles cell)

If the polarization or charge-transfer resistance (R_p) is known, the electrochemical reaction rate can be calculated. Double layer capacitance measurements can provide information on adsorption and desorption phenomena. In some systems, a C_{dl} measurement may not represent the double layer capacitance. Rather it may indicate the degree of film formation or the integrity of an organic coating.

The impedance of a capacitor diminishes as the frequency increases, while the impedance of the resistor is constant. Thus above a certain frequency, the impedance of the capacitor, C_{dl}, becomes much smaller than the impedance of the resistor, R_p. Since C_{dl} is in parallel with R_p, the capacitor acts as a short and effectively removes the resistor from the circuit (meaning the electron will mostly move through the capacitor). At the highest frequencies, the impedance if the capacitor will also become much smaller than R_s, thus, the high frequencies behavior of the Randles cell is controlled almost entirely by R_s.

However, at the lowest frequencies, the capacitor acts as open circuit and is effectively removed from the circuit (meaning at lowest frequencies, the impedance of the capacitor is too large, the electron mostly move through the resistor). The impedance of the Randles cell is then the combined resistance values of the two series resistor R_s and R_p.

Thus, at both the high and the low frequency limits, the Randles cell behaves primarily as a resistor. The imagine component is very small, the phase angle is close to 0 degree, and the impedance does not change with frequency.

At intermediate frequencies, the impedance of capacitor begins to have an effect and cell becomes more capacitive. The imagine component becomes significant, the phase angle can start to approach 90 degrees, and the cell impedance becomes frequency dependent.

iii.1 The complex plane plot (Nyquist plot)

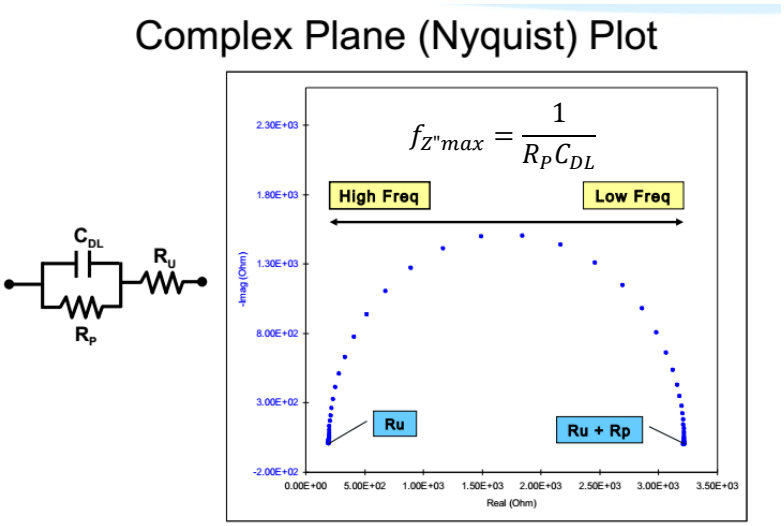


Fig. i-2. Complex plane plot for a simple electrochemical system.

The complex plane plot plotted the imaginary impedance component (Z") against the real impedance component (Z′) at each excitation frequency. The plot in Fig. i-2 illustrates the expected response of the simple circuit in Fig. i-1.

At high frequencies, the impedance of the Randles cell was almost entirely created by the solution resistance, R_s. The frequency reaches it high limit at the left most end of the semicircle, where the semicircle touches the x axis. At low frequency limit, the Randles cellalso approximates a pure resistance, but now the value is (R_s + R_p). The frequency reaches its low limit at the rightmost end of the semicircle.

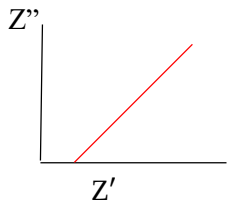
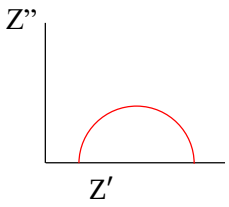
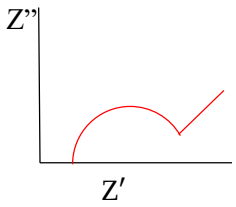
The complex plane plot has several advantages. The primary one is that the plot format makes it easy to see the effects of the solution resistance. Besides, the shape of the curve (often a semicircle) does not change when the solution resistance changes. Consequently, it is possible to compare the results of two separate experiments that differ only in the position of the reference electrode. Another advantage of this plot is that it emphasizes circuit components that are in series, such as R_s.

The complex plane plot has also some disadvantages. For example, frequency does not appear explicitly. Secondly, although the solution resistance and charge transfer resistant can be easily read directly from the complex plane plot, the electrode capacitance can be calculated only after

the frequency information is known. As shown in Fig. i-2, if R_p is known, the capacitance (C) can be calculated from the frequency corresponding to the top of semicircle.

Although the complex plane plot format emphasizes series circuit elements, if high and low impedance networks are in series, the low impedance circuit may not be seen on the plot, since the larger impedance controls plot scaling.

If system is kinetically slow, large R_p and only limited frequency region where mass transfer significant. If R_p is small, then the system is kinetically facile.

Diffusion control (Mass – transfer control)	**Kinetic control**	**Mix kinetic – diffusion control**
Rate determining step is diffusion process	Rate determining step is kinetics process	Rate determining steps are both slow diffusion process and slow kinetics process
		

iii.2 The Bole plot

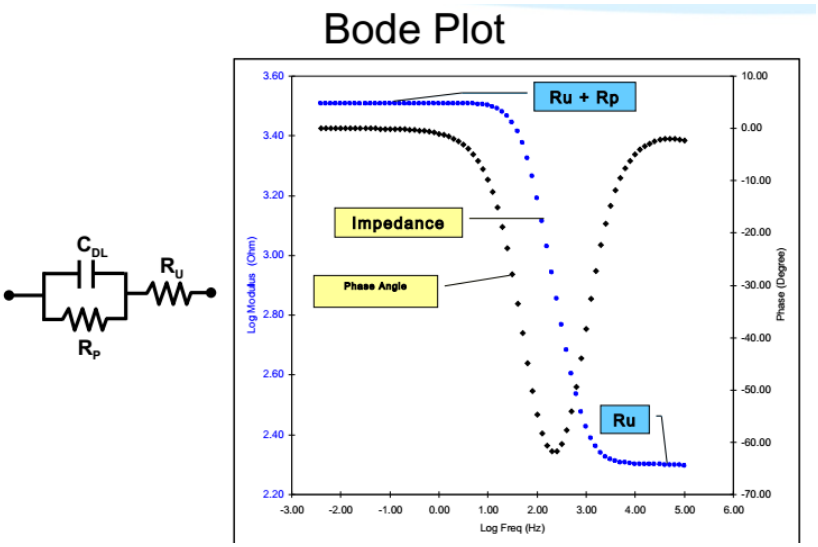


Fig. i-3. Bole plane plot for a simple electrochemical system.

Fig. i-3 shows a Bole plot for the same data pictured in the complex plane plot in Fig. i-2. The Bole plot format gives the absolute impedance, $|Z|$, as calculated by Eq. i-4, and the phase shift, θ as a function of frequency, f.

$$|Z| = \sqrt{Z'^2 + Z''^2} \qquad \text{(i-4)}$$

The Bole plot has some distinct advantages over the complex plane plot. Since frequency appears as one of the axes, it is easy to understand from the plot how the impedance depends on the frequency. The plot use logarithm of frequency to allow a very wide frequency range to be plotted on one graph, but with each decade given weight. The Bole plot also show the magnitude, $|Z|$, on a log axis. This can be an advantage when the impedance depends strongly on frequency, as is the case with capacitor. Besides, the values of Rs, Rp, Cdl can be obtained from the Bole plot as shown in Fig. i-3.

On some electrochemical processes, there is more than one rate-determining step. Each step represents a system impedance component and contributes to an overall reaction rate constant. The electrochemical impedance experiment can often distinguish among these steps and provide information on their respective rates or relaxation times.

Complex plane plot (Nyquist plot)	**Bode plot**
- **Frequency is not obvious.** - **Small impedances can be swamped by large impedances.**	- Frequency is explicit. - Small impedances in presence of large impedances can be identified easily.